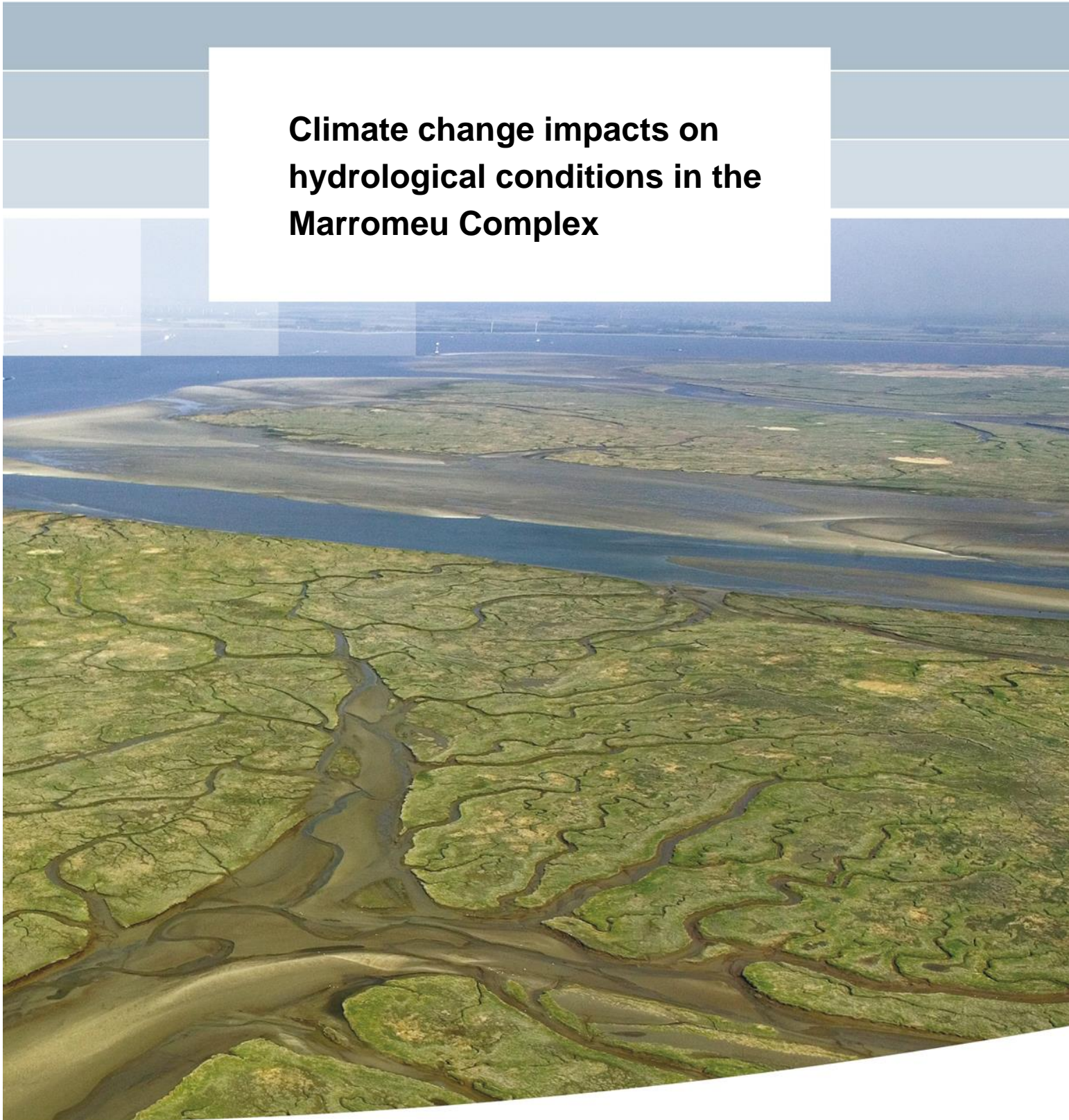**Climate change impacts on hydrological conditions in the Marromeu Complex**

Climate change impacts on hydrological conditions in the Marromeu Complex

Frederiek Sperna Weiland
Laurène Bouaziz
Jaap Schellekens

Deltares

Title
Climate change impacts on hydrological conditions in the Marromeu Complex

Keywords
Marromeu Complex, Mozambique, climate change, droughts, wetlands, ecosystems

Summary

Background and methodology

The Marromeu Complex is located in the Zambezi Delta in Mozambique. It is a protected RAMSAR wetland site. Ecosystems as well as human activities may experience negative impacts from future temperature increases and changing rainfall patterns due to climate change. This study estimates the changes in hydrological conditions in the Marromeu complex and the possible impacts. The figure below provides an overview of the study approach. For this assessment data from four global climate models (GCMs) for two future scenarios were used for the future time horizons 2030 and 2050. The variation between the GCMs and thus the uncertainty of the projections was largest for the drier period from March to August.
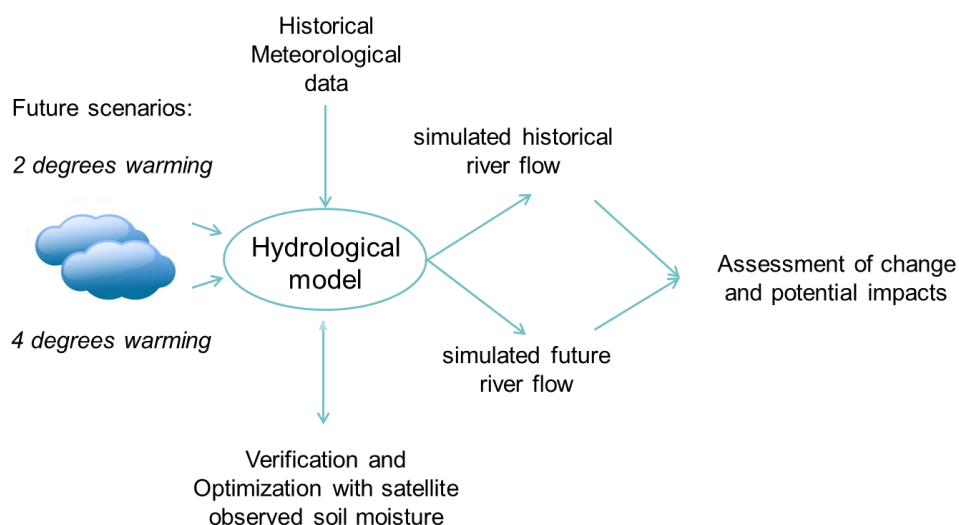

Figure A Study approach with the model and datasets included.

Hydrological and meteorological changes

Precipitation is overall projected to decrease by 2030 for all seasons except for the dry season where increases and decreases are equally likely to occur. By 2050 there is a tendency towards decreases up to -50% although (small) increases are possible as well. The variation in the projections increases, except for the rainy season (December to March). Here the direction of change is unclear and varies between -5 and +4 %. The start of the rainy season will be more variable in the future and a late onset (beginning of December) will occur more often than previously.

Deltares

Title
Climate change impacts on hydrological conditions
in the Marromeu Complex

Client	**Project**	**Attribute**	**Pages**
WWF Netherlands	11202660-000	11202660-000-ZWS-0012	75

As a result of decreasing rainfall and increasing temperatures, up to ~2 degrees by 2050, the evaporation deficit will increase and thus soil moisture and groundwater recharge (up to -5%) will decrease. Groundwater levels may on average decrease with 4 cm and decreases of up to 13 cm may occur during the dry season.

Based on literature review a sea level rise of approximately 0.30 meters was derived specifically for the coastline of the Marromeu Complex.

Consequences for the Marromeu Complex

Production of maize, corn and sugarcane will require more irrigation water during the dry season due to the projected increase in evaporation and decrease of soil moisture. Crop growing conditions will become less favorable and small-scale farming yields may reduce, given their limited resilience to climate change.

Increased drought and a more variable onset of the rainy season will affect biodiversity. On the inland boundary the mangrove forests may retreat and freshwater grassland can disappear.

River flow from the Cheringoma Escarpment will likely decrease. A reduction of wet season flow (as projected by 3 out of 4 scenarios) will also reduce the flow of freshwater in the wetland area downstream which in turn may lead to further upstream penetration of saline water.

The population of Sofala, Mozambique will approximately double every 25 years. This will likely result in an increasing pressure on the use of resources and available land.

The projected sea level increase will exacerbate flooding and possibly loss of land due to erosion and land submerging in the delta area. The higher sea level will also mean that saline water will reach further land inward and cause increased land salinization.

Recommendations

Implementation of small-scale rain-water harvesting and storage would provide water for small-scale rainfall-fed agriculture and households in the dry season.

Continued conservation and expansion of the mangroves are necessary to protect the area from coastal erosion and flooding.

Restriction of clear cutting and burning land for cultivation in the upstream catchments is necessary to maintain the natural water holding capacity of the soil.

The projected reduction in groundwater recharge and likely increases in salinization asks for sustainable use of the available water resources.

Title
Climate change impacts on hydrological conditions in the Marromeu Complex

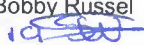| Client	Project	Attribute	Pages
WWF Netherlands	11202660-000	11202660-000-ZWS-0012	75

A detailed groundwater analysis, including a local groundwater model, would help to assess salinization and decreasing groundwater levels as well as the interaction with the Zambezi River and the possible groundwater flow from the escarpment.
s
The outcomes of this study were limited by the availability of local data on river flows, groundwater levels, land use and vegetation occurrence. Improved monitoring would help to assess the current state and changes therein.

Version	Date	Author	Initials	Review	Initials	Approval	Initials
1.0	Mar. 2019	Frederiek Sperna Weiland		Bobby Russel		Gerard Blom	
		Laurene Bouaziz					
		Jaap Schellekens					

Status
final

Contents

Appendices

Acknowledgement

1 Introduction

WWF has requested Deltares to conduct a climate impact analysis for the Marromeu Complex located on the coastline in the Central part of Mozambique. This analysis supports the development of a restoration strategy and the improved and sustainable management of the complex. The analysis provides WWF with information that can support the definition of sustainable conservation and restoration strategies to be developed considering the changing climate conditions. The results are available for use in further studies and stakeholder assessments.

For this assessment we follow an approach using models and tools developed by Deltares and VanderSat. River flows, soil moisture, evapotranspiration and groundwater recharge are simulated with the distributed hydrological model Wflow (Schellekens et al., 2014). Focus is on the period 1979 to 2014 for which peer-reviewed validated global meteorological datasets are available.

Soil moisture data derived from satellite observations provides an important source to quantify the severity of historical drought conditions. Because there is no river flow data available in the Marromeu complex we have also used the satellite derived soil moisture data to validate and optimize model and use the model to assess changes in future soil moisture conditions.

The climate impact analysis focusses on the changes in drought conditions and related decrease in water availability for ecosystems and domestic and agricultural use. The climate projections are based on the IPCC 5th assessment report – the latest version of the internationally established climate scenarios.

Socio-economic information has been obtained from WWF and literature review. In the last section the results of the climate impact assessment are translated into consequences for the Marromeu Complex using the available socio-economic data.

2 Data and Methods

2.1 Study area

Background

The Marromeu complex is located in the lower Zambezi Delta and covers an area of approximately 11,000 km^2. The complex became a Ramsar site in 2004. It is bordered in the North-East by the Zambezi River, in the South-East by the Indian Ocean and in the west by the Cheringoma Escarpment. It is inhabited by Buffalo, Elephant, Antelope, Zebra, Hippopotamus, Lions, Leopards, Cheetahs, Wild Dogs, Spotted Hyena and a variety of water birds (Crane Foundation, 2018).

Agricultural activities are in the Eastern part of the complex. This mainly concerns large scale irrigated sugar cane production, that has slowly extended into the wetland areas, and some smaller scale crop production of mainly maize, corn and rice. The eastern part is also the area where most people live – the population of the complex is estimated at 120,000 thousand (Beilfuss et al. 2001). The complex includes the Marromeu Special Reserve as well as four surrounding hunting concessions. Military and commercial hunting has decimated wildlife populations during and immediately following Mozambique's civil war and ongoing hunting activities delay wildlife recovery. Large parts of the complex are hard or impossible to access due to dense vegetation. Hunters do access more inaccessible areas over water. Clear-cutting and fires are widespread in the upland areas.

The area used to be severely influenced by the discharge variability of the Zambezi River which was the main source of water for the complex and caused seasonal flooding that supported the wildlife, fisheries, agricultural activities and biodiversity. Due to the regulation of the Zambezi River at Cahora Bassa and the construction of dikes, roads and railways, discharge to the Salone River that flows from the Zambezi to the complex has been severely reduced and the river is silting up (Beifuss and Bento, 2003). There are plans to rehabilitate the Salone and to divert water from the Zambezi to the Salone. A feasibility study on this topic was started in 2017.

At present the inundation of the Zambezi Delta is mainly dependent on local rainfall-runoff from the Cheringoma Escarpment and local rain within the reserve (Working Group for Conservation and Sustainable, 2003). The Mungari, Ruave, Sanga, and Zuni Rivers have their source on the crest of the Cheringoma Escarpment and flow down meandering along the edge of the Zambezi Delta. These water resources sustain wetlands, lakes and thus wildlife on the western half of the delta that no longer receive floodwaters from the regulated Zambezi River (Bento and Beilfuss, 2003). This study focusses on changes within the complex and the rivers originating on the Cheringoma escarpment.

Composite satellite image (Landsat 7 ETM, July 2003) of the Marromeu Complex, showing the Zambezi Delta, Cheringoma escarpment, and other regional features. Map produced by Richard Beilfuss and Carlos Bento.
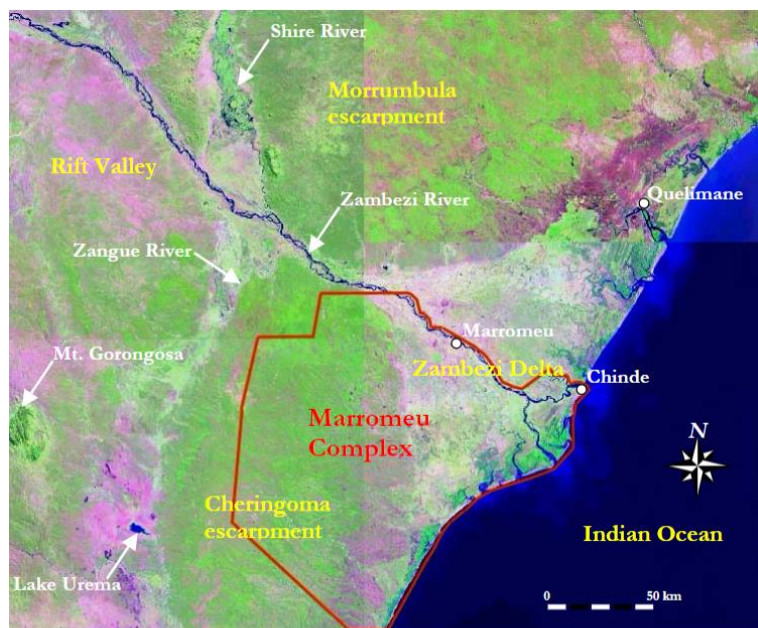
Figure 2.1 Overview of the Marromeu Complex delineated with red and its location in the Zambezi Delta at the Southern Bank of the Zambezi (source: Beilfuss and Bento).

Model area

The area considered in the modelling and soil moisture analysis includes the full river catchments entirely located within the Marromeu Complex, delineated in black in Figure 2.2. It was explicitly decided not to include the Zambezi River in the model because of its complexity, size and current hydrological disconnection from the Marromeu Complex.
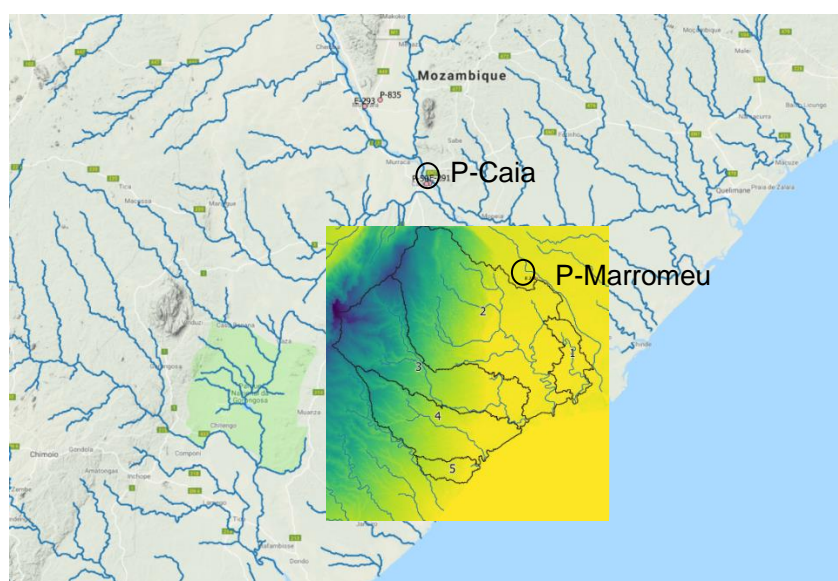
Figure 2.2 Map of the catchment areas included in the model (delineated in black and numbered 1 to 5) together with the two precipitation stations (black circles) nearest to the complex.

Based on steepness / elevation (i.e. of the escarpment and the wetland areas) and vegetation types like forests, agricultural crops and wetland vegetation, the complex has been divided in representative sub-areas used for analysis of the data, see Figure 2.3.
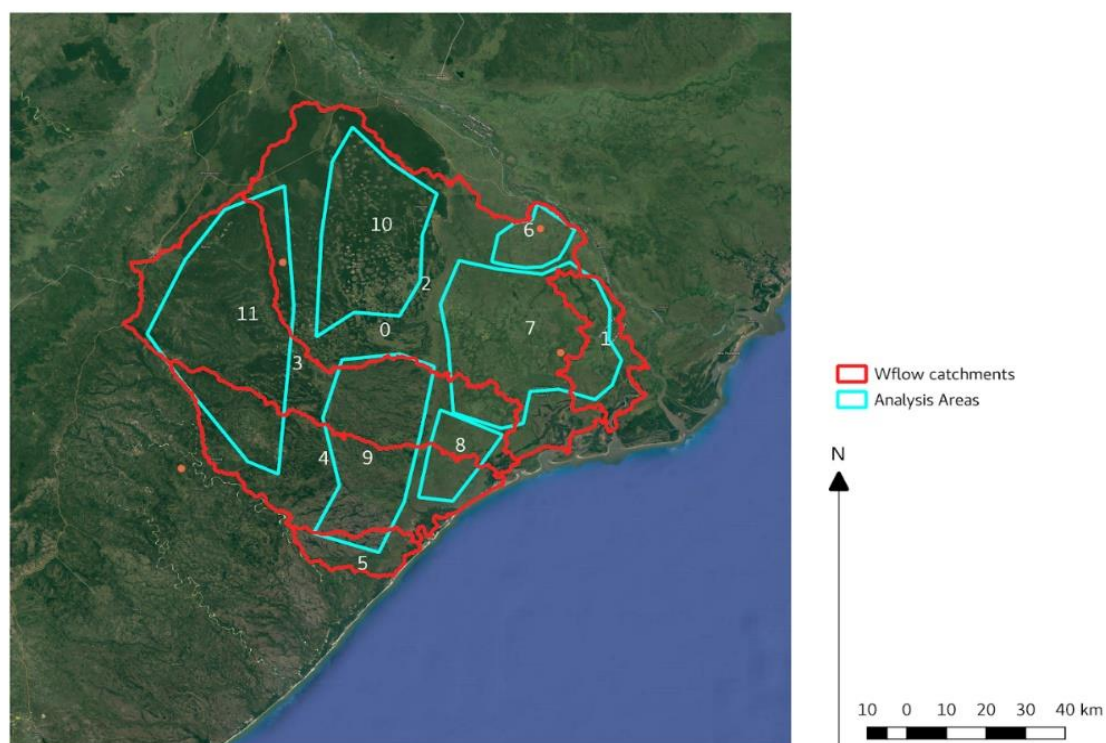
Figure 2.3 areas used in the analysis. 1 to 5 are the wflow catchment 6-11 are areas with more or less homogeneous vegetation and topographical properties.

2.2 Approach

With this assessment we want to analyse potential future changes in hydrological conditions in the Marromeu complex due to climate change with a specific focus on droughts and their possible impacts. Figure 2.4 outlines the assessment design.

1. River flow, soil moisture, evaporation and groundwater are simulated for the historical period 1979-2014 with the hydrological model (Wflow) using historical meteorological datasets.

2. In the absence of observed river flow data the hydrological model is verified and optimized based on satellite soil moisture observations as a proxy.

3. After optimization the hydrological model is used to simulate future river flow, soil moisture, evaporation and groundwater for the years 2030 and 2050.

4. The model is forced with climate datasets for the RCP4p5 and RCP8p5[1]. The former refers to a global average temperature increase of 2 degrees by 2100, the latter to 4 degrees warming.

5. For all variables the change between the historic period and the future time horizons is assessed and potential impacts are discussed.
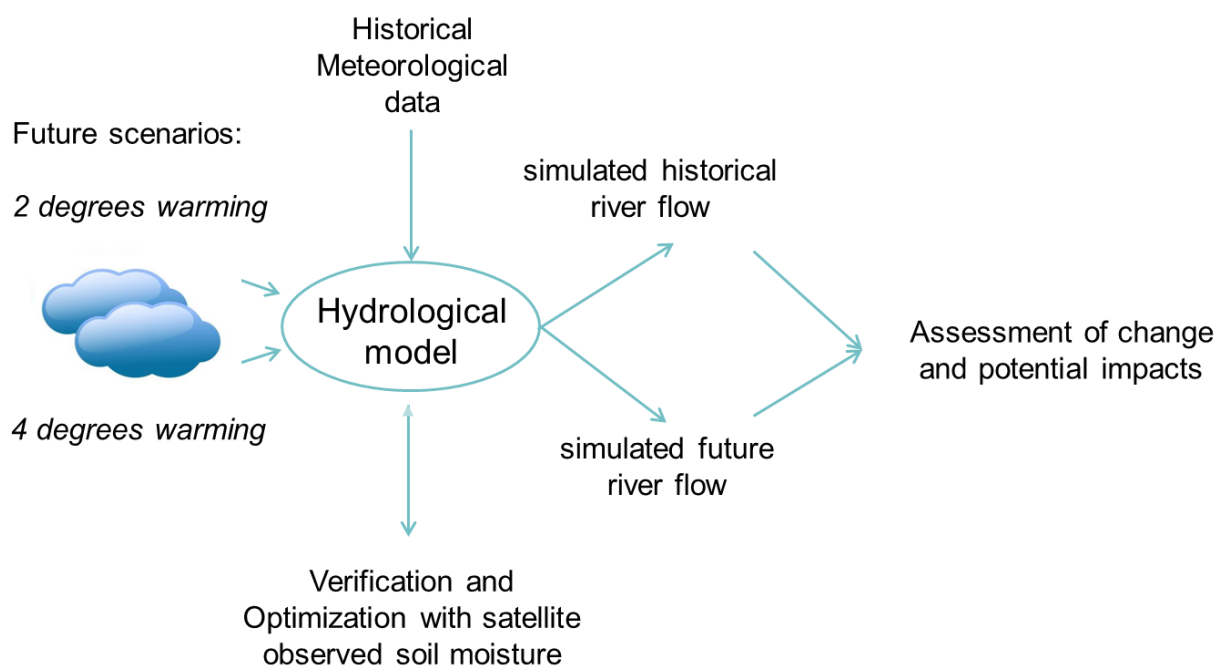

Figure 2.4 Assessment design with the model and datasets included.

---

[1] *Representative Concentration Pathways used by IPCC to convert future development scenarios into quantified greenhouse gas concentrations for climate models resulting in quantified future warming projections.*

2.3 Hydro-meteorological data

2.3.1 Historical meteorological data

2.3.1.1 Local meteorological observations

Local precipitation data was provided by WWF Mozambique. This data originates from ARA-Zambeze. The timeseries cover the period 2009 to near present. We have analysed the data for two locations near the complex. The meteorological station in Marromeu which is located on the North-East border of the area and the station in Caia located north of the complex.

2.3.1.2 Global meteorological data

The global dataset Multi Source Weighted Ensemble Precipitation (MSWEP; Beck et al., 2016) is frequently used at Deltares to force Wflow hydrological models. The dataset combines precipitation from satellite, re-analysis and station observation data. The different datasets are averaged based on their performance. The dataset is available at a daily time-step and its spatial resolution is 0.25 degrees. Temperature and potential evaporation were obtained from the eartH2Observe dataset (Schellekens et al., 2017). Potential evaporation was calculated with the widely used physically based Penman-Monteith equation (Monteith, 1965). Within the hydrological model the potential evaporation is transferred to crop specific evaporation.

2.3.1.3 Comparison of precipitation data

In Fig. 2.5 to 2.7 we compare the local station data from the two stations with the global dataset spatially averaged over catchment 1. Overall the products are quite similar which confirms reasonable performance of the global product. There are some differences. For Caia we see a large deviation in rainfall amount for the year 2009 compared to the other station and the global product. In addition, the daily observed precipitation data at Marromeu for the dry period is nearly continuously dry. This resulted in very dry conditions in the hydrological model and as discussed with WWF we doubted this was representative for the entire area.

Indeed, a high degree of spatial variability of the precipitation is expected in the study area, based on the difference between the two available stations and the presence of both coastal and mountainous areas. By using the global product to force our model we are able to represent this spatial variability in the model. Finally, for climate change analysis a long time series is required (at least 30 years) which also requires the use of the long global data time series.
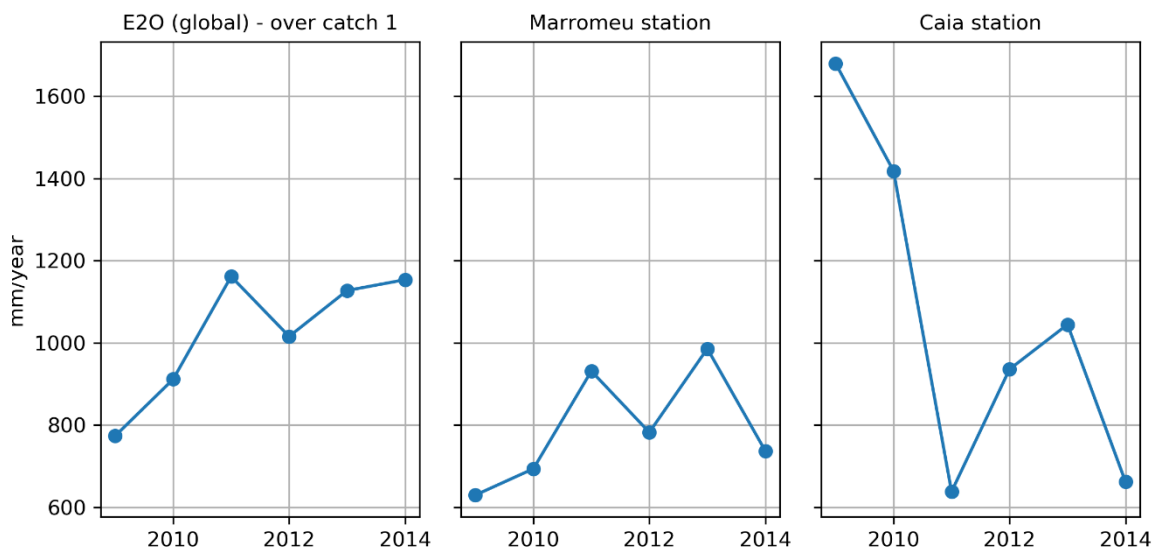
Figure 2.5 Comparison of yearly precipitation over catchment 1 with the global product (E2O), the Marromeu station and Caia station
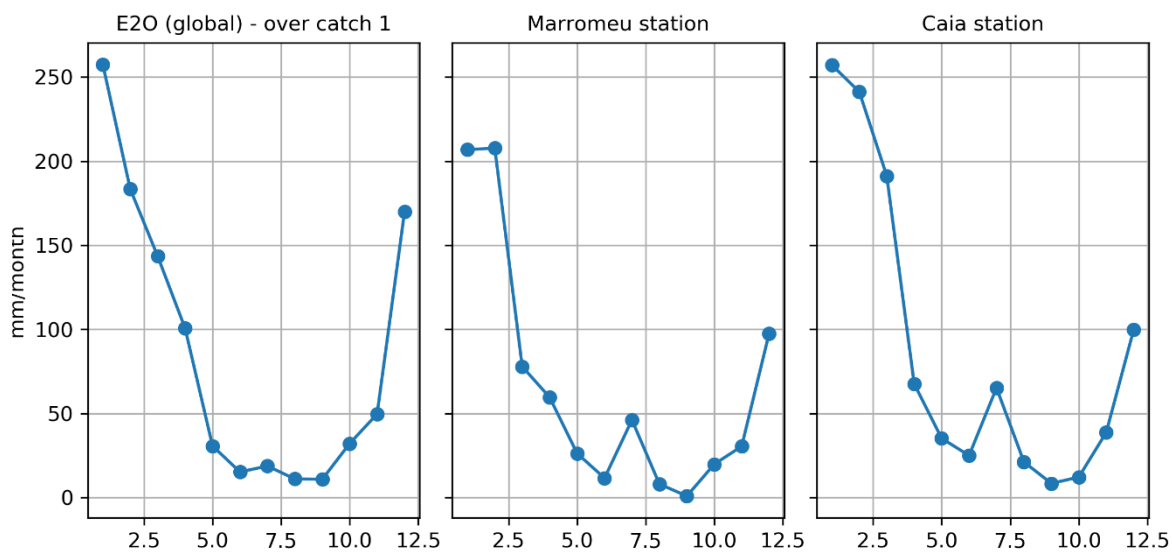

Figure 2.6 Comparison of monthly precipitation over catchment 1 with the global product (E2O), the Marromeu station and Caia station
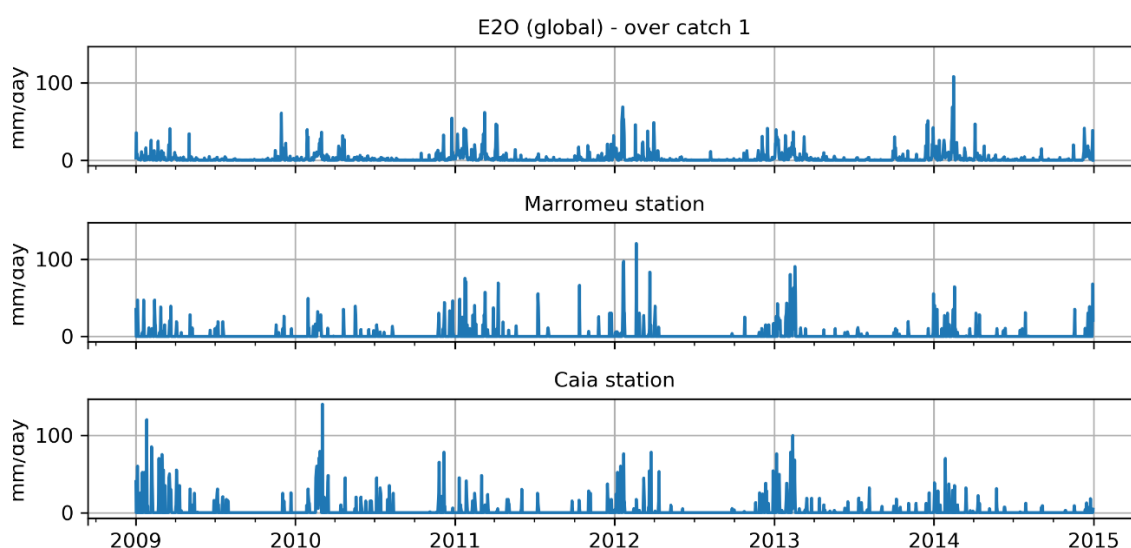
Figure 2.7 Comparison of monthly precipitation over catchment 1 with the global product (E2O), the Marromeu station and Caia station

2.3.2 Future rainfall, evaporation and temperature projections

This study focuses on changes in future hydrological conditions caused by climate change. To this end climate datasets from the 5th Assessment report of the Intergovernmental Panel on Climate Change (IPCC-AR5; IPCC, 2013) have been used. Two RCPs were selected, RCP4.5 (the moderate change scenario) and RCP8.5 (the worst case scenario). Focus is on the future time-horizons 2030 and 2050, for both the historical period and the future periods a time period of 30 years is used, because natural climate variability is assumed to be covered in a 30 year period.

For the calculation of future changes in river flow we used datasets from General Circulation Models (GCMs) that were part of the international inter-sectoral impact model inter-comparison project (ISI-MIP). The ISI-MIP project developed future climate projections that were later used as input for the IPCC 5th assessment report.

The database contains open bias-corrected GCM data existing of global daily grids with a resolution of 0.5 degrees from 4 GCMs: NorES1-M, IPSL-CM5A-LR, GFDL-ESM2M, HadGEM2-ES. These bias-corrected GCMs have been considered in this study.

Part of the ISI-MIP project focused on the bias-correction of the GCM precipitation data. Hereto they applied an advanced bias-correction method (Hempel et al., 2013). The method preserves the absolute changes in monthly temperature, and relative changes in monthly values of precipitation. It is a modification of frequently used simpler transfer function, considered too simple by Van der Zaag et al. (in prep) and considers both correction of the monthly mean and correction of the daily variability around the monthly mean.

2.3.3 Surface water level data

Water level data has been provided by ARA-Zambeze for a number of gauges. Unfortunately, none of those are located in the complex. We have data for two stations located downstream of the Cahora Basa dam in the Zambezi main river, Tete and Caia. The time-series covers the period 1955 – 2017. The construction of the dam resulted in a decrease in seasonality in the Zambezi river discharge, i.e. a decrease of dry season minimum discharge and increase of wet

season maximum discharge. This affects the Zambezi river water that could potentially flow into the Marromeu complex during high flows, if the Salone River was not disconnected from the complex by dams and other infrastructure.

2.3.4 Satellite soil moisture

Wetlands are areas with higher soil moisture content than the surrounding land (Müller et al., 2012). Satellite derived soil moisture is a good estimator of the wetness of the wetland and has been included in this study because it provides valuable information on changes in drought conditions and can be used to improve the parameterization of the hydrological model. For the period 2015 to 2018 there data available from the SMAP satellite data from NASA which provides L-band data and a rather good estimate of the moisture conditions. Before 2015 we rely on C-band satellite data. As part of the analysis the C-band data was optimized to create time-series of continuous data using both SMAP and the C-band data.

2.3.5 Sea Level Rise (SLR) and cyclone projections

In this region tropical storms that sometimes evolve into tropical cyclones occur with a frequency of about twice per year and mostly from January until March (INGC, 2009). In Figure 2.8 the tracks and severity of cyclones over the period 1980 to 2050 are shown. To assess future changes in cyclone frequency and sea level rise we have based ourselves on existing literature of modelling studies based on the IPCC 4th and 5th assessment report.
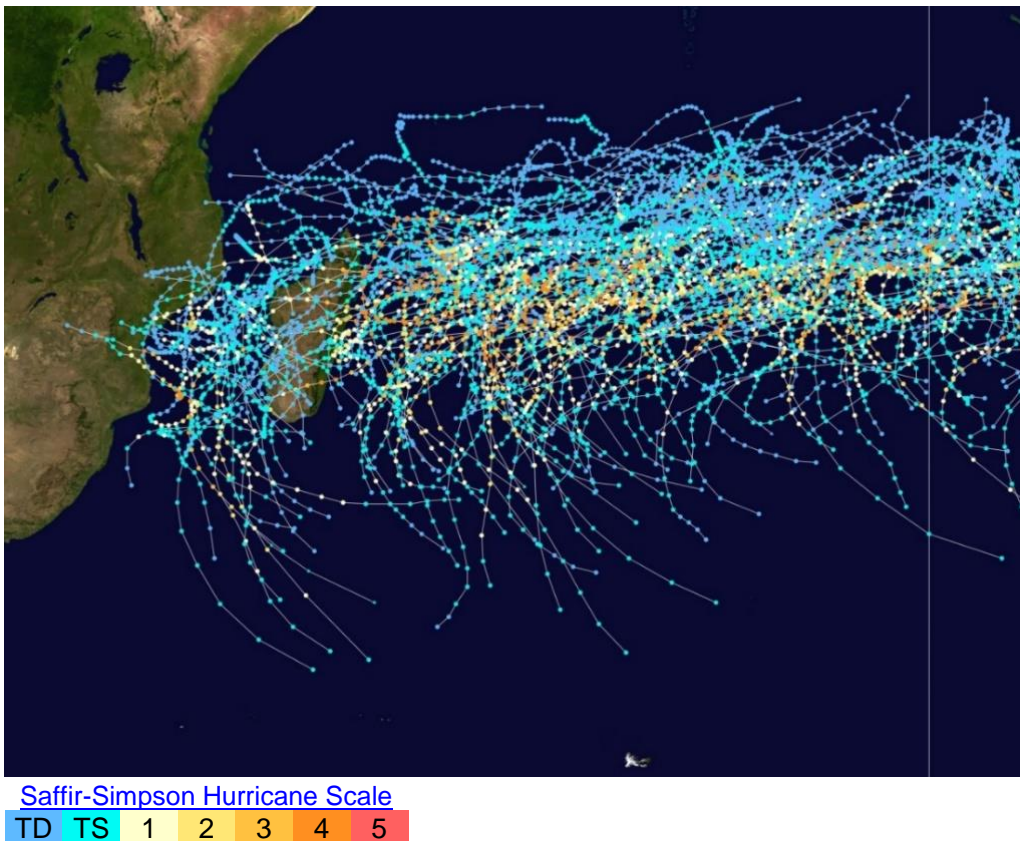

Saffir-Simpson Hurricane Scale

| TD | TS | 1 | 2 | 3 | 4 | 5 |

Figure 2.8 Southwest Indian Ocean cyclone tracks 1980-2005, taken from http://en.wikipedia.org/wiki/ Tropical_cyclone_basins.

Climate change impacts on hydrological conditions in the Marromeu Complex

2.4 Wflow hydrological model

Figure 2.9 shows the Wflow-sbm model structure. Within the Wflow model the water enters the model as precipitation. Part of the precipitation is stored as interception in the vegetation and the remaining water is available for infiltration in the soil according to a fraction of paved and unpaved area. The soil in Wflow-sbm is considered as a 4-layer bucket, divided into a saturated store and an unsaturated store. Water that cannot infiltrate into the soil is routed overland using the kinematic wave method. Soil evaporation, transpiration and open water evaporation occur from the soil based on the transformation of Penman-Monteith calculations into actual evapotranspiration within the model. Transfer from the unsaturated store to the saturated store is controlled by the saturated hydraulic conductivity at water level depth and the ratio between the unsaturated store and the saturation deficit. Vegetation may extract water from the saturated store through capillary rise which results in a flux from the saturated store to the unsaturated store. Lateral flow from the saturated store from one grid cell to another grid cell is based on the difference of water level of both pixels following Darcy's law. When the water level of the saturated store is at the surface, water may exfiltrate and will be added to the river flow.
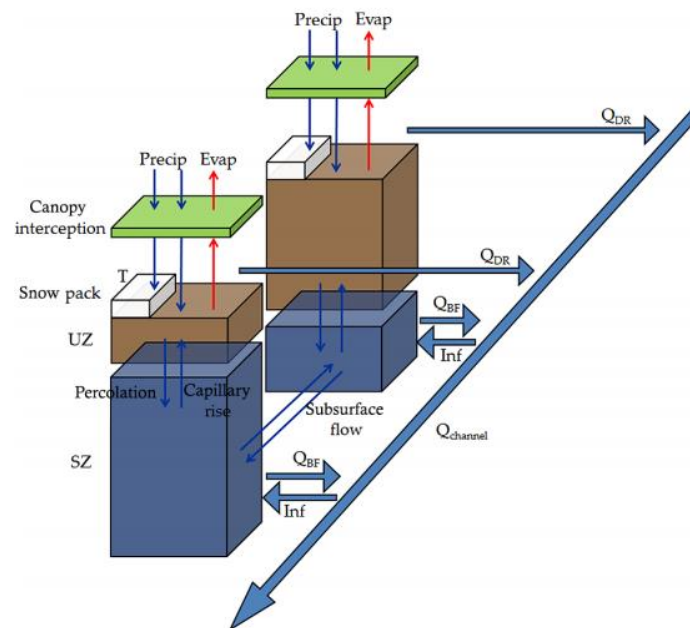

Figure 2.9 Open Streams Wflow_sbm model structure, adapted from (Schellekens et al., 2014). Symbol definitions are as follows: Precip, precipitation; Evap, evaporation; T, temperature; UZ, unsaturated zone; SZ, saturated zone; Qchannel, total runoff; QDR, direct runoff; QBF, baseflow; and Inf, water flow from the river channel to the saturated zone.

3 Results

3.1 Historical soil-moisture time-series and spatial patterns from satellite data

To account for the complexity and spatial heterogeneity of the complex (i.e. irrigated land, forests, hill slopes, wetlands) the area has been divided in sub-areas for which individual soil moisture time-series have been generated. The map of the sub-division of the complex in areas of similar topographic and vegetation properties is provided again in Figure 3.1. The first analysis of the data showed (unexpectedly) that the vegetation cover in the steeper area was too dense of the L and C-Band data to provide reliable soil moisture estimates. As such, for those areas we can use data between 2015 and 2018 only. For the lower delta areas we can use the combination of longer time-series. A more in-depth analysis is provided in Appendix A.

Figure 3.2 shows the monthly climatology for soil moisture determined from the period 2015-2018 for the Marromeu Complex as outlined in Figure 2.1. The intra-annual cycle of wet and dry months can clearly be seen. The soil moisture is expressed with a number between 0 (completely dry) and 1 saturated. The plots show that the southern and eastern areas are wettest in the wet periods. In the driest month (October) the whole of the area becomes almost equally dry. The wettest month from a soil moisture perspective is April.
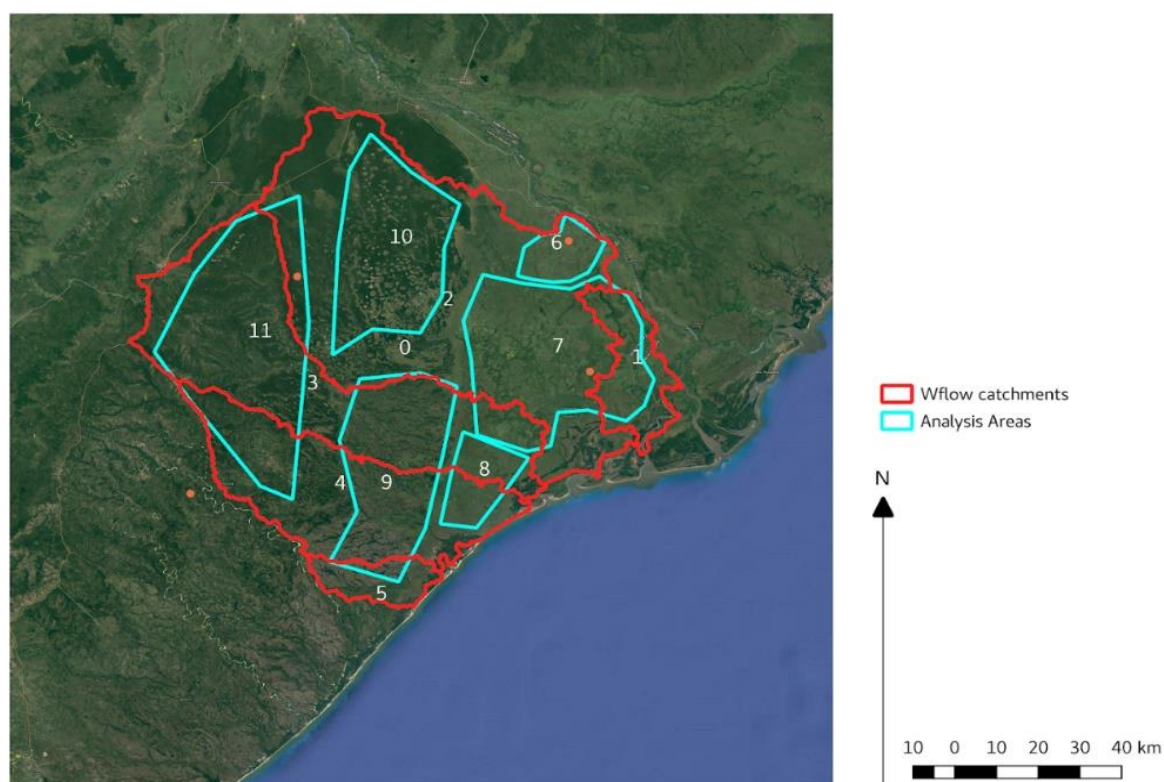

Figure 3.1 areas used in the analysis. 1 to 5 are the wflow catchment 6-11 are areas with more or less homogeneous vegetation and topographical properties.
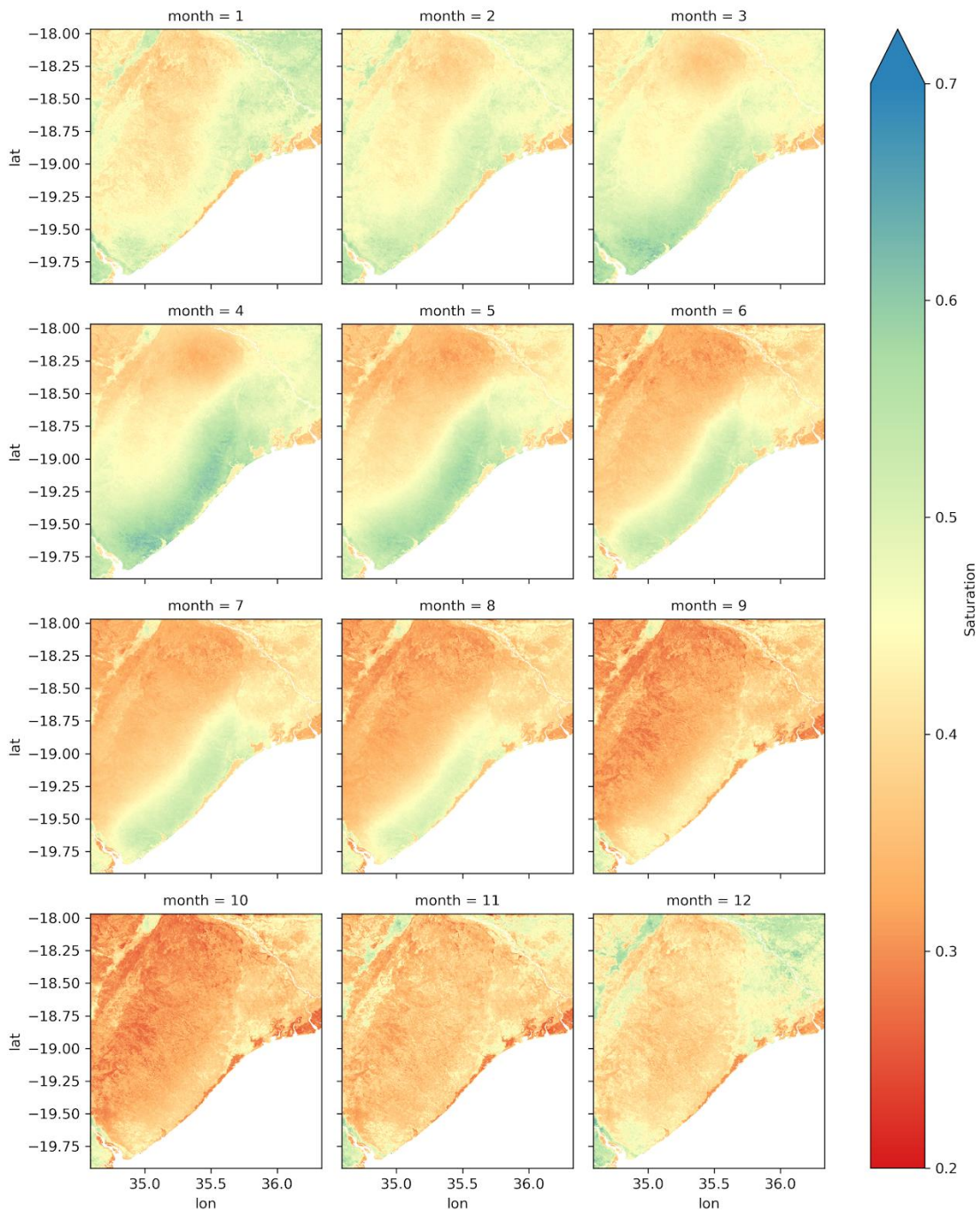
Figure 3.2 Monthly climatology of apparent saturation (between 0 and 1) over the period 2015-2018 derived from L-Band soil moisture. Month 1 corresponds to January, month 12 is December.

Figure 3.3 shows the long soil moisture record for area 6, 7 and 8 respectively, those in the east of the complex. The blue (long term) and orange (short term) lines are 14 day rolling mean averages. The green lines show the 365 days rolling mean. There is considerable difference between the years with the beginning of the record (2002-2007) being relatively dry.
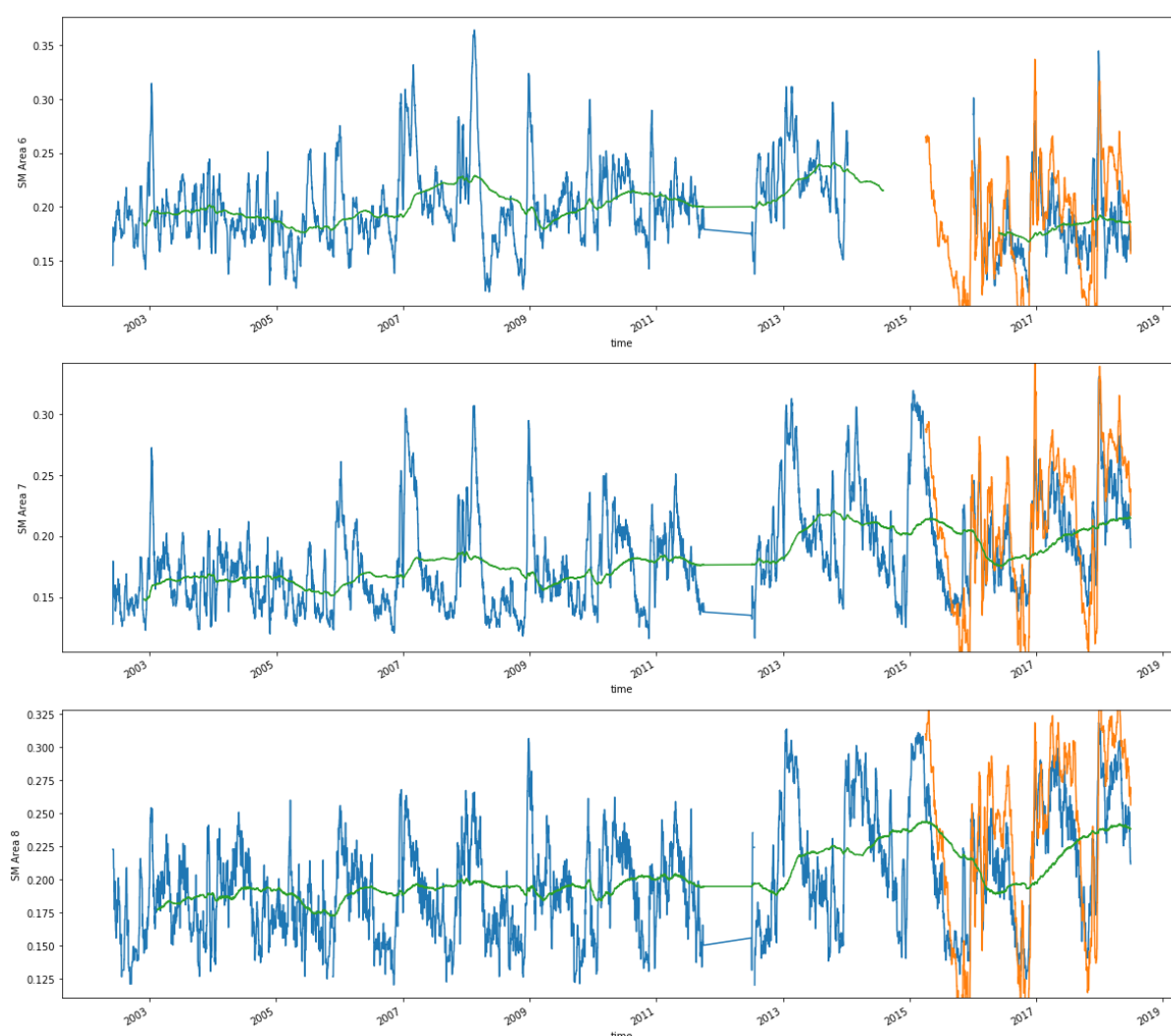

Figure 3.3 long term soil moisture record (14 day rolling mean) for area 6,7 and 8. The orange line shows the short term record (the L band), the green line the 365 day rolling mean.

3.2 Comparison modelled and satellite-based soil-moisture for the historical period

There is no river flow data available to validate the discharges simulated with the hydrological model. We therefore rely on a comparison between satellite observed soil moisture and soil moisture simulated with the hydrological model to optimize the model. The comparison of satellite-based soil moisture and modelled soil moisture shows discrepancies due to uncertainty in both model and satellite observations. However, for some areas, monthly patterns are comparable (see Fig. 3.1 for the location of area 8) and there is a relatively constant bias over time. Based on these results (and extended results included in Appendix A) we assume that the model can be used for a sensitivity analysis of the impact of various climate change scenarios on the drought conditions in the area.
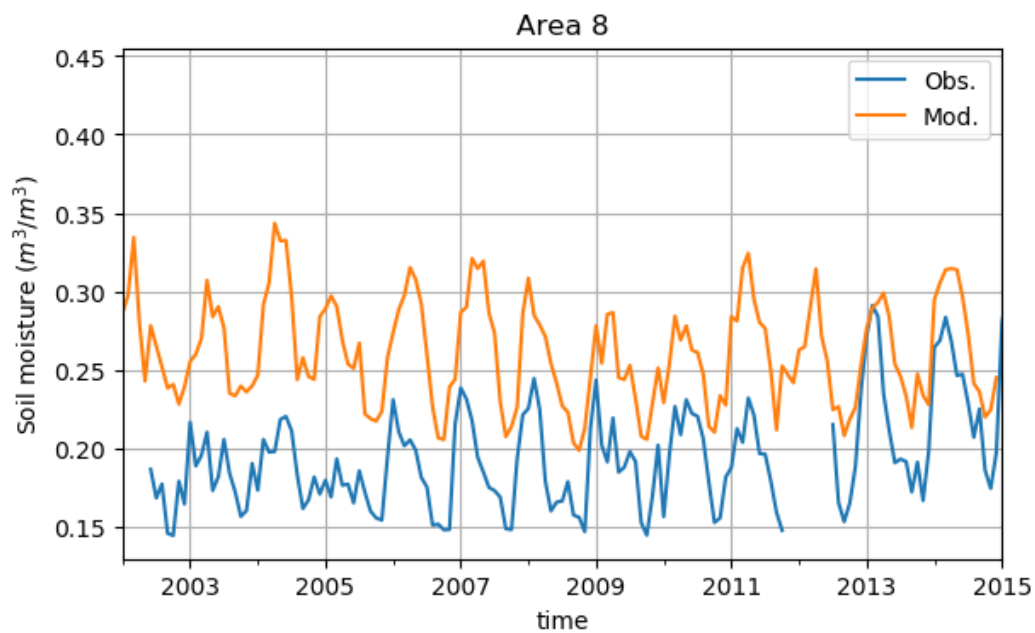
Figure 3.4 Comparison of observed (VanderSat) and modelled soil moisture in area 8
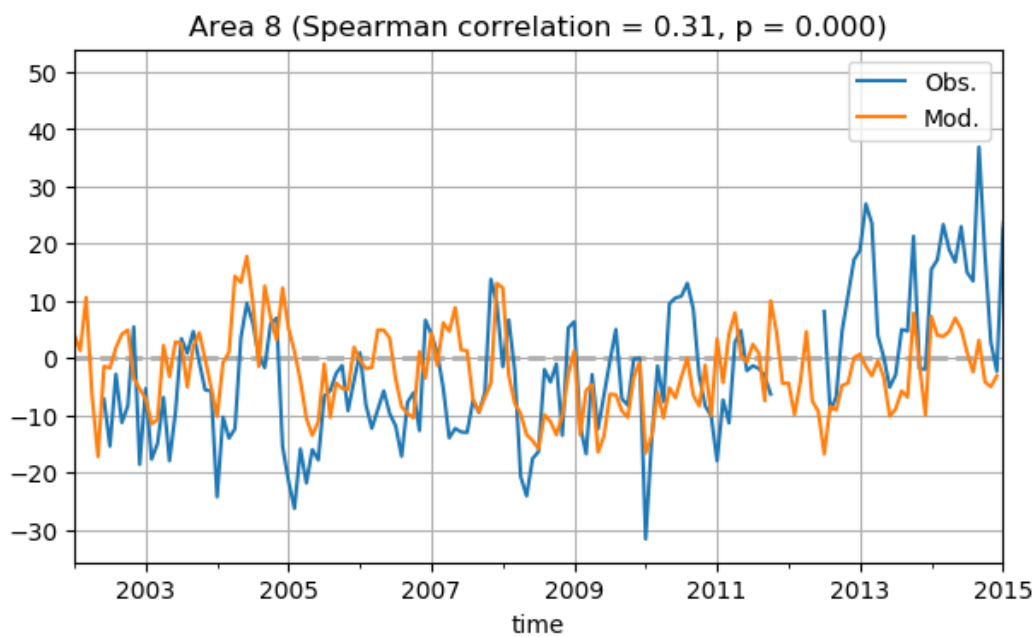
Figure 3.5 Comparison of soil moisture anomalies (deviations from mean) for observed and modelled soil moisture in area 8

Climate change impacts on hydrological conditions in the Marromeu Complex

Mean monthly modelled soil moisture are shown in Figure 3.6. When compared to satellite derived values (see Fig. 3.2), we see similar patterns of wetter lowland areas compared to the highlands. Both modelled and observed datasets indicates that the months September and October are the driest of the year.

Figure 3.6 Mean monthly modelled soil moisture (m³/m³)

3.3 Future projections of temperature and precipitation

The first part of the assessment of potential changes in precipitation and temperature focusses on monthly average changes. This is followed by a more in-depth analysis in which changes in variables specifically of interest to the Marromeu Complex are investigated. Therefore the year has been divided into four seasons that correspond specifically to the seasons as experienced in Mozambique:
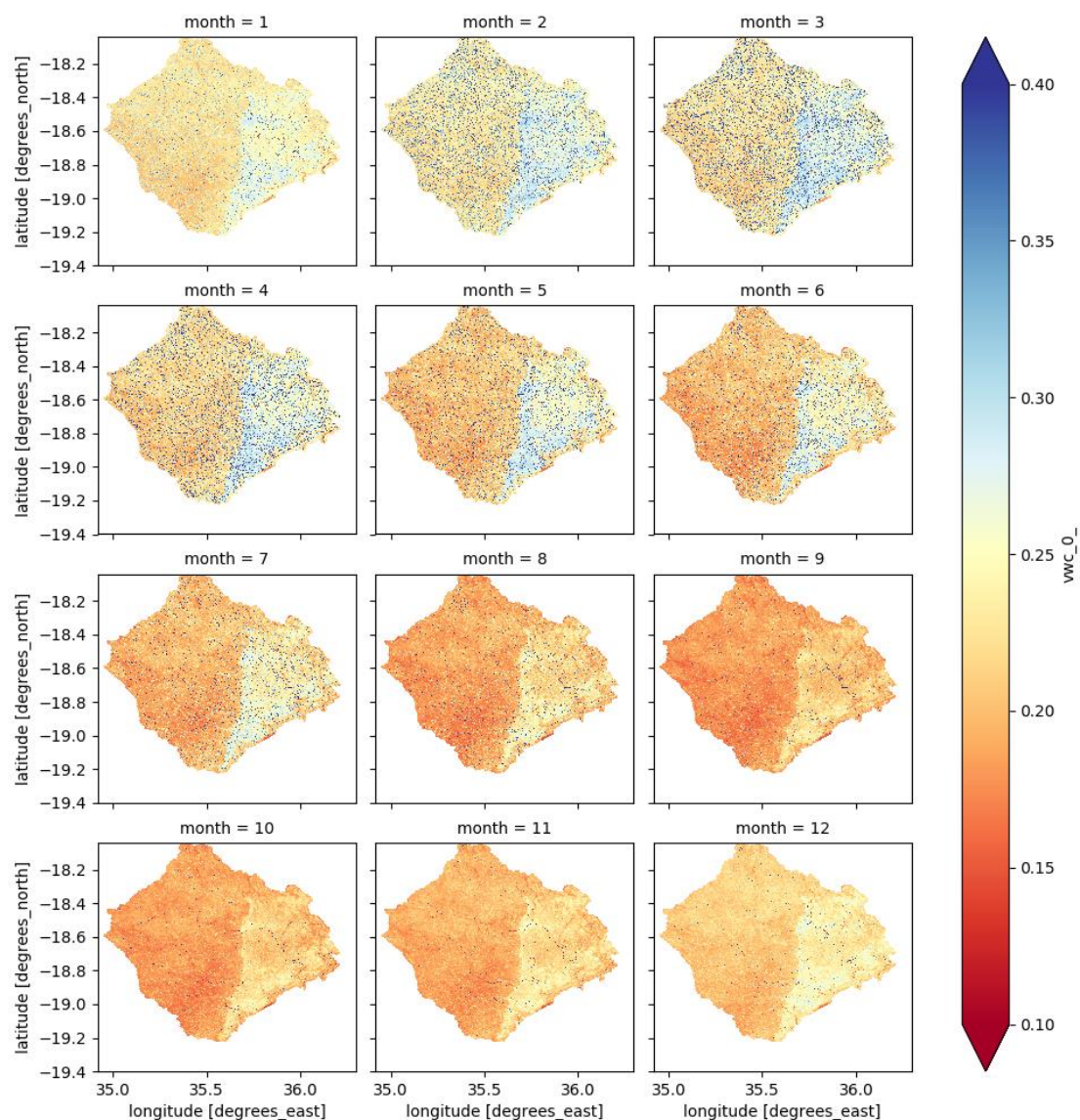
- Oct – Nov: Start wet season

  - In this period the first rain events start to occur after the long dry period.

- Dec – April: Rainy season

  - During this period most severe rainfall events occur and the rainfall frequency is high.

- May: Post rainy season

  - This is the transition period to the dry season during which rainfall diminishes.

- June – September: Dry season

  - During this period there can be very long periods of zero or very little rain.

3.3.1 Projected increase in temperature

Based on bias-corrected data from the selected 4 GCMs we have derived changes in temperature. We selected two Representative Concentration Pathways (RCPs). RCP4p5 refers to a global average temperature increase of 2 °C by 2100 and RCP8p5 refers to an increase of 4 °C by 2050. On average, and in line with three out of four models an increase in temperature is projected of approximately 1 °C by 2030 and 1.5 to 2 °C by 2050 for RCP4p5. The temperature increase is largest for the dry period, i.e. the months September to November. The GCM gfdlesm2m deviates from the other GCMs for 2030 showing more monthly variation in projected change. RCP8p5 projects increases of approximately 2 °C throughout the year by 2050.

Change in temperature RCP4p5 2030
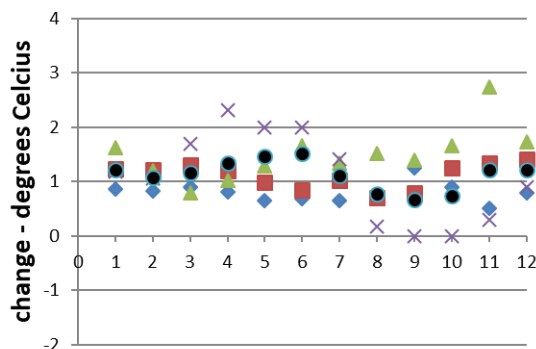
Change in temperature RCP4p5 2050

Figure 3.7 Projected change in temperature for 2030 (left) and 2050 (right) for RCP4p5 for the selected GCMs indicated in different colours and the ensemble mean change (black dots). The numbers 1 to 12 correspond to the months January to December.

Change in temperature RCP8p5 2030

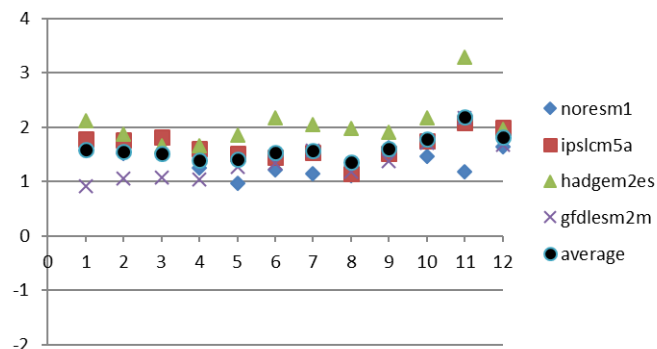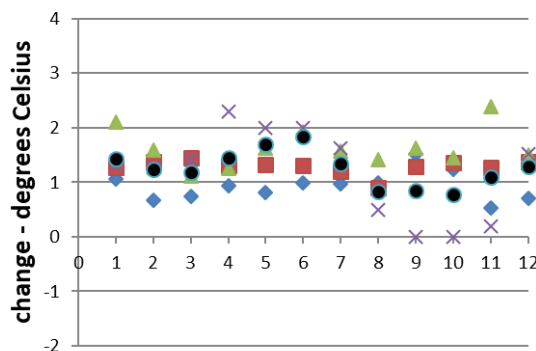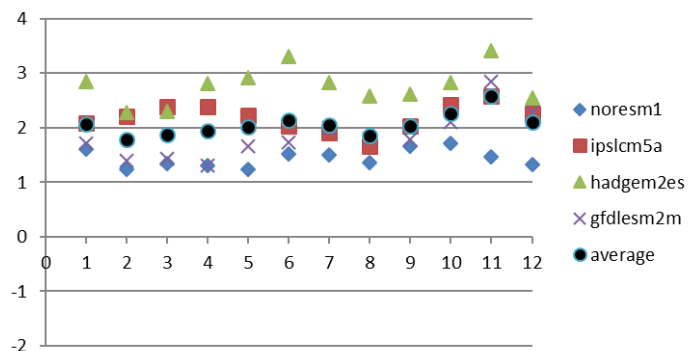## Change in temperature RCP8p5 2050

Figure 3.8 Projected change in temperature for 2030 (left) and 2050 (right) for RCP8p5 for the selected GCMs indicated in different colours and the ensemble mean change (black dots).

3.3.2 Projected change in monthly precipitation

The changes projected by the individual GCMs for precipitation show a very mixed signal. The main signal we see is a projected likely decrease for September to November by 2050 of up to ~40%. There are indications of precipitation increases (~10 to 20%) for at least February. These projections are in line with Price et al. (2017). By 2030 the projected changes as well as the variation for the GCMs is still smaller. Largest decreases for 2030 can be found for the months December and January. As a result of this analysis we now have spatially varying projections that can be used to prepare the input for the future scenario runs with the hydrological model.
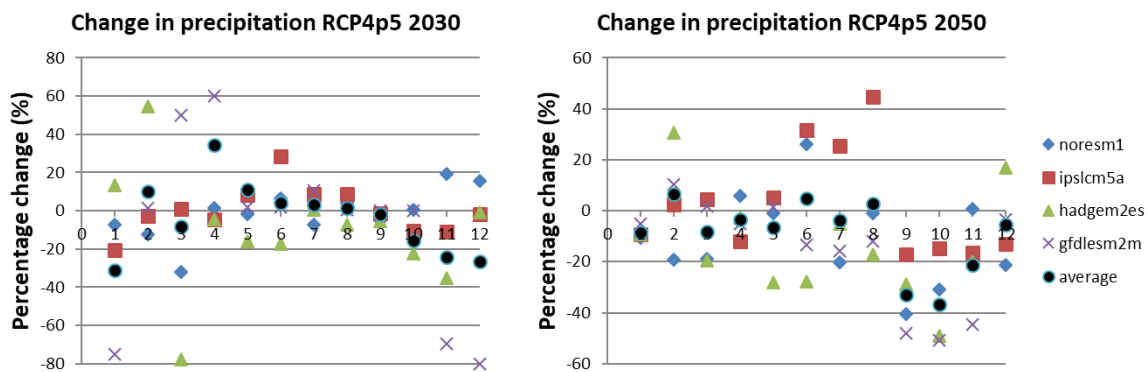
Figure 3.9 Projected change in precipitation for 2050 for RCP4p5 for the selected GCMs indicated in different colours and the ensemble mean change (black dots).
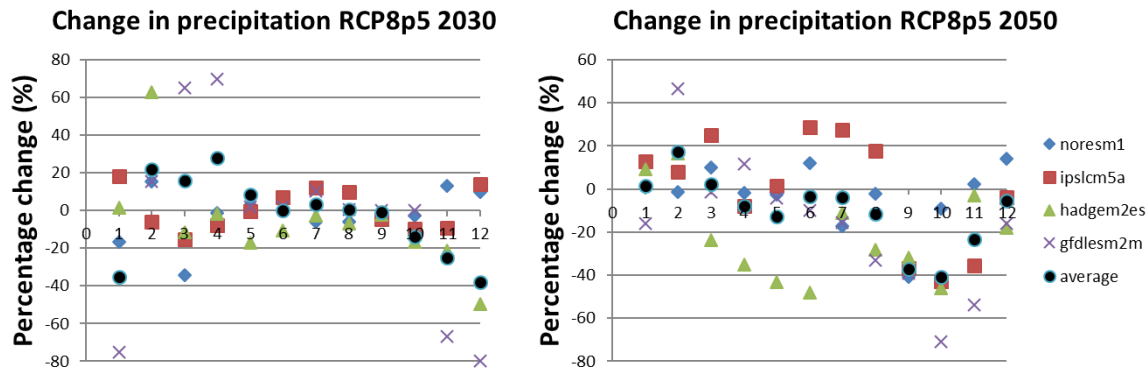
Figure 3.10 Projected change in precipitation for 2050 for RCP8p5 for the selected GCMs indicated in different colours and the ensemble mean change (black dots).

Because both for temperature and precipitation we see similarities between the changes projected by the individual GCMs we decided to work with the ensemble mean projected changes. We obtained 4 different future scenarios. A number that is still feasible to handle for the hydrological simulations. We focus on the years 2030 and 2050 and for both time horizons we consider RCP4p5 and RCP8p5. For precipitation this results in the mean projected changes displayed in Figure 3.11. Figure 3.11 shows that for October to December there is a high likelihood of precipitation decreases. For the months March to August, that covers a large part of the dry season, the variability between the climate models is large. And although the scenarios we use for 2050 for RCP4p5 and RCP8p5 mainly project decreases it should be considered that small increases in precipitation may occur as well.

Figure 3.11 Historical and future monthly precipitation for the Marromeu complex.

3.3.3 Projected change in seasonal rainfall amounts

For all individual seasons the average change in rainfall was assessed. For both the near (2030) and far (2050) future all GCMs and both RCPs were grouped to estimate projected change including the uncertainty range, following the same app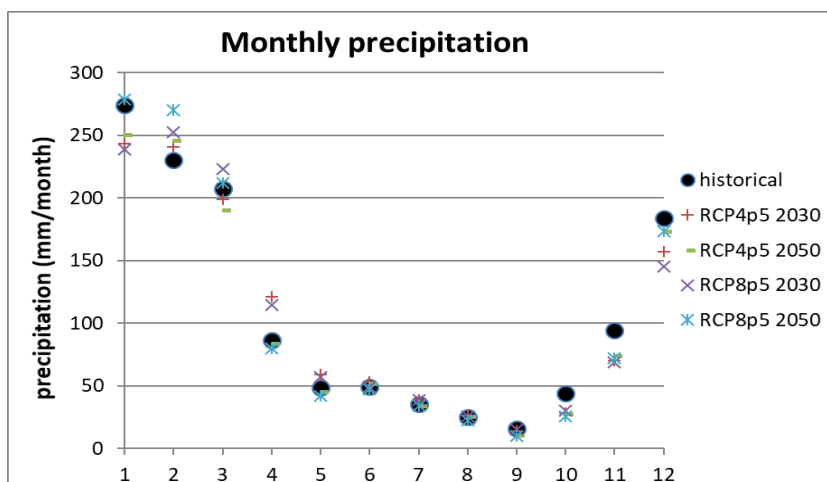roach as Lesk et al. (2017) implemented for the Kafue basin. The full range (grey line) includes all projections and is thus including possible outliers. For the green line the most extreme projected increases and decrease is excluded. The confidence on this projected range (green) is higher and the discussion of results will focus on the green range only.

By 2030 decreases in rainfall are likely for all seasons except for the dry season where increases and decreases are equally likely. Absolute dry season rainfall amounts are already small for current climate conditions. The decrease of rainfall could especially be large (-11 to -46 %) for the pre-rainy season. This is the time of the year where the conditions in the complex are driest. For 2050 the range of projected change, and thus the uncertainty increases. For the pre-rainy, post-rainy and dry season decreases seem more likely and these can be over -50%. Increases in rainfall could also occur for the pre-rainy (+ 11%) and post rainy (+ 8%) season, providing another scenario to be considered. For the rainy season the range of projected changes is small (-5 to +4%) and increases and decreases seem equally likely.
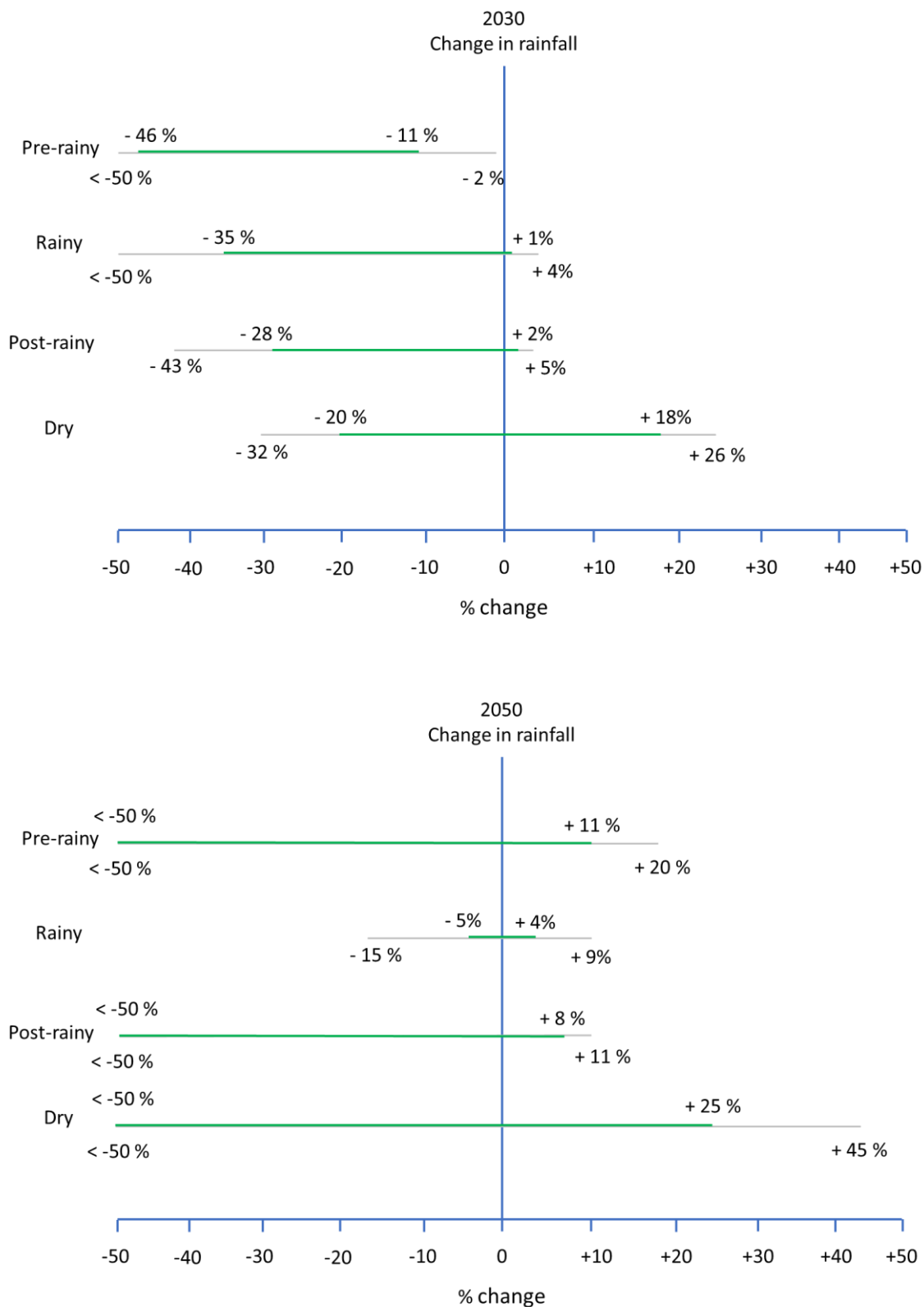
Figure 3.14 Projected range of change in seasonal rainfall for 2030 (top) and 2050 (bottom)

3.3.4   Projected change in length of dry period
The impacts of droughts are worst when the length of the dry period is long. Here we assessed whether the length of the dry period could potentially increase in the future. To assess the length of the dry period we calculated 5-day precipitation sums and assumed that a drought has come to an end when over a period of 5 days the precipitation is more than 20 mm. The data from the 4 GCMs was pulled together for the historical period and the 4 future scenarios. From each GCM time-series we calculated the length of the dry period for the historical period, 2030 and 2050. The box-plots that were constructed based on this data are shown in Fig. 3.12.
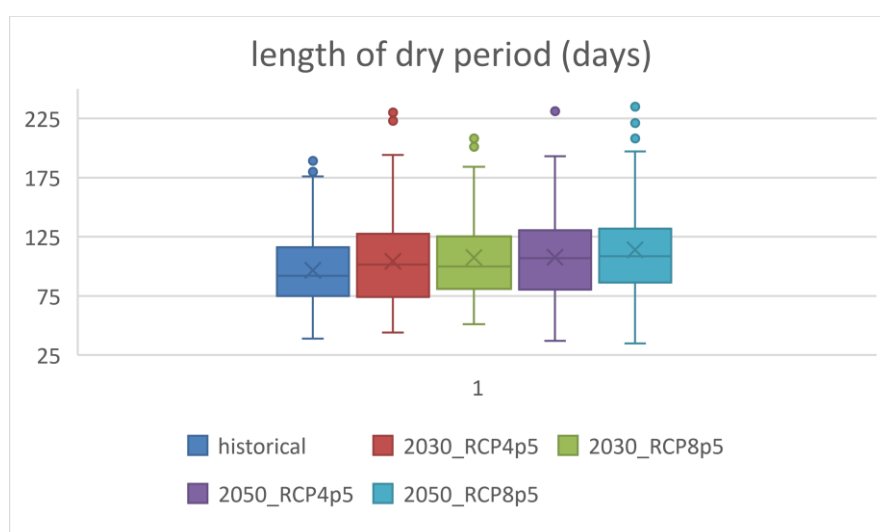
Figure 3.12 Box-plots of the length of the dry period for the historical period and the future pathways RCP4p5 and RCP8p5 for the time horizons 2030 and 2050.

The boxplots include all GCM data we have available for this assessment and therefore provide a reliable estimate with realistic uncertainty bounds. The GCMs indicate a likely tendency towards a small increase in the length of the dry-period as this is projected for both future time horizons and both climate change scenarios. The projected changes in dry period duration is from on average 96 days historically to 113 days in the far future under the worst-case scenario, RCP8p5. In the future the inter-annual variability may increase as well – this increase can only be clearly found for RCP4p5. This indicates that there will be years with shorter dry periods than previously observed and there will also be years with longer dry periods for which adaptation strategies should be prepared.

3.3.5 Projected change in the start of the rainy season

To assess the potential change in the start of the rainy season the rainfall of October and November was analysed. The following criteria were used for the definition of the onset:

•   The average 5-day rainfall sum of the days before this day was below 5 mm
•   The average 5-day rainfall sum of the given day is higher than 20 mm

These criteria make sure that there was a long period of very little rain in advance of the start of the rainy season, while the rainfall amount of the given day is much higher. The results are displayed as bar charts in Fig. 3.13. The number zero at the x-axis corresponds to the first day of October, the start of the pre-rainy season. The number 61 corresponds to the 30th of November after which the rainy season starts. To include as much information as possible the 30 year periods for all GCMs were included in the analysis. For the historical period the start date varies between the first of October and the beginning of December, yet there is a stronger tendency towards the end of October / beginning of November. For the future scenarios the rainy season start can still vary between the 1st of October and beginning December similarly to what has been observed in the past. However, in the future the variation seems to be larger, a start at the beginning of October could be equally likely to a start in the beginning or halfway November. The uncertainty tends to increase. For Rcp8p5 a late start after the 10th of December is more likely than for RCP4p5, but still only occurs for a few years.
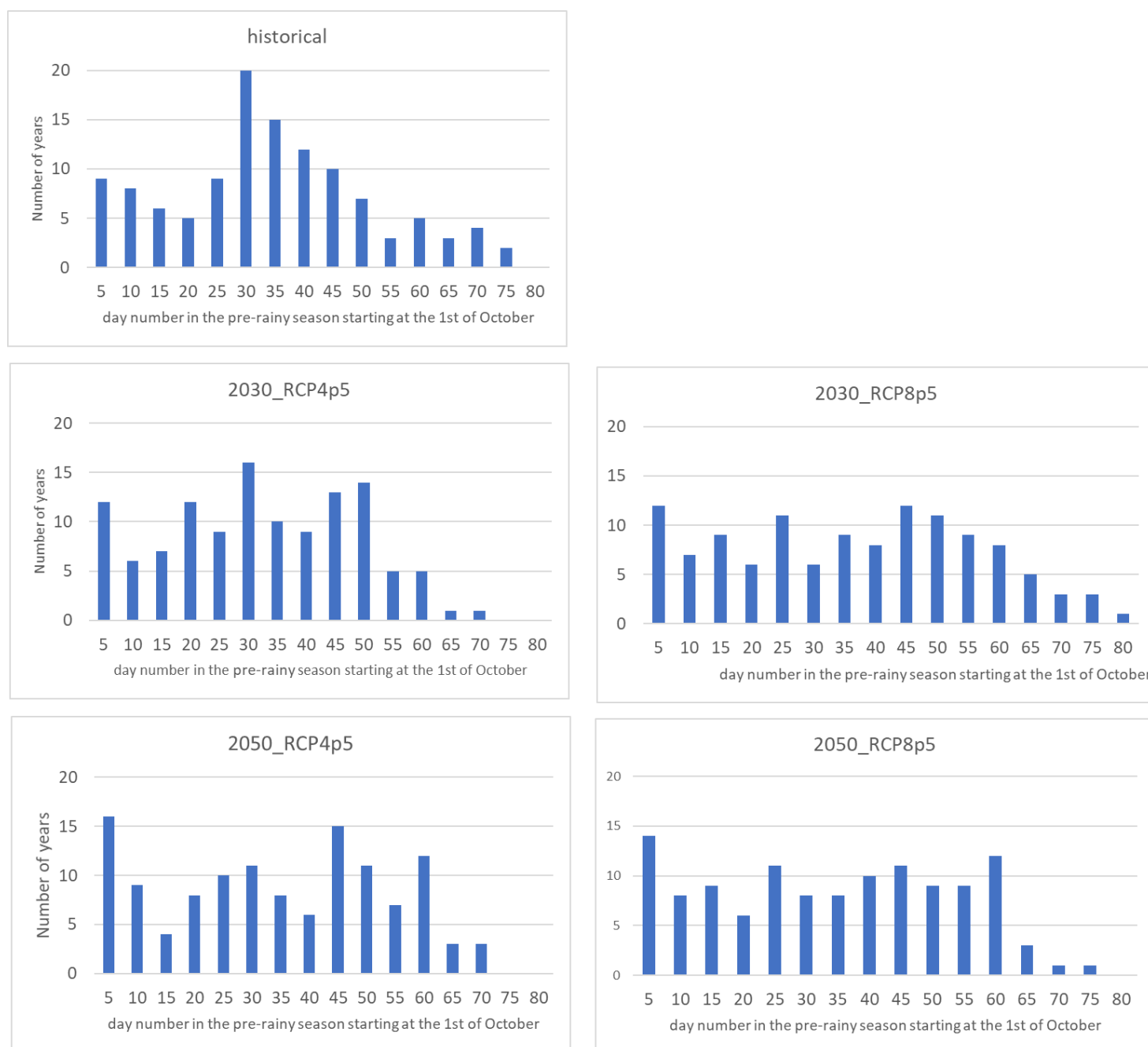
Figure 3.13 Histogram of the occurrence of the start of the rainy season in one of the 5-day intervals in the pre-rainy season, starting at the first of October (day = 1) and ending at the end of November (day = 61). The number of years correspond to the number of years in the 30-year periods taken from all 4 GCMs. For the historical period (top), near future (middle) and far future (bottom) for both RCP4p5 (left) and RCP8p5 (right).

3.4 Future changes in hydrological conditions

3.4.1 Spatial changes in precipitation and evaporation
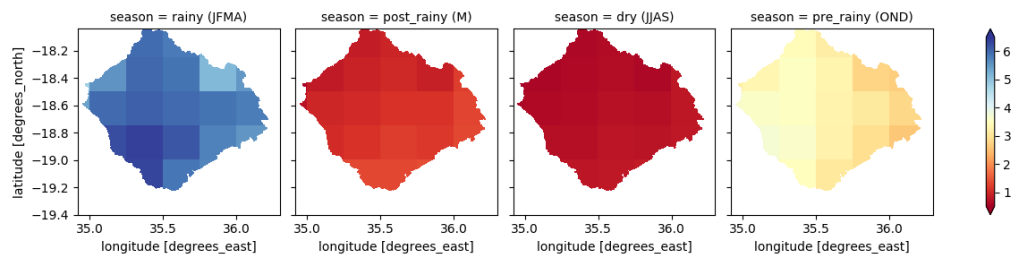
Figure 3.15 Mean daily precipitation (mm/d) during historical period per season

Figure 3.16 Changes in mean yearly precipitation (%) for the different scenarios relative to historical precipitation (1979-2014) for the different seasons

The maps in Figure 3.15 show mean daily precipitation for the historical period for the rainy season (January to April), the post-rainy season (May), the dry season (June to September) and the pre-rainy season (October to December).The maps in Figure 3.16 display the projected changes in precipitation over the Marromeu complex for the individual grid cells of the bias-corrected GCM data used. Overall annual precipitation decreases in each sc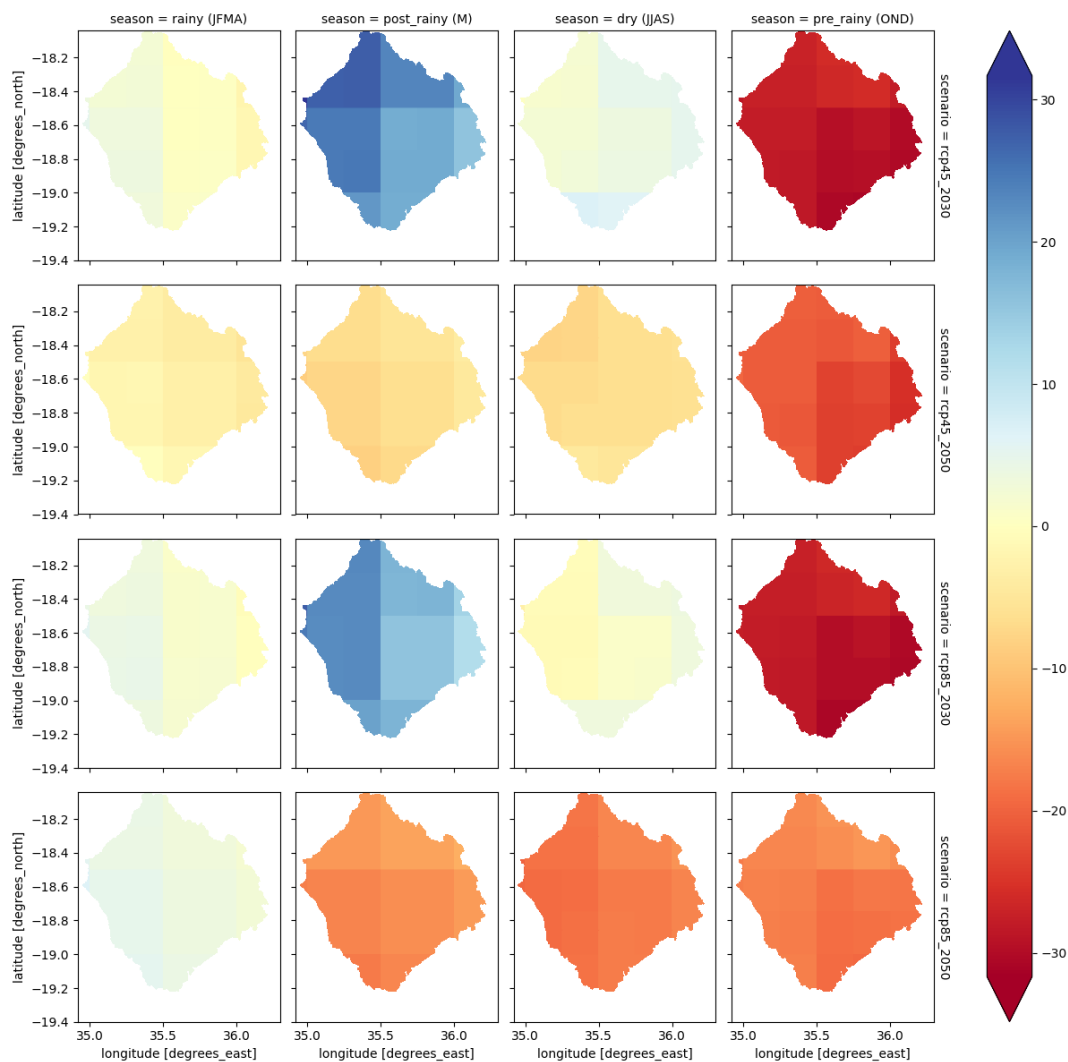enario. The largest decrease occurs for RCP4.5 2050, the smallest decrease occurs for RCP8.5 2050 this is mainly a result of precipitation increases in the wet season. Precipitation decreases in the pre-rainy period in each scenario over the entire study area. Both far future scenarios show a decrease of precipitation from May to December, while the near future scenario shows an increase in precipitation in the post-rainy period.

Figure 3.18 shows that potential evaporation will increase in each scenario and each season. The largest increase occurs for RCP8.5 2050. As expected increases in potential evaporation are in line with the projected temperature increases. The combination of a decrease in precipitation in the dry season and an increase in potential evaporation will result in drier conditions in the future.
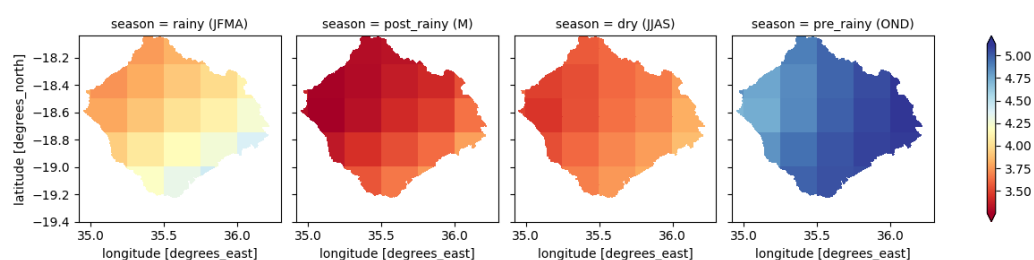

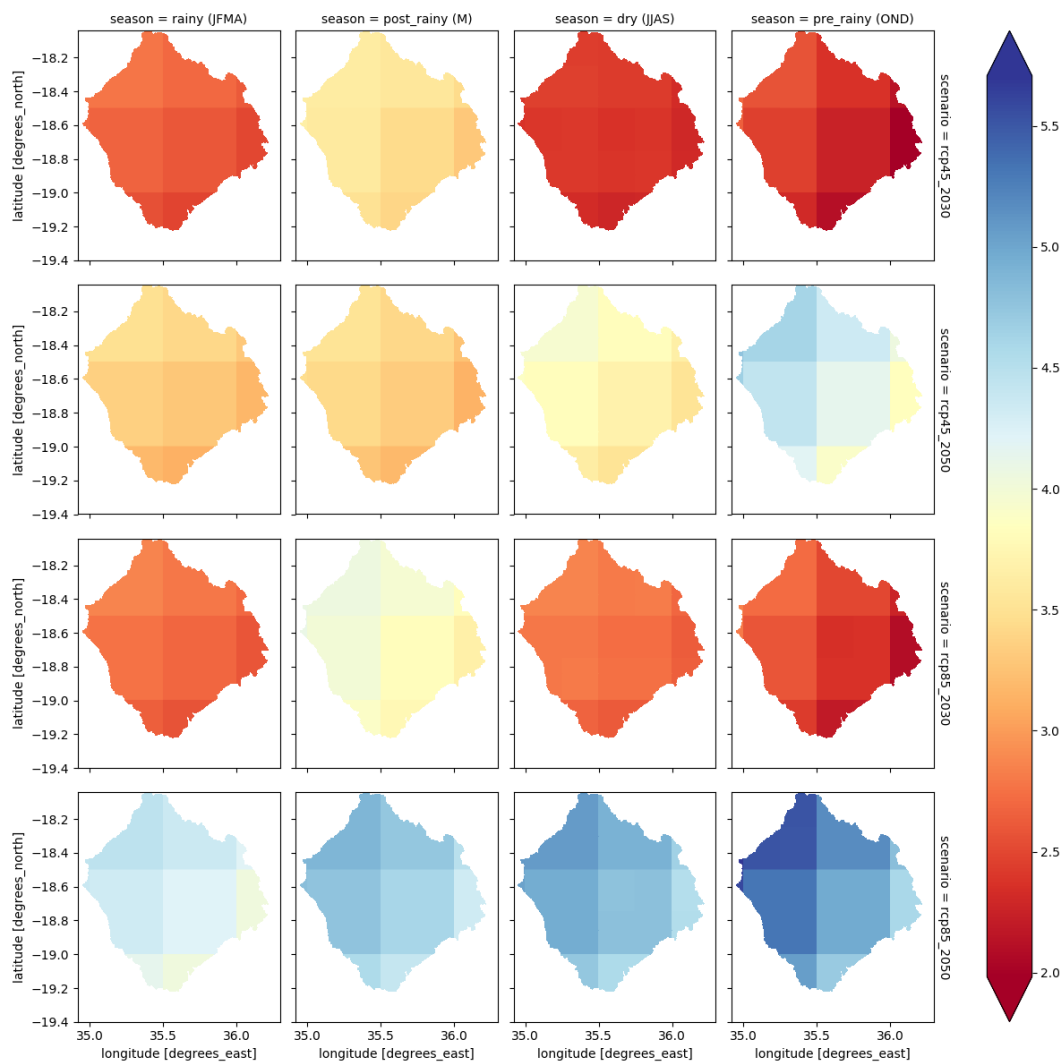*Figure 3.17 Mean daily potential evaporation (mm/d) during historical period per season*

Figure 3.18 Changes in mean yearly potential evaporation (%, derived from MSWEP temperature data) for the different scenarios (rows) relative to historical potential evaporation (1979-2014) for the different seasons (columns)

3.4.2   River flow → indicator of surface water availability
The remainder of precipitation that does not evaporate, that is not stored in vegetation and does not infiltrate into the ground becomes runoff. The runoff from all catchment cells flows to the river and is from there routed downstream as river flow. We analyzed the river discharge for all catchments at a location chosen downstream in the river. We use the difference between historic and future modelled river flows is an indicator of future fresh water availability. Changes in river discharge projected by the 4 scenarios for catchment Area 3 (one of the larger catchments see for the exact location Fig. 3.1) are shown in Figure 3.19 together with the absolute discharge amounts. The scenarios show a decrease of runoff from October to January for all scenarios., RCP 8.5 2050 is the only scenario with an increase in runoff during the wet period (Feb-March). It is also visible in the spatial variations (Figure 3.20). For the near future runoff in the period March to July is higher than previously while for the far future runoff decreases are projected for this period. Although decreases are projected for the period June up until October the absolute discharge is very low in this period and changes are negligible. In Appendix B we have included discharge graphs for all five sub-catchments in the complex. The change signals for the catchment 2 to 5 are similar with decreasing runoff from October to January and a possibility of an increase in wet season runoff according to only one of the scenarios. For catchment 1, the smallest catchment in the Eastern corner next to the sea there is a likely discharge decrease nearly throughout the year. This catchment is not influenced by the mountain range, in addition precipitation increases over this area are projected to be smallest compared to the other catchments (see Fig. 3.16). Because of the limited variation between the catchments and the relatively small size of catchment area 1, we focus the analysis of monthly time-series in graphs on Area 3. The discussion of the results can be extrapolated to catchment 2 to 5. In catchment 1 the decreases in discharge, groundwater level and soil moisture will be larger and thus the fresh water availability will be lower.

Figure 3.20 shows the rivers with an average discharge of more than 0.1 m³/s for the historical period and the different scenarios for all seasons. A decrease of flowing river extents is observed in the drier seasons and the more extreme scenarios.

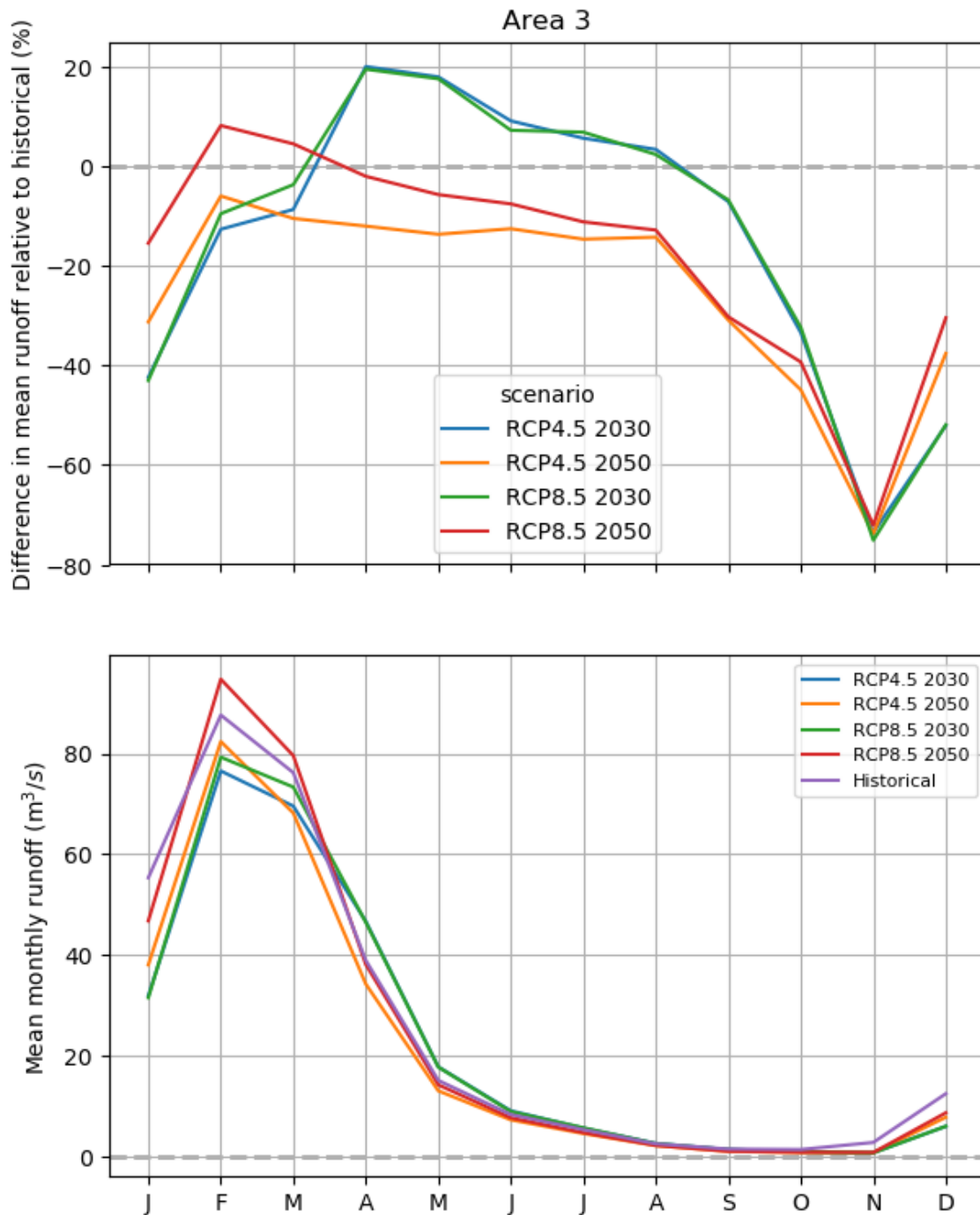*Figure 3.19 Top: Changes in mean monthly runoff (%) for the different scenarios relative to the historical model run in catchment area 3, below: mean monthly discharge (m³/s) for the different scenarios and historical period*
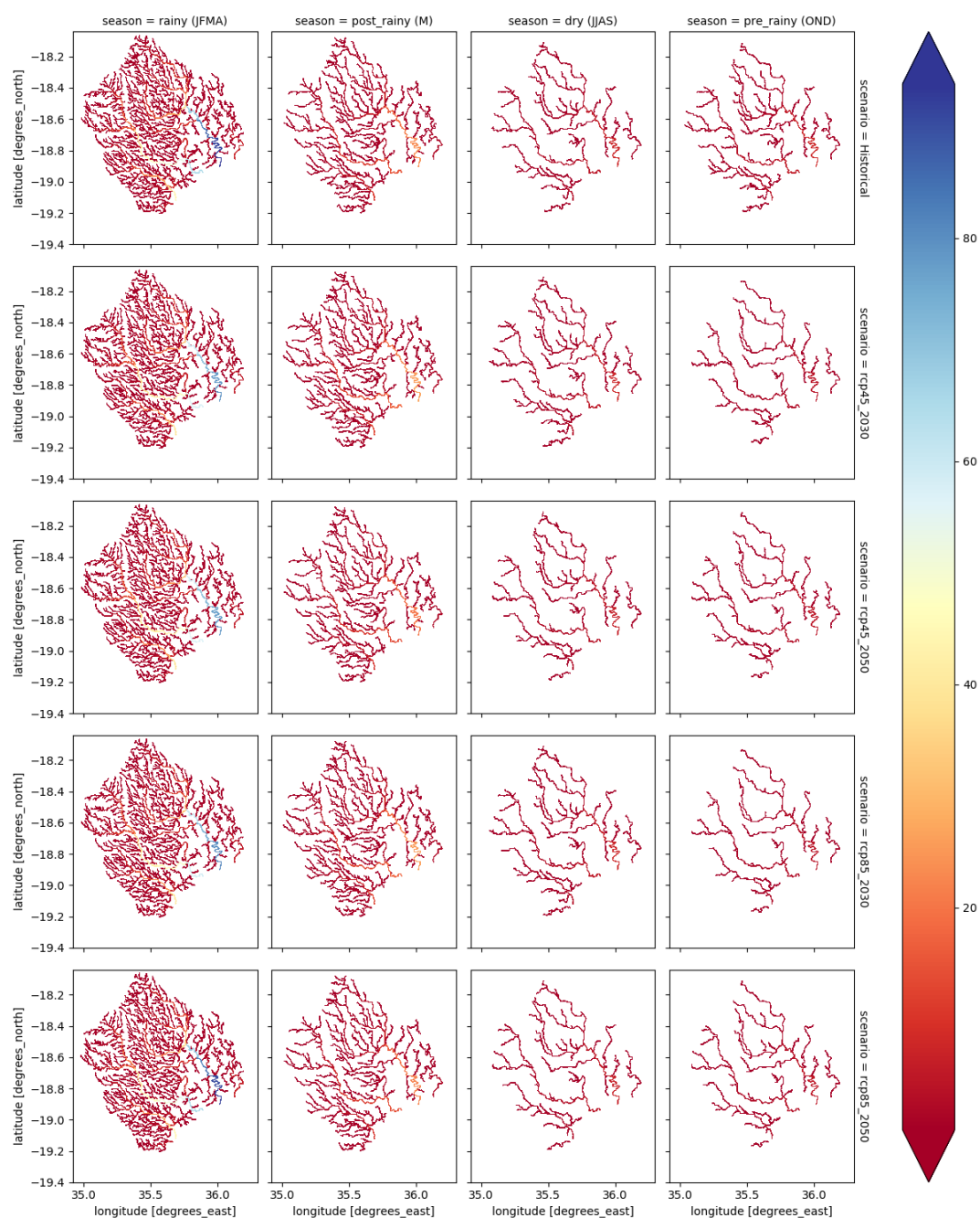
Deltares

Figure 3.20 Mean daily discharge (m³/s) for the historical period (upper row) and the different scenarios (lower 4 rows) for the different seasons (columns) for the Marromeu Complex.

The changes in lowest discharge (5th percentile) and highest discharge (95th) percentile have also been assessed for catchment area 3. The 5th percentile discharge refers to the discharge of the dry season. Figure 3.21 shows for Area 3 that the lowest discharges will likely decrease with 30 to 40 %. Yet, even under the historical climate conditions the river discharge is (close to) zero. High flows will likely decrease, Only RCP8p5 projects minor increases for 2050.
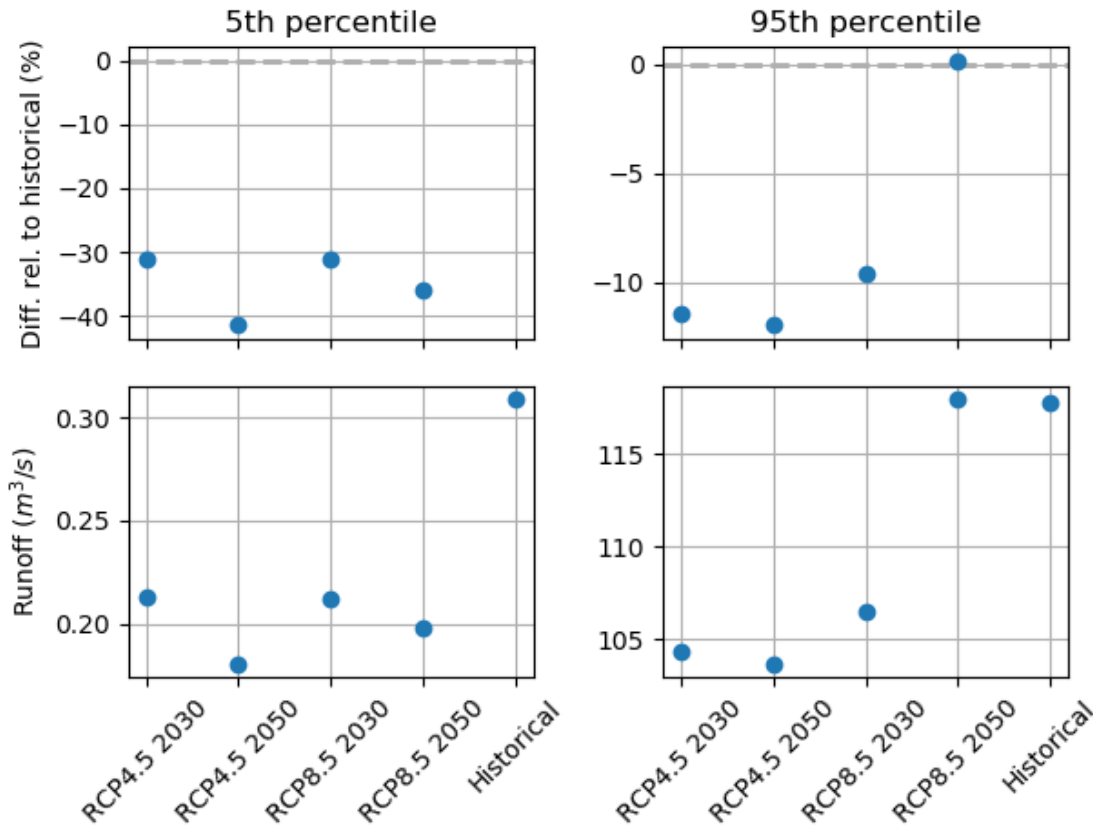
Figure 3.21 Top: changes in extreme values (5th and 95th percentile) for the different scenarios. Below: absolute values of 5th and 95th percentiles for the different scenarios

3.4.3 Groundwater levels

Groundwater levels are calculated by the wflow-sbm model, however it should be noted that these values could not be validated with measured data and that they are therefore highly uncertain. Groundwater depths mainly decrease during the rainy season for all scenarios, except RCP8.5 2050. Here we have included as additional area for analysis Area 6 because groundwater is not necessarily bounded by catchment boundaries. In addition large irrigated areas are located here. In March in Area 6, groundwater levels decrease with an average of 13 cm. At the end of the dry season (in September), the difference is about 4 cm on average.

Figure 3.22 Top: Changes in mean monthly groundwater level depth (%) for the different scenarios relative to the historical model run in areas 3 and 6. Below: mean monthly groundwater depth (cm) for the different scenarios and historical period (cm below surface)

3.4.4 Groundwater recharge → Indicator of change in groundwater availability for use

Groundwater recharge is the amount of water that percolates through the soil to the groundwater and herewith replenishes the groundwater reservoir. Within the Marromeu complex groundwater is used for irrigation water, drinking water and groundwater levels are important to maintain the complex specific vegetation. To sustainably use the groundwater, annual recharge should be in line with the annual use. We cannot estimate the actual groundwater use but we can assess whether the replenishment decreases. Figure 3.23 shows the area average change in groundwater recharge for the catchment area 3 and area 6. In the latter area we expect the most irrigated agriculture to be located.

Groundwater recharge decreases for all scenarios except for RCP8.5 2050. The decrease is largest after the dry period (more than 50%), especially in area 6. Since problems with groundwater salinization have already been observed, especially near the large scale sugar cane production site, groundwater abstractions should be regulated.

The spatial variability of groundwater recharge for the historical period and the scenarios is shown for the different seasons in Figure 3.24 where we see that recharge takes place during the wet season and will likely decrease according to most scenarios, except for RCP8.5 2050.

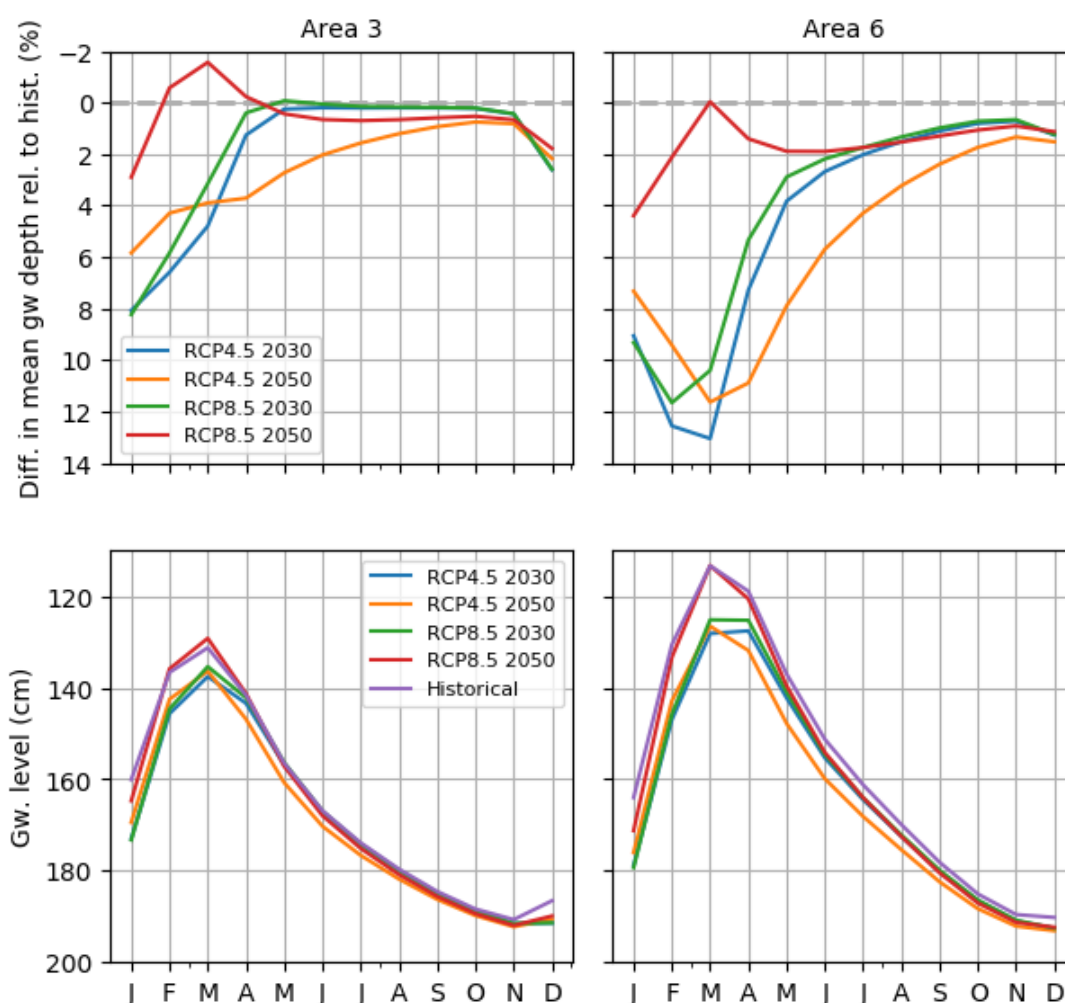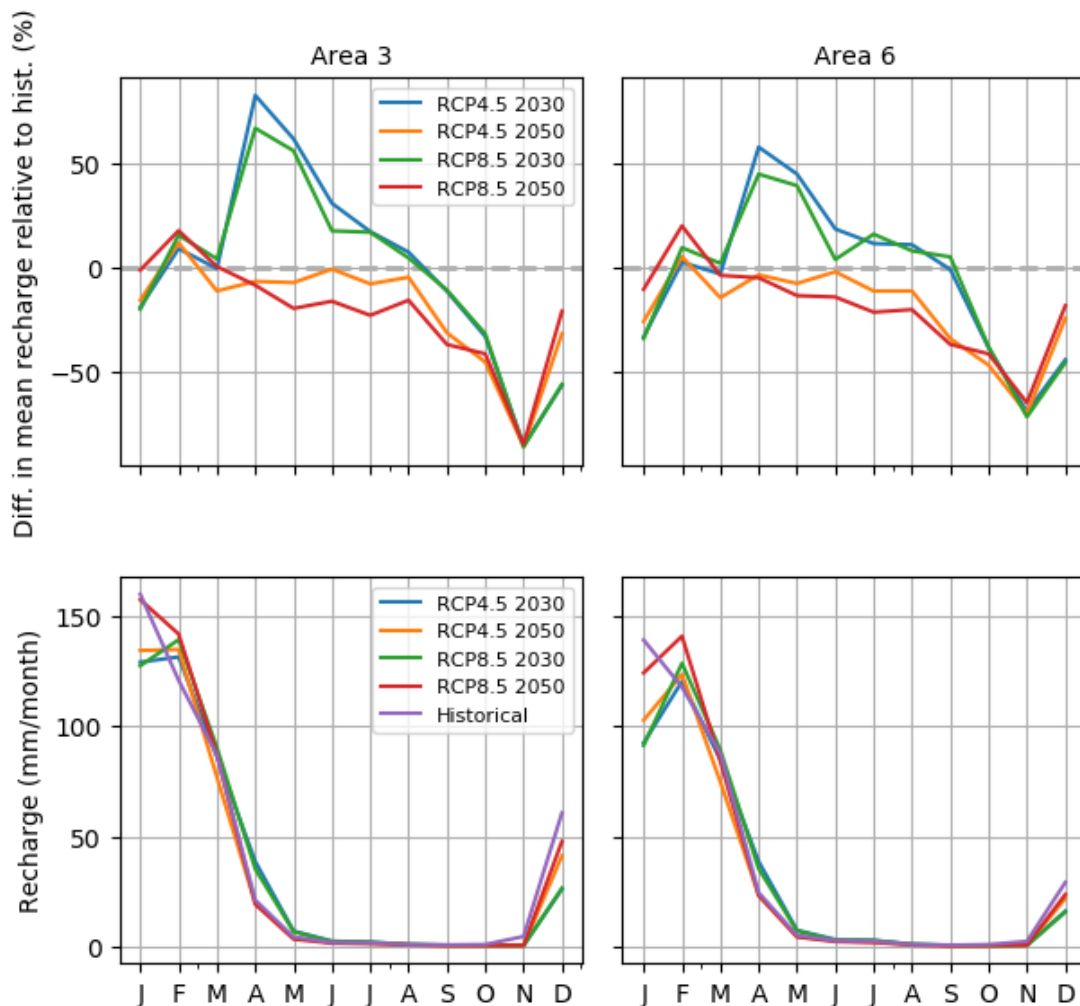*Figure 3.23 Top: Changes in mean monthly recharge (%) for the different scenarios relative to the historical model run in areas 3 and 6. Below: mean monthly recharge for the different scenarios and historical period*
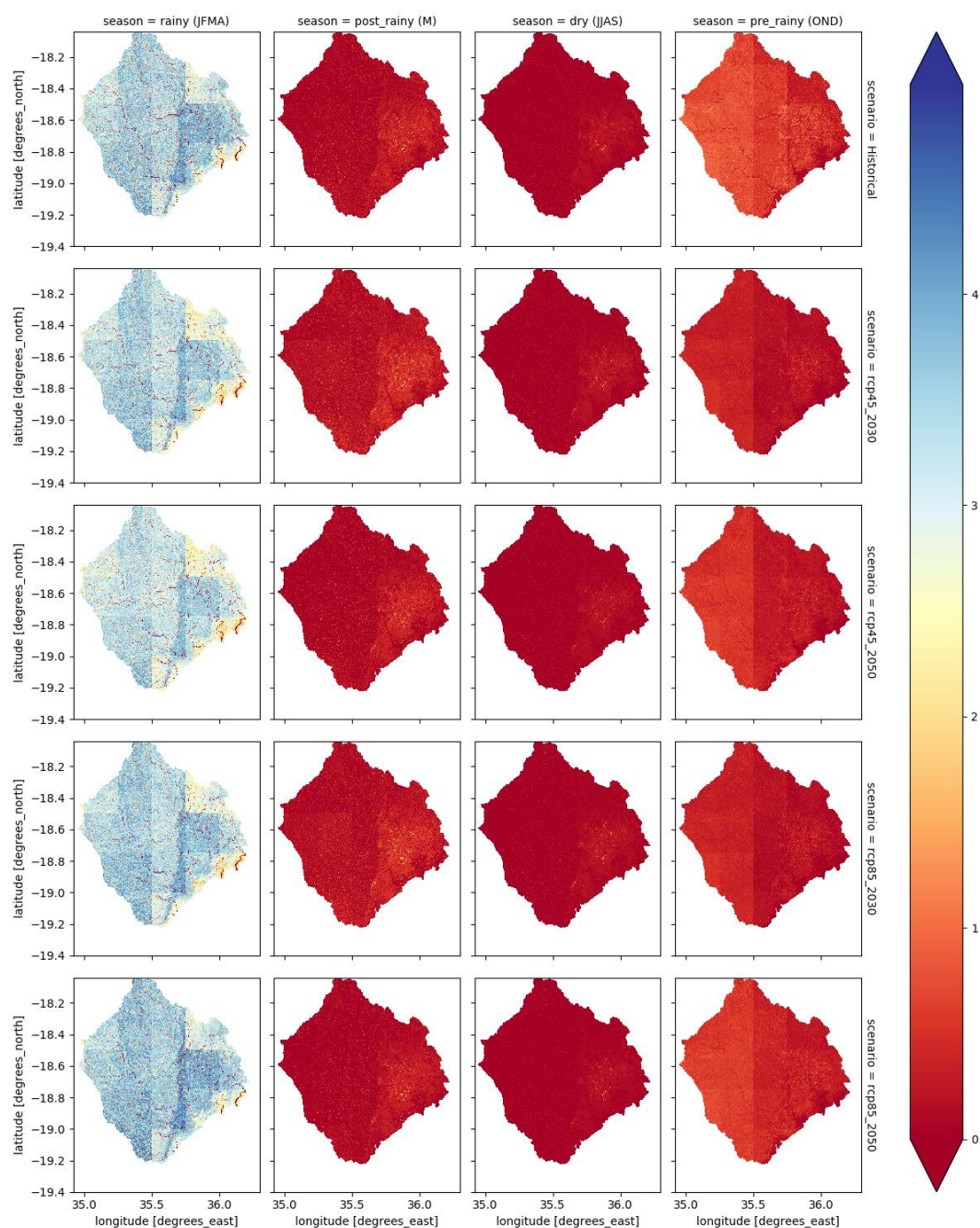
Figure 3.24 mean daily recharge (mm/d) for the historical period and the different scenarios for the different seasons

3.4.5   Evaporation deficit → Indicator of drought and irrigation need
Evaporation deficit is the difference between potential and actual evapotranspiration for a given crop and a deficit can limited crop growth or lead to crop losses. Potential evaporation indicates how much water would be evaporated by a crop under perfect growing conditions, i.e. assuming no limitations on water availability. Actual evaporation quantifies the actual amount of water evaporated and is (nearly) always lower than potential evaporation due to limited water availability for the crop. The difference is an indicator of the severity of droughts. But even more important, it is an indicator of the need for irrigation, whereas the reduction in fresh water availability shown in the past paragraphs are an indication that further restrictions on irrigation may be needed in the future dry seasons. According to the FAO cropping calendar, irrigation of rice and sugarcane occurs at the end of the dry season (November and December) and might require up to 15% more water during extreme conditions due to the increased evaporation deficit of the studied scenarios.

The evaporation deficit for the historical period and the different scenarios was calculated per month using the monthly mean potential evaporation (Ep) and actual evaporation (Ea):

Storage deficit = Ep – Ea (mm/month)

The relative change of storage deficit compared to the historical period was calculated following:

$$Relative\ change\ (\%)\ \ = \left(\frac{E_{P,\ mean\ monthly,\ scenario} - E_{a,\ mean\ monthly,\ scenario}}{E_{P,\ mean\ monthly,\ historical} - E_{a,\ mean\ monthly,\ historical}} - 1\right) * 100$$

The graphs in Figure 3.25 indicate an increase in the highest evaporation deficit (95% value). The lowland area and the agricultural area in the east are especially affected (area 6 compared to area 3). The increase in evaporation deficit is large and further increasing after the dry season and in the months March, April and May.
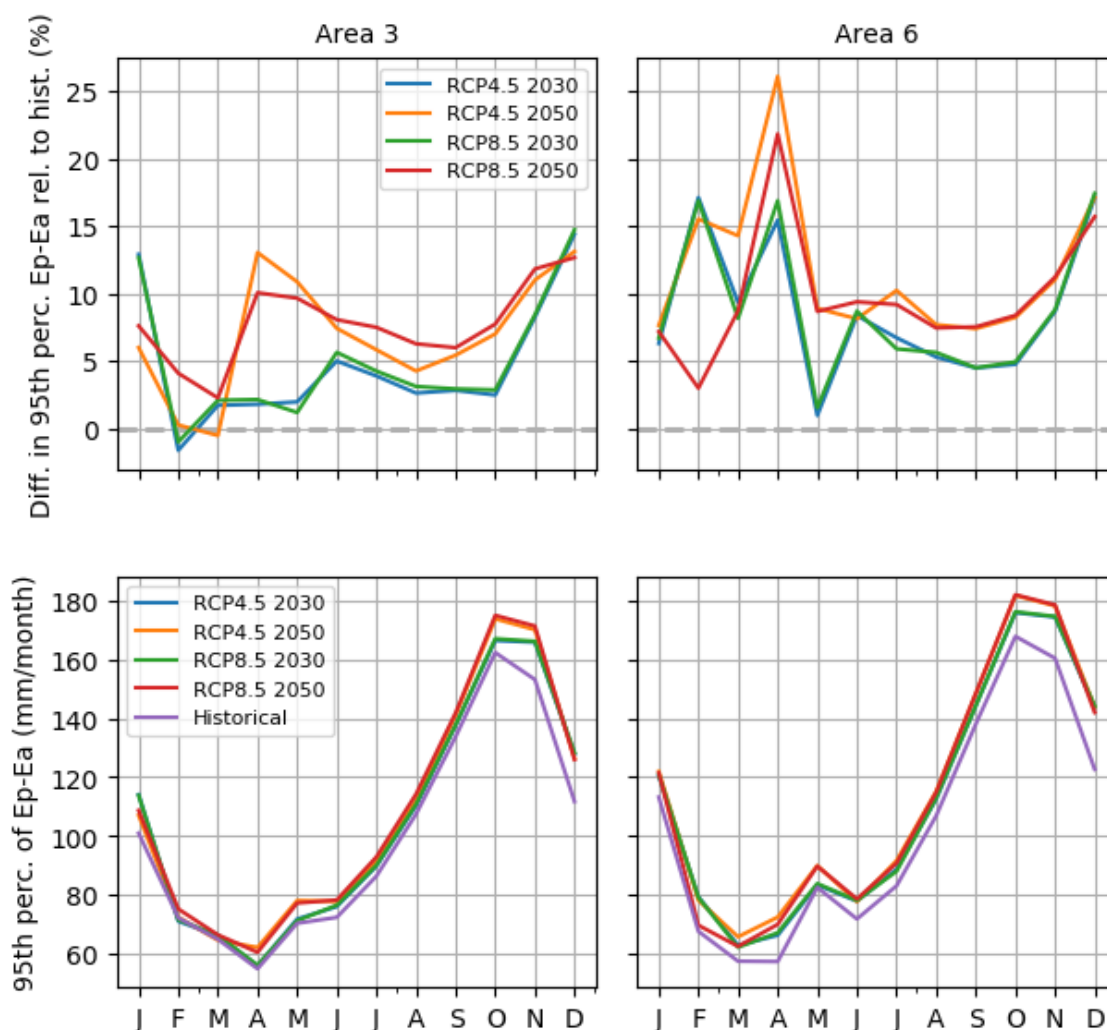
Figure 3.25 Top: Changes in the 95th percentile of the difference between potential and actual evaporation (%) for the different scenarios relative to the historical model run in areas 3 and 6. Below: 95th percentile of the monthly difference between potential and actual evaporation for the different scenarios and historical period

The evaporation deficit increases mostly in the pre-rainy season (October to December) over the entire study area for all scenarios compared to the historical situation, as also shown in Figure 3.26.
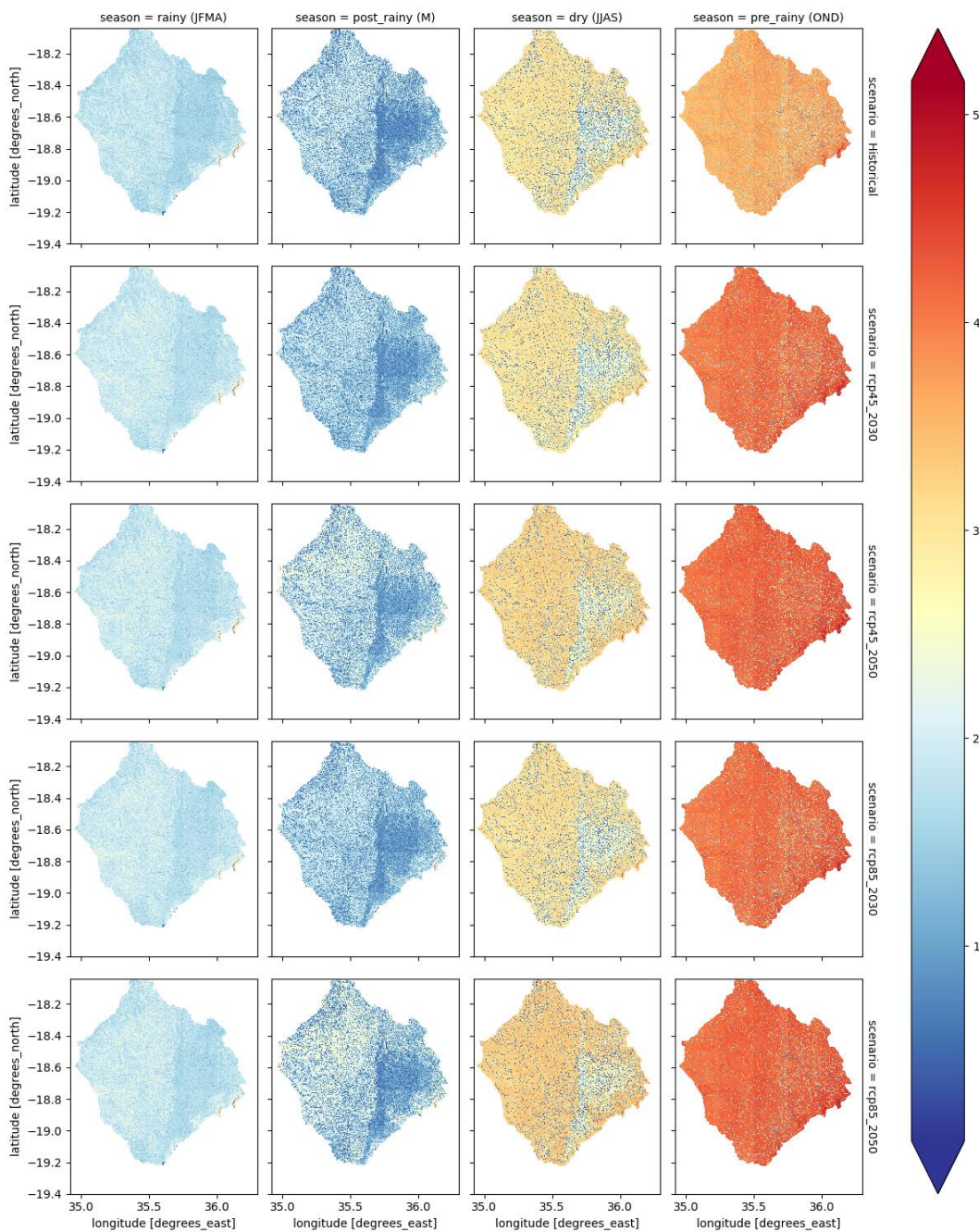
Figure 3.26 Mean evaporation deficit (potential evaporation minus actual evaporation) for the historical period and the different scenarios (rows) and the different seasons (columns).

3.4.6 Soil moisture → Indicator of the severity of the drought conditions

Using the hydrological model we have assessed the potential future changes in soil moisture conditions. With decreasing soil moisture the crop yield and productivity will also decrease. In addition, natural vegetation is expected to degrade with decreasing moisture conditions possibly leading to limitation of vegetation for food for wildlife. In addition, the infiltration capacity could potentially decrease as a result of drier soils affecting natural vegetation

The graphs in Figure 3.27 clearly indicate decreases in soil moisture conditions, nearly throughout the year. Again we see strong decreases for October and November.
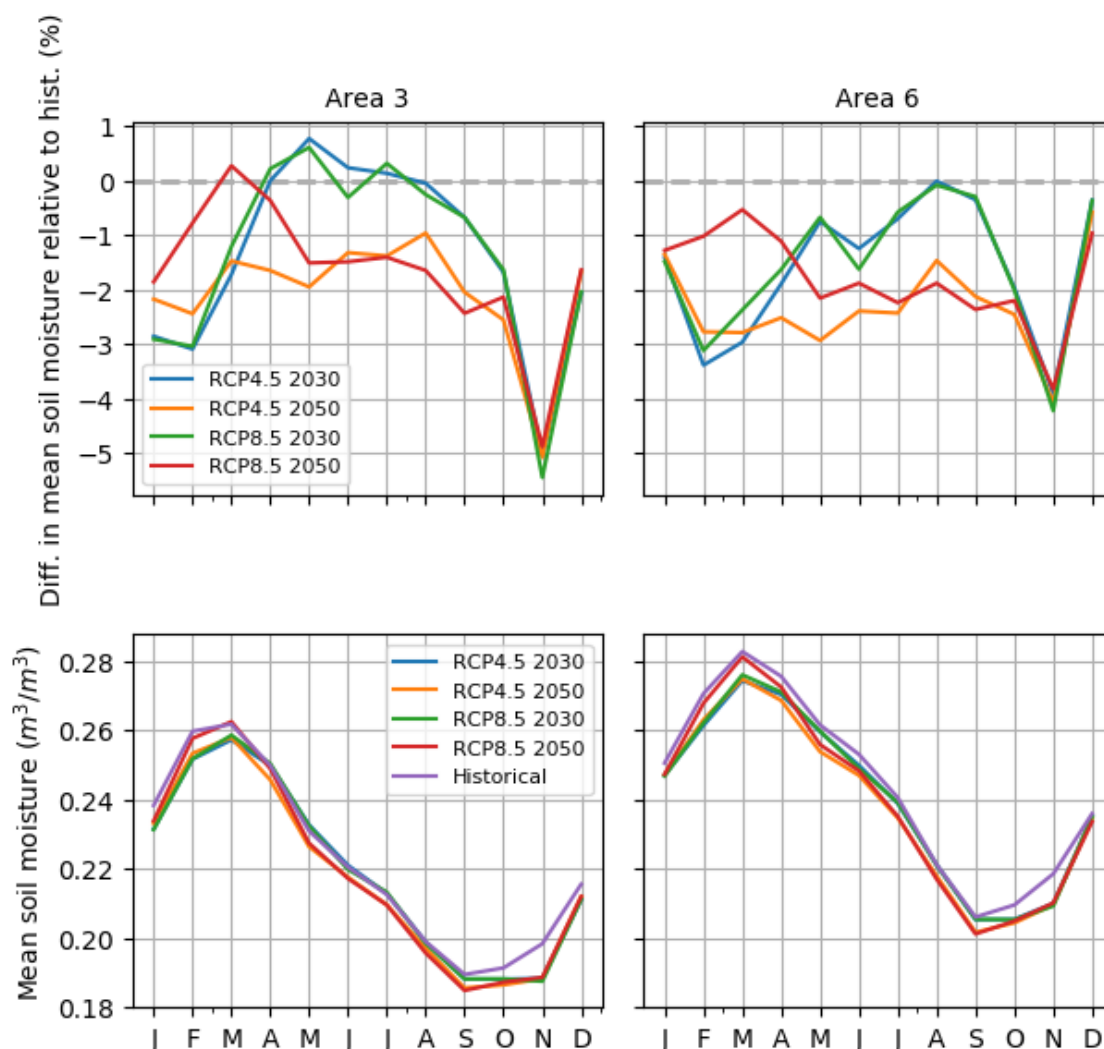
Figure 3.27 Top: Changes in mean monthly soil moisture (%) for the different scenarios relative to the historical model run in areas 3 and 6. Below: mean monthly soil moisture for the different scenarios and historical period

In an earlier study on the Marromeu complex by IHE (IHE,2014) the presence of signs of karstic erosion along the Cherringoma escarpment for almost its entire length from South-West to North-East was mentioned. An analysis was made of the satellite-based soil moisture product to investigate the likely emergence of karstic waters at the foot of the escarpment. Unfortunately, this cannot be identified from the available data, the analysis is included in Appendix C.

3.4.7   Changes in river discharge Zambezi → potential inflow to Marromeu Complex
The Zambezi used to supply water to the Marromeu complex through the Salone River. The development of infrastructure and dams in the Salone River has led to a disconnection of the complex from the Zambezi River and herewith the freshwater influx has been severely reduced.

In addition, the construction of the Cahora Basa dam in the Zambezi upstream of the complex has altered the flow regime of the river. The seasonal variation of the river has decreased and thus the peak flows that were the main source of inflow to the Salone have become less high. Amit Singh (2017; collaboration between IHE and Deltares) investigated the influence of the Cahora Basa dam on the discharge seasonality of the Zambezi. They investigated the water level data for Tete and Caia and found that after the construction of the dam there was a 60 – 80 % increase in dry season water level and 20 – 40 % reduction in wet season water levels. At Tete, the timing, duration, magnitude and frequency of the water level has been significantly altered. Given that no significant changes were found in the precipitation, the changes in water levels of the lower Zambezi River can be attributed to the dam operations at Cahora Bassa.

The figure below illustrates these changes best. It displays the water level statistics for Tete station. The timeseries have been divided into pre-regulation (1955-1974), the period needed for the reservoir to become fully operational (1975-1994) and the data for the period that the reservoir was fully operational (1995-2015). From the boxplots it can clearly be seen that the differences between months has decreased and flows for the months February to May have clearly become lower.
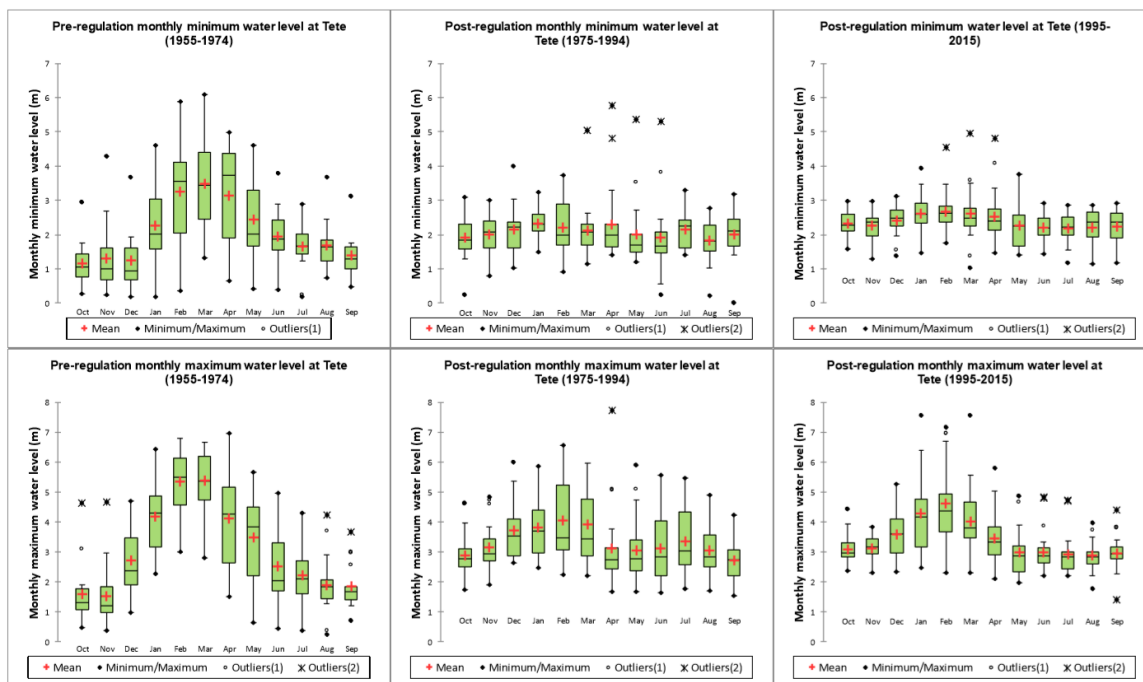
Figure 3.28 statistics of monthly minimum and maximum water levels pre and post-regulation at Tete; taken from Singh (2017).

Deltares

3.4.8 Surface water extent analysis

Figures 3.29 and 3.30 show a composite image of surface water extent based on Landsat images (provided by USGS/Google and processed in Google Earth Engine) between respectively 1998 and 1992, and 2012 and 2015. These figures depict the disconnection of the Salone River with the Zambezi River.
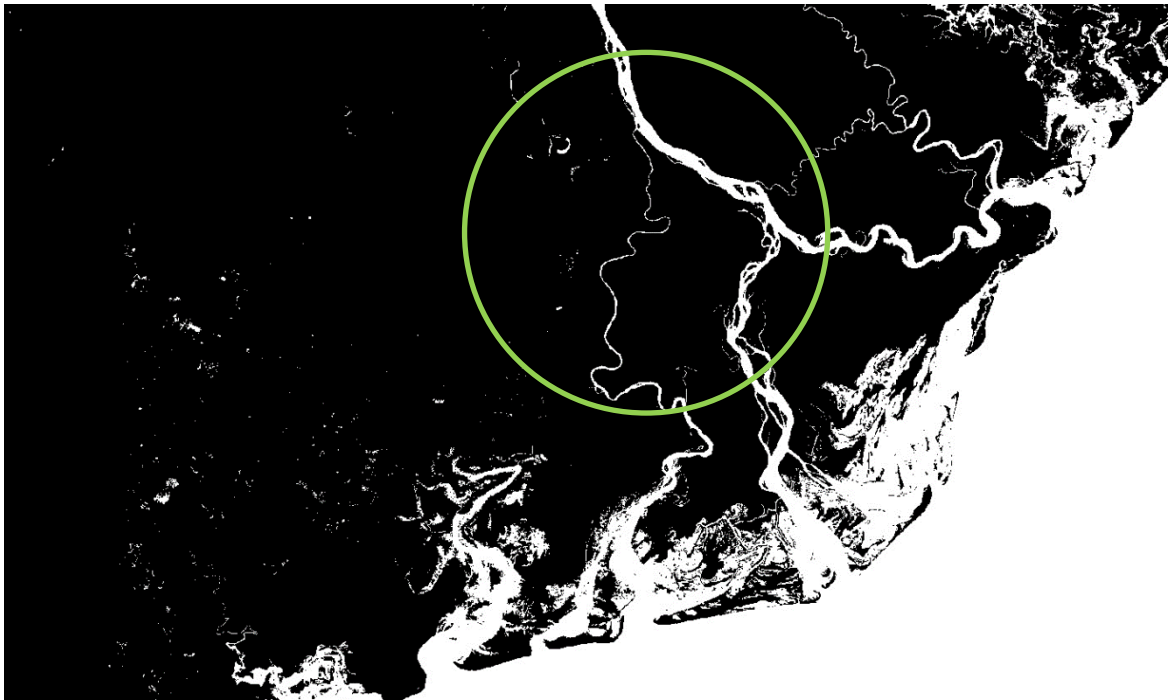
Figure 3.29 Approximation of satellite surface water extent over the period 1998-1992.
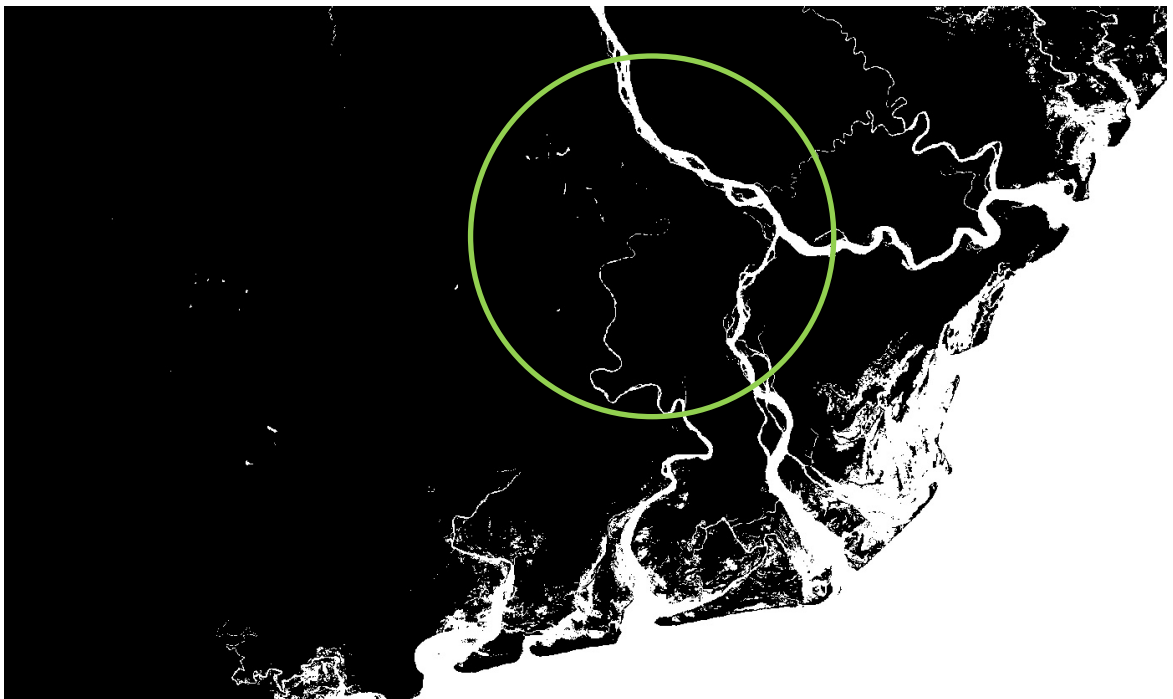
Figure 3.30 Approximation of satellite surface water extent over the period 1998-1992.

While these images can show changes in water surface extent over a long period, we are also interested in seasonal changes in surface water extent as this might provide information on connectivity of wetlands in different seasons and the temporal existence of pools that will dry-up towards the end of the dry season.

The Sentinel-1 mission, carried out by the European Space Agency (ESA), consists of a constellation of two satellites (Sentinel 1A and 1B) with on board a C-band synthetic aperture radar (SAR). The satellites were launched in 2014 and provide radar backscatter, cloud free, images of the top layer of the soil. Radar backscatter is mainly influenced by the water content through the dielectric constant, geometry and roughness of the surface, and can therefore be used for surface water extent mapping. Unfortunately, the Sentinel-1 data seemed to highly overestimate the surface water extent at the end of the dry season. This overestimation was confirmed by a comparison with optical cloud-free image of the Sentinel-2 satellite.

This implies that the Sentinel-1 data contains biases and can therefore not be used. Sentinel-2 data does not provide regular full coverage. Especially during the wet period, clouds and clouds-shadow are present in the images. Composite images would have to be obtained by using a set of images and removing the cloud disturbance. More details of the assessment are provided in Appendix D. It can be concluded that a seasonal surface water extent analysis requires more extensive and in-depth analyses to provide reliable output and this cannot be included in the current assessment.

3.4.9 Sea level rise, cyclone frequency and severity

Climate change can in principle impact both the mean sea level and the storminess (winds, rain, storm surge) of a given coastal region. One of the missions of the Intergovernmental Panel on Climate Change (IPCC) is to provide comprehensive scientific assessments on environmental consequences of projected climate changes. Their reports contain an overview on the effects of increased emissions on different environmental variables and are therefore the official source for such figures. The most recent IPCC publication is Assessment Report 5 (AR5), see IPCC (2013) and references therein. A new report with recommendations by the IPPC, Assessment Report 6 (AR6), is foreseen for 2021. In the assessment below we have therefore not only reviewed 2013's AR5 but also more recent research that will in principle be used in AR6.

3.4.9.1 Sea level rise

Projections of global mean sea level rise are given in AR5 for the four RCPs. The projections of global mean sea level rise until 2100 for these four scenarios are presented in Figure 3.31, relative to 1986–2005 (reproduced from IPCC, 2013).

The solid lines in Figure 3.31 show the median projections, the dashed lines show the likely ranges for RCP4.5 and RCP6.0, and the shading the likely ranges for RCP2.6 and RCP8.5. The figure shows a projected global mean sea level rise of between, 0.15 – 0.35 m in 2050 and between 0.30 – 1.0 m in 2100. Regionally the changes in mean sea level may differ from the global change in mean sea level, e.g. related to (changes in the) non-uniform characteristics of the earth's gravitational field. Figure 3.32 (reproduced from IPCC, 2013) suggests that in the coastal region close to Marromeu the relative mean sea level change varies between 0.4 – 0.9 m in the period 2081 – 2100 relative to 1986 – 2005 for the different emission scenarios considered by IPCC. Note that the upper bound of this range comes close to the upper bound of the range projected by IPCC for the global mean sea level rise (point projection of 0.75m for RCP8.5 in 2100, cf. Figure 3.33). Besides regional variations, there are also other uncertainties that are not fully accounted for in Figure 3.32. Most importantly, the uncertainties related to response of the ice masses on Antarctica and Greenland to rising temperatures (see

e.g. Rahmstorf, 2010, Lowe and Gregory, 2010). Recently, Le Bars et al. (2017) took into account the uncertainties in the AR5 sea level rise data (Church et al., 2013) and subsequent research of Deconto and Pollard (2016) to determine a high-end sea level rise probabilistic projection including rapid Antarctic ice sheet mass loss. Figure 3.33 shows their main result in which there is a high probability of the global sea level rise of 1.8 m.
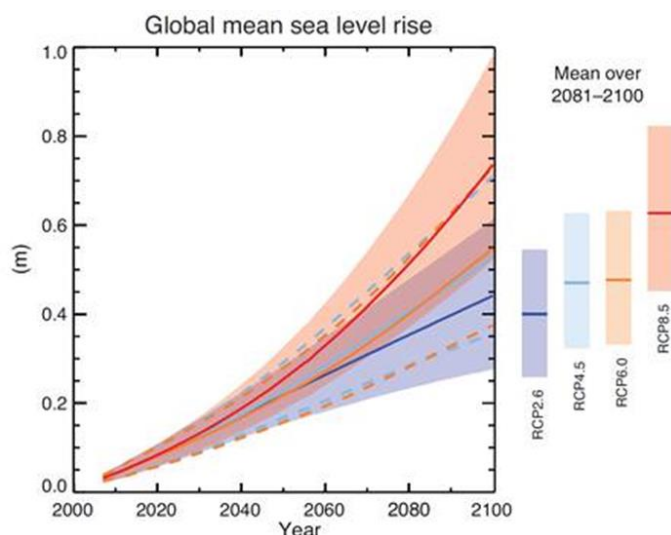

Figure 3.31 IPCC projections of global mean sea level rise relative to 1986–2005 for the four emission scenarios considered by IPCC (IPCC, 2013, Fig. TS.22).
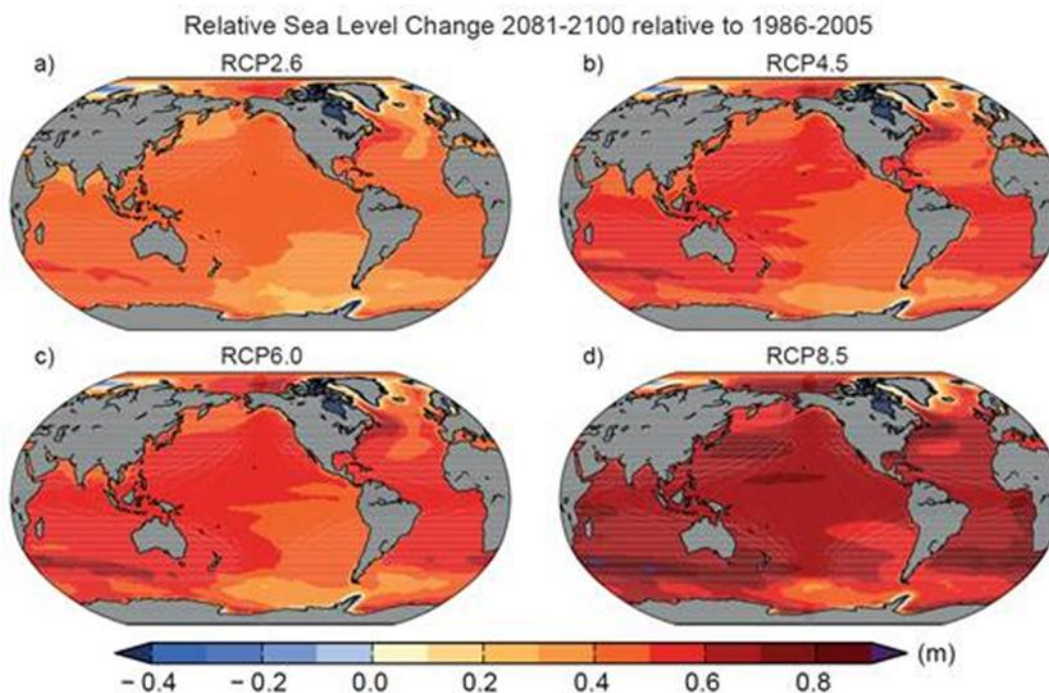

Figure 3.32 IPCC projections of regional relative sea level changes relative to 1986–2005 for the four considered emission scenarios by IPCC (IPCC, 2013, Fig. TS.23).
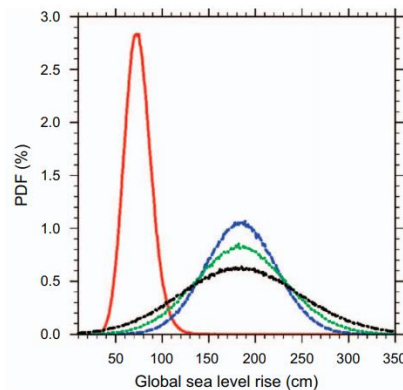
Figure 3.33 Probability distributions of the global total sea level rise in 2100 compared to 1985–2005 for the RCP8.5 scenario for IPCC AR5 (red), Antarctic mass loss (blue), including temperature dependent Antarctic mass loss (green) and ensemble uncertainty (black). Taken from Le Bars et al. (2017, Fig. 1).

Given the latest IPCC assessment report and further uncertainties discussed above, we recommend that a sea level rise figure of 0.9 m with an uncertainty range of 0.4 m to 1.8 m be accounted for in the coastal region close to Marromeu up to the end of this century. For 2050, given the lower uncertainties in the projections at such term (cf. Figure 3.33) and that also at such term the likelihood of the collapse of the Antarctica and Greenland ice-sheets is low, we estimate a sea level rise figure close to the upper bound of the range projected by IPCC for the global mean sea level rise of 0.30 m with an uncertainty range of 0.20 m to 0.35 m.

3.4.9.2 Storminess

During the wet season tropical cyclones regularly occur in Mozambique. The country's coast line is situated at the western boundary of a tropical cyclone belt – the south-west Indian Ocean basin. Cyclones that originate in the tropical latitudes of the Indian Ocean may move towards the east coast of Africa and may make landfall along the coast of Mozambique or pass very close to the coast. If such tropical cyclones make landfall they may cause extreme surge and wave setup along the coast and extreme rainfall and winds above land. These can lead to serious floods. The actual effects of each storm on coastal water levels will vary depending on local characteristics (e.g. shape and depth) and the vulnerability of the affected locations. The actual impact further depends on the local exposure, i.e. on the infrastructure and populations affected by such inundation. Examples of tropical cyclones are cyclone Eline that made landfall in Inhambane in February 2000 and the more recent Dineo (February 2017) also hitting Inhambane. And likely the most severe, cyclone Idai, that made landfall March 2019 and severely impacted Mozambique, including Sofala province, with strong winds and large scale flooding caused by both the cyclone itself and the accompanying heavy rains.

There are large uncertainties (conflicting) in terms of effects of climate change on the tropical cyclone climate affecting Mozambique and the Marromeu region in particular. Observations suggest a southward shift in their trajectories and landfall locations and increase of intensity (due to its correlation with the sea surface temperature), see INGC (2009) and Pat et al. (2010). In terms of projections there is much uncertainty and results from different studies are to certain extent conflicting (see e.g. Malherbe et al., 2011, 2012 and 2013, Emanuel et al., 2008, Muthige et al., 2018). In global terms, according to Stocker et al. (2013) projections for the 21st century indicate that it is likely that the global frequency of tropical cyclones will either decrease or remain essentially unchanged, concurrent with a likely increase in global mean tropical cyclone maximum wind speed. Malherbe et al. (2011) reports a northward shift in the preferred landfall position along the southern African east coast. The most recent study of Muthige et al. (2018) reports based on downscaling of AR5 data a future decrease in the number of tropical cyclones making landfalls over Mozambique and an associated decrease in associated rainfall as long as the 2 °C global warming threshold is met. Our overall conclusion based on the reviewed literature is that the uncertainty is large and it is best to assume that there will be no changes.

3.5 Socio-economic and ecological consequences for the Marromeu Complex

Overall the results of this assessment indicate that the drought problems in the complex will likely increase in the future. Below we specify the most relevant changes and their expected impacts, the latter are based on literature review of mainly the current situation in the larger Zambezi Delta and expert judgement.

According to the FAO cropping calendar, irrigation of maize, wheat and sugarcane is needed during (the end of) the dry season and will require more irrigation water due to the increased evaporation deficit projected by the studied scenarios. Evaporation deficit will increase and soil moisture will decrease, with changes up to 5% for the dry season, thus crop growing conditions will become less favorable.

According to van Logchem et al. (2012) crop yield of for example maize can reduce with 11% by 2050 in Mozambique because of increasing temperatures and decreases in rain. Ecologically this will likely exacerbate the already observed vegetation changes like the retreat of Mangrove forests at the inland boundary and change of wetland grassland to dry land grassland or more woody vegetation (Beilfuss et al. 2001). Increased drought and a more variable start of the rainy season will also affect the population of water birds and possibly larger mammals like elephants. These limitations in water availability can lead to competition for freshwater between human and nature during periods of drought (Price et al., 2016). In the past restrictions on water use have already been issued (source: WWF Mozambique). Further restrictions may be required especially because groundwater recharge will probably decrease with approximately 5% during the driest months (except for RCP8p5 by 2050). With the hydrological model decreases in groundwater level were assessed at 4 cm on average and 13 cm for the worst-case scenario in the dry season.

River flow from the Cheringoma Escarpment will likely decrease. Decreases in absolute flows are largest for the months October to January (i.e. the rainy season) for all scenarios, except for RCP8p5 for 2050. A reduction of wet season flow will also reduce the water availability in the wetland area and consequently may result in permanent drying of wetland area. In addition, reduced river flows may lead to further salinization of surface water and land with consequences for natural vegetation, aquatic organisms and cropping areas.

This study does not include flood modelling or assess flood impacts, however RCP8p5 does project increases in rain and consequently river flows by 2050, therefore extreme floods could still occur. To assess the likelihood further analysis is needed. Moderate floods could improve the conditions in the complex and could bring some of the seasonality in wetness back.

As a result of the disconnection of the Marromeu complex from the Zambezi River through the dams placed in the Salone the seasonally occurring floods have significantly decreased and woody savanna species and more upland grassland species are replacing the flood tolerant grassland species. In addition, abandoned alluvial channels and sand bars are now vegetated with grassland species (Beilfuss et al. 2001).

The population of Mozambique is rapidly increasing. In coastal east Africa on average the population doubles approximately every 25 years (Price et al., 2016) this is in line with the Mozambican projections for Sofala where the Marromeu Complex is located and where the increase is expected to be largest in rural areas. This will likely result in an increasing pressure on the use of resources and available land, possibly accompanied by habitat fragmentation and deforestation through cultivation of land in the Marromeu complex. Evergreen forest has in the past already been lost by unsustainable clear cutting and burning.

The increase in sea level rise will affect flooding and loss of land due to erosion and land submergence in the delta area. The delta is very flat, the main part of the area ranges between 0 and 24 metres above sea level (WWF Moz, 2016). With increases in sea level rise of ~0.30 metres by 2050 and a storm severity comparable to current climate conditions the influence of the sea, and thus salinization, will reach further inland. Exact figures for saline intrusion of the Marromeu complex are not available but for the larger Zambezi Delta there are indications of 50 to 80 kilometer. The total extent of saline grasslands, partly replacing the freshwater grasslands, has increased by about 5% since 1960 (Beilfuss et al., 2001) and will likely further increase. In the North-East close to the village Marromeu, land has been cultivated by Sena Sugar Estates (Beilfuss et al., 2001) and groundwater extractions have locally increased the salinity levels and caused the salinization to reach further inland. This will only be exacerbated by sea level increases.

The mangroves help to protect the delta area from coastal erosion and dampen the waves during high tides. In addition, they provide an excellent carbon stock (Stringer et al., 2014). Shapiro et al. (2015) concluded that the mangrove area in the Zambezi delta has increased approximately 10% over the past 2 decades. Further inland mangroves are diminishing due to human influences and dryer soil conditions.

4 Conclusions and recommendations

4.1 Conclusions

The assessed changes have been derived from a set of 4 GCMs for 2 representative climate scenarios for the near (2030) and far future (2050). The consistency between the GCMs is large for the months October to December in the rainy season. From March to August the variation in changes projected by the different GCMs is larger and the uncertainty thus as well. This should be taken in account when using the results of this study.

Overall it can be concluded that drought conditions in the Marromeu complex will likely become more severe in the future.

The freshwater supply to the wetlands from rainfall and the rivers from the escarpment will overall decrease whereas evaporation will increase. This negatively impacts agricultural conditions, the freshwater availability for households and will affect the existing water depended ecosystems.

The projected sea level rise of 0.20 – 0.35 meters will cause increased salinization further inland, submerging of the delta area and coastal erosion.

4.2 Recommendations:

4.2.1 Recommendations for adaptive management
Implementation of small-scale rain-water harvesting and storage would provide water for small-scale rainfall-fed agriculture and households in the dry season, see also Van Logchem et al., 2012.

The projected reduction in groundwater recharge and likely increases in salinization ask for sustainable use of the available water resources. We understand that for the large scale sugarcane production water is already retrieved from outside the complex (source: WWF).

The mangroves are an important means to: (1) protect the area from coastal flooding and erosion, (2) store carbon and (3) can on small scale be used for human activities. Protection and possibly the extension of the mangrove area is recommended.

In the Gorongoza national Park the natural vegetation is affected by land cultivation for agriculture and cattle. It is unclear whether this frequently occurs in the Marromeu complex as well, however even small scale clear cutting and burning in the upstream catchments will not only affect the vegetation it will also result in increased runoff and reduce the natural water holding capacity of the soil. Awareness raising and restrictions on land cultivations can help.

4.2.2 Recommendations for monitoring and further research
Data and information on the biodiversity, human activities, land use and meteorological and hydrological conditions are sparse and scattered. Improved monitoring of groundwater levels, salinization of ground- and surface water and river levels would help in the assessment of the change in the natural conditions of the complex. In addition, land use, ecosystem and vegetation mapping would improve the impact assessment.

There is a LIDAR dataset available that covers (most of) the Marromeu complex. If this data is processed it will provide a detailed map of the elevation of the terrain. This can be used to assess how far the sea will come land inward with the projected sea level rise.

This project did not include the development and use of a local groundwater model, whereas, if observation data became available, a groundwater model could help to better quantify the change in groundwater levels, increase in salinization and possibly the groundwater connection of the complex to the Zambezi River.

5 References

Beck, H. E., van Dijk, A. I. J. M., Levizzani, V., Schellekens, J., Miralles, D. G., Martens, B., and de Roo, A.: MSWEP: 3-hourly 0.25° global gridded precipitation (1979–2015) by merging gauge, satellite, and reanalysis data, Hydrol. Earth Syst. Sci., 21, 589-615, https://doi.org/10.5194/hess-21-589-2017, 2017.

Beilfuss, R., Moore, D., Bento, C., and P. Dutton, 2001. Patterns of vegetation change in the Zambezi Delta, Mozambique. Working paper 3. Zambezi basin Crane and Wetland conservation program.

Church, J. et al., 2013: Sea level change Climate Change 2013: The Physical Science Basis. Contribution of Working Group I to the Fifth Assessment Report of the Intergovernmental Panel on Climate Change ed T F Stocker, D Qin, G-K Plattner, M Tignor, S K Allen and J Boschu (Cambridge: Cambridge University Press).

Deconto, R.M. and Pollard D., 2016: Contribution of antarctica to past and future sea-level rise. Nature, 531, 591–7.

Emanuel, K. A., R. Sundararajan, and J. Williams, 2008: Hurricanes and global warming: Results from downscaling IPCC AR4 simulations. Bull. Amer. Meteor. Soc., 89, 347–367.

Hemer, M.A., Y. Fan, N. Mori, A. Semedo and X. L. Wang, 2013: Projected changes in wave climate from a multi-model ensemble. Nature Climate Change, doi:10.1038/nclimate1791 (http://www.nature.com/nclimate/journal/vaop/ncurrent/full/nclimate1791.html).

Hempel, S., Frieler, K., Warszawski, L., Schewe, J., and Piontek, F.: A trend-preserving bias correction – the ISI-MIP approach, Earth Syst. Dynam., 4, 219-236, https://doi.org/10.5194/esd-4-219-2013, 2013.

IHE, 2014: Feasibility Study to Reconnect the Salone River to the Main Zambezi – A Hydro-geomorphological Approach

INGC, 2009: Synthesis report. INGC Climate Change Report: Study on the impact of climate change on disaster risk in Mozambique. [van Logchem B and Brito R (ed.)]. INGC, Mozambique.

IPCC, 2007: Climate Change 2007: The Fourth Assessment Report of the Intergovernmental Panel on Climate Change.

IPCC. 2013. Climate Change 2013: The physical science basis. Contribution of working group I to the fifth assessment report of the Intergovernmental Panel on Climate Change. Cambridge University Press, Cambridge, United Kingdom and New York, NY, USA.

Jeff Price, Rachel Warren, Jeremy Vanderwal, Amy McDougall, Stephen Cornelius and Heather Sohl, PROJECTED CHANGES IN CLIMATE AND BIODIVERSITY IN WWF PRIORITY PLACES. VOLUME 3 – BIODIVERSITY, Version 2.0 July 23, 2016.

Lesk, C., De Mel, M., and Horton, R. 2017. Climate Change in the Kafue Basin in the Zambezi Watershed. New York: Center for Climate Systems Research, Columbia University.

Le Bars, D., S. Drijfhout and H. de Vries, 2017: A high-end sea level rise probabilistic projection including rapid Antarctic ice sheet mass loss. Environmental Research Letters, 12(4).

Lowe, J. A. and J. M. Gregory, 2010: A sea of uncertainty: How well can we predict future sea level rise? Nature Reports Climate Change, 42-43. Available at http://www.nature.com/climate/2010/1004/full/ climate.2010.29.html.

Malherbe, J, Engelbrecht, F, Landman, W and C. Engelbrecht, 2011: High resolution model projections of tropical cyclone landfall over southern Africa under enhanced anthropogenic forcing. South African Society for Atmospheric Sciences 27th Annual Conference, Hartbeespoort, South Africa, 22-23 September 2011.

Malherbe J, F.A. Englebrecht, W.A. Landman and C.J. Engelbrecht, 2012: Tropical systems from the South West Indian Ocean making landfall over the Limpopo River Basin, southern Africa: a historical perspective. Int. J. Climatol., 32 1018–32.

Malherbe J, F.A. Englebrecht and W.A. Landman, 2013: Projected changes in tropical cyclone climatology and landfall in the South West Indian Ocean region under enhanced anthropogenic forcing. Clim. Dyn., 40 2867–86.

Müller, T., Mapaura, A., Wursten, B., Chapano, C., Ballings, P. and R. Wild, 2012. Vegetation survey of Mount Gorongosa, Occasional Publications in Biodiversity No. 23, Biodiversity Foundation for Africa.

Muthige, M.S., J. Malherbe, F.A. Englebrecht, S. Grab, A. Beraki, T.R. Maisha and J. Van der Merwe, 2018: Projected changes in tropical cyclones over the South West Indian Ocean under different extents of global warming. Environ. Res. Lett., 13,. https://doi.org/10.1088/1748-9326/aabc60.

Monteith, J. L.: Evaporation and environment, Sym. Soc. Exp. Biol., 19, 205–234, 1965.

Patt A, Varela R, Nhantumbo I, Bizikova L, 2010: The Social Dimensions of Adaptation to Climate Change in Mozambique. Development and Climate Change Discussion Paper Number 16, The World Bank, Washington, DC, USA.

Jeff Price, Rachel Warren, Stephen Cornelius and Heather Sohl, Climate Change Impacts on WWF Priority Places and Species Volume 2 – Climate Modelling. Version 2.0 March 1, 2017

Rahmstorf, S., 2010: A new view on sea level rise. Nature Reports Climate Change, 44-45. Available at http://www.nature.com/climate/2010/1004/full/climate.2010.29.html.

Schellekens, J.: OpenStreams wflow documentation release 1.0RC1, Deltares, available at: http://wflow.readthedocs.org/en/ latest/ (last access: 25 September 2015), 2014.

Schellekens, J., Dutra, E., Martínez-de la Torre, A., Balsamo, G., van Dijk, A., Sperna Weiland, F., Minvielle, M., Calvet, J.-C., Decharme, B., Eisner, S., Fink, G., Flörke, M., Peßenteiner, S., van Beek, R., Polcher, J., Beck, H., Orth, R., Calton, B., Burke, S., Dorigo, W., and Weedon, G. P.: A global water resources ensemble of hydrological models: the eartH2Observe Tier-1 dataset, Earth Syst. Sci. Data, 9, 389-413, https://doi.org/10.5194/essd-9-389-2017, 2017.

Semedo, A., R. Weisse, A, Behrens, A. Sterl, L. Bengtsson and H. Günther, 2013: Projection of global wave climate change towards the end of the 21st century. Submitted to J. Clim.

Shapiro, Aurélie C., Carl C. Trettin, Helga Küchly, Sadroddin Alavinapanah and Salomão Bandeira, (2015). The Mangroves of the Zambezi delta: Increase in Extent Observed via Satellite from 1994 to 2013. Remote Sensing, 7, 16504–16518.

Singh, A. 2017: Historical analysis of change in rainfall, flow regime and river morphology. MSc Thesis WM-WRM. 17-23, UNESCO-IHE.

Stocker, T.F., D. Qin, G.-K. Plattner, L.V. Alexander, S.K. Allen, N.L. Bindoff, F.-M. Bréon, J.A. Church, U. Cubasch, S. Emori, P. Forster, P. Friedlingstein, N. Gillett, J.M. Gregory, D.L. Hartmann, E. Jansen, B. Kirtman, R. Knutti, K. Krishna Kumar, P. Lemke, J. Marotzke, V. Masson-Delmotte, G.A. Meehl, I.I. Mokhov, S. Piao, V. Ramaswamy, D. Randall, M. Rhein, M. Rojas, C. Sabine, D. Shindell, L.D. Talley, D.G. Vaughan and S.-P. Xie, 2013: Technical Summary. In: Climate Change 2013: The Physical Science Basis. Contribution of Working Group I to the Fifth Assessment Report of the Intergovernmental Panel on Climate Change [Stocker, T.F., D. Qin, G.-K. Plattner, M. Tignor, S.K. Allen, J. Boschung, A. Nauels, Y. Xia, V. Bex and P.M. Midgley (eds.)]. Cambridge University Press, Cambridge, United Kingdom and New York, NY, USA.

Stringer et al., The Zambezi River Delta Mangrove Carbon Project: A Pilot Baseline Assessment for REDD+ Reporting and Monitoring, Center for Forested Wetlands Research U.S. Forest Service, 2014.

Van Logchem, B. & Queface, A.J. (eds.). 2012. Responding to Climate Change in Mozambique: Synthesis Report. Maputo INGC.

WWF Mozambique, 2016. Sustainable Finance for Protected Areas System in Mozambique Socioeconomic Assessment on Mangrove Forests in the Zambezi delta Contract No: 08-FY16-40000062, Final Report.

A   Preparation and validation of soil moisture

Here, the analysis of the high resolution soil moisture of the area is described. The analysis focuses on the following steps:
- Process the soil moisture for the period 2002 to 2018. Here 2015-2018 has the highest quality data
- Match the recent data to the long timeseries
- Examine the spatial variations in the soil moisture over the area
- Examine the temporal variation over the area

Location and analysis areas
The analysis was done over the whole area as well as over a number of sub-areas as shown in Figure A.1.
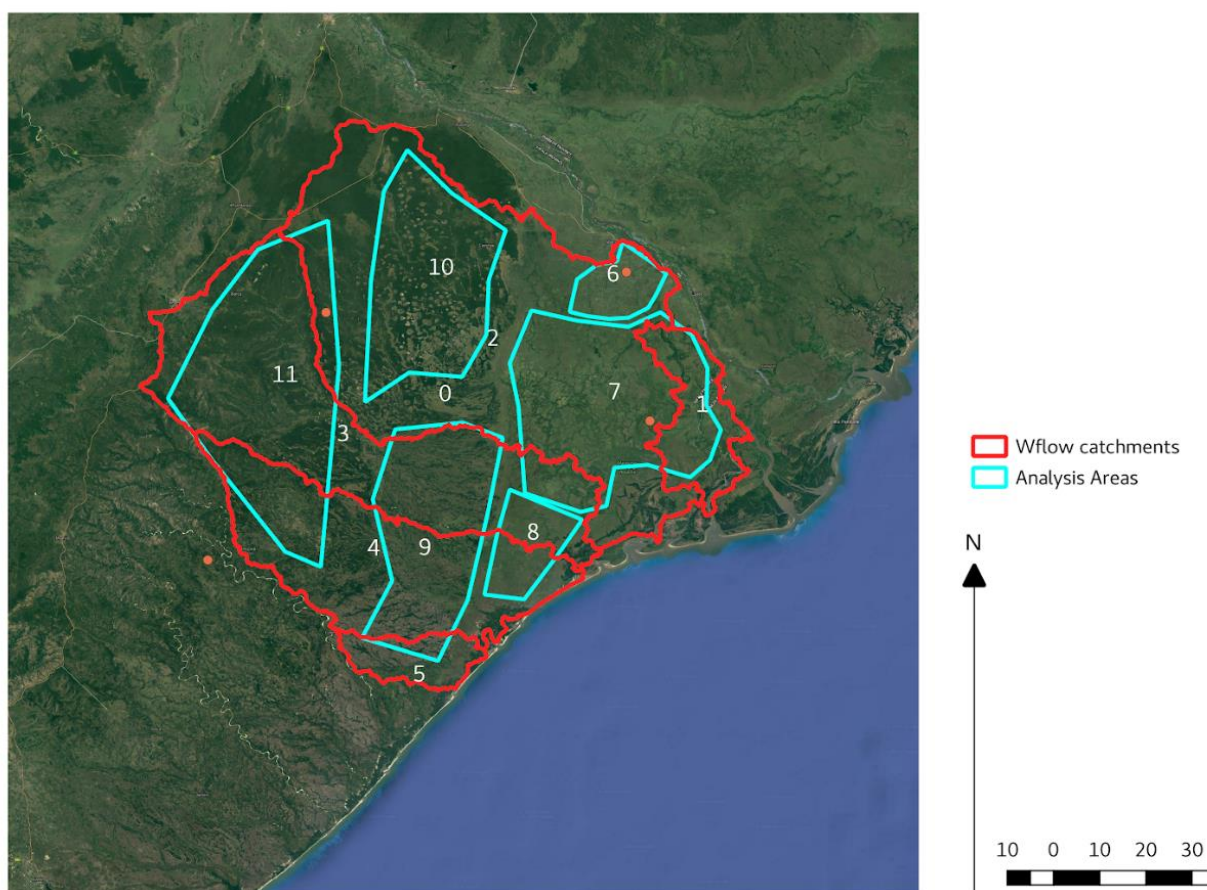
Figure A.1 Areas used in the analysis. 1 to 5 are the wflow catchment 6-11 are areas with more or less homogeneous vegetation and topographical properties.

Spatial analysis

The first analysis of the data showed that (unexpectedly) the vegetation cover in the steeper area was too dense of the L and C-Band data to provide reliable soil moisture estimates. As such, for those areas we can use data between 2015 and 2018. The area for which reliable data is present roughly coincides with the areas 1, 6, 7 and 8 in Figure A.1.

Figure A.2 shows monthly climatology for soil moisture determined from the period 2015-2018. The yearly cycle of wet and dry months can clearly be seen. The soil moisture is expressed in m3/m3. We can also scale to soil moisture to the estimated porosity to derive a number between 0 (completely dry) and 1 saturated. In Figure A.3 the apparent saturated based on the soil moisture is shown.

The plots show that the southern and eastern areas are wettest in the wet periods. In the driest month (October) the whole of the area becomes almost equally dry. The wettest month from a soil moisture perspective is April.
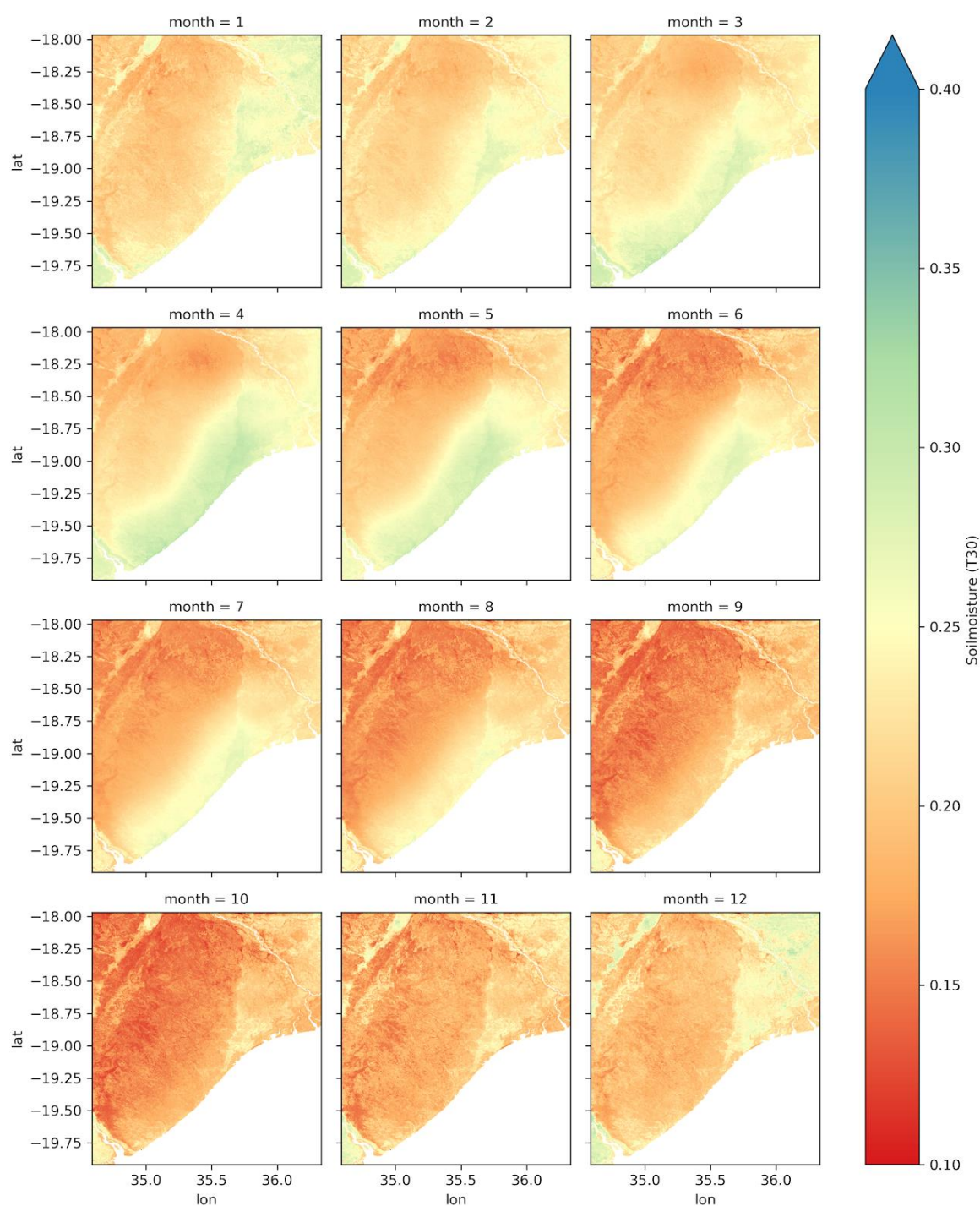
Figure A.2 Monthly climatology of L-Band soil moisture [m3/m3] over the period 2015-2018. here a root zone transformation with a T value of 30 has been applied.
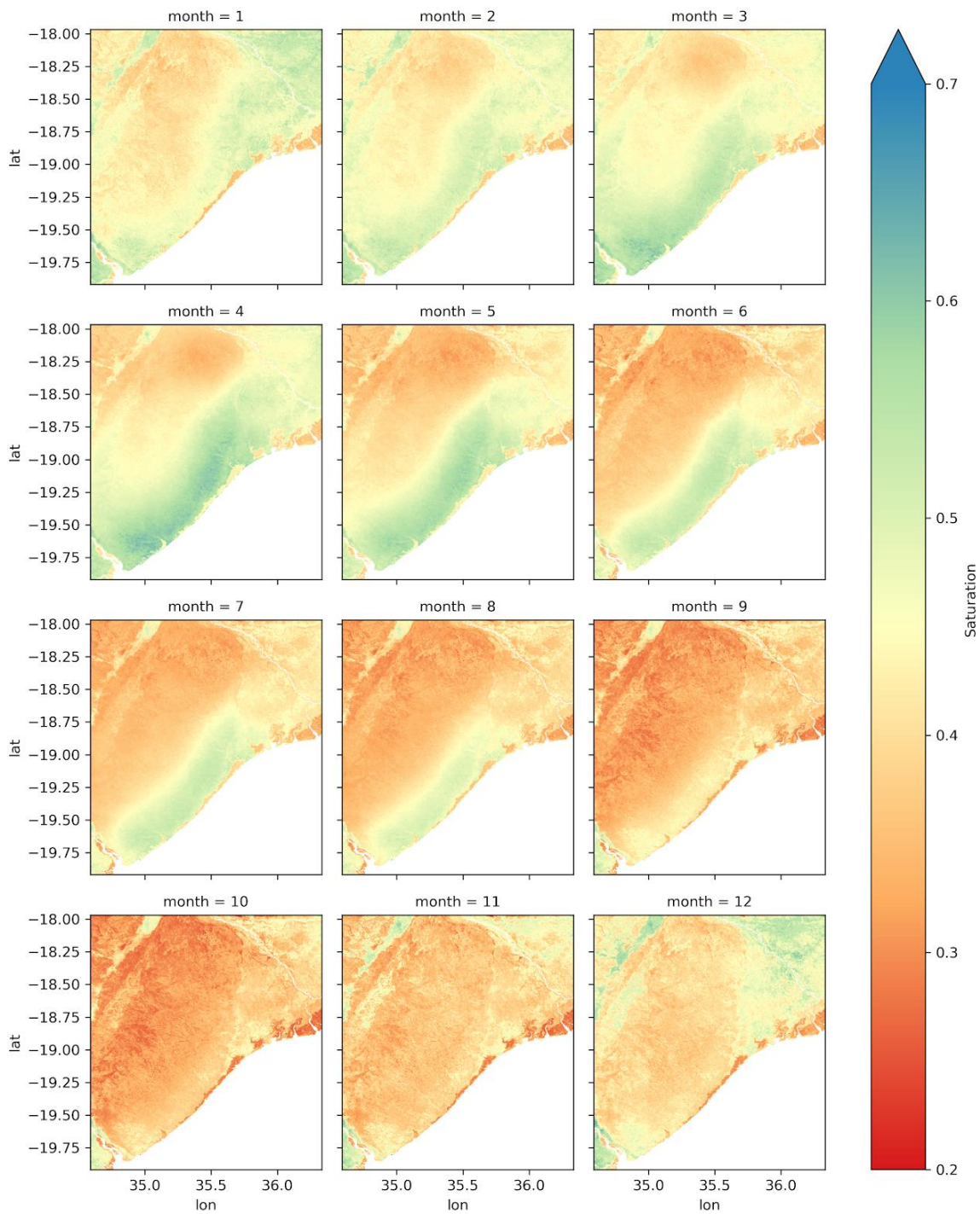
Figure A.3 Monthly climatology of apparent saturation (between 0 and 1) over the period 2015-2018.

Climate change impacts on hydrological conditions in the Marromeu Complex

Timeseries

Time series of average soil moisture (using T=5) have been generated for all the areas defined in Figure A.1. In Figure A.4 two plots are shown. The first plot show the average soil moisture for areas 6,7 and 9 while the second part of that figures shows the average of the areas 9, 10 and 11. Areas 8 and 11 show the largest range between dry and wet periods although the largest wet peak in early 2017 is clear in all areas and very pronounced in area 7. Area 6 is a relative small area that most probably includes irrigation (evident from the circular structures that can be seen in areas photography). However, an irrigation signal is not detected in the measurements.

Figure A.4 Timeseries of 14 day average soil moisture for areas 6,7 and 8 (top panel) and areas 9, 10 and 11 (bottom panel)

The average monthly climatology determined over 2015-2018 over the areas 6-1 is shown in Figure A.5. This figure shows the same pattern as Figure A.2 where we can see that area 10 and 11 show the least variation within a year.
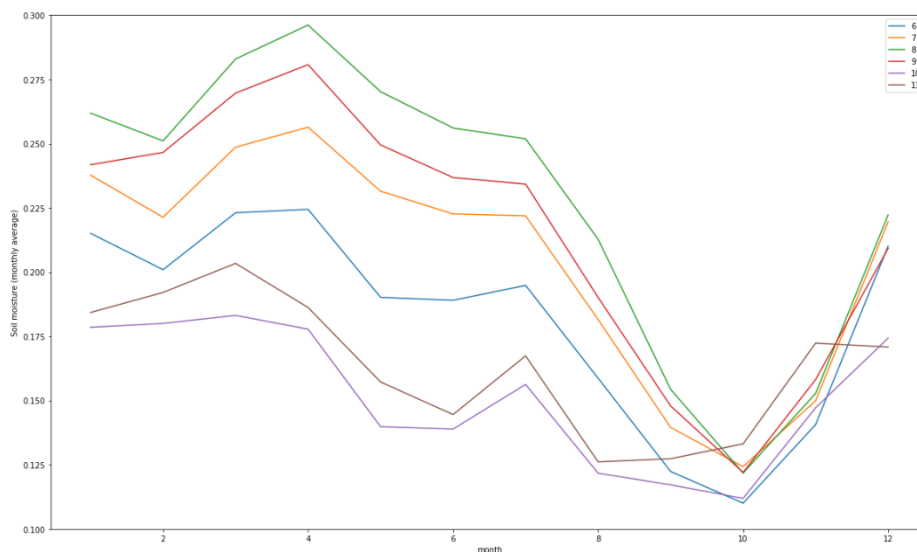
Figure A.5 Monthly soil moisture climatology for the period 2015-2018 for the L band for the areas 6-11.

Matching of C to L-Band

Using the C band data we can go further back in time and show longer time series. however, the quality of the C-Band data is relatively low in this area and we only feel confident using it in areas 1, 6, 7 and 8.

For the Area 6, 7 and 8 we matched the long time record (C-Band) to the short and better time record of the L band. Figure A.6 shows two panels. The top one shows the raw L and C band as well as the C band matched to the L band using the 0.1 and 0.9 percentiles. The bottom panel shows the same data but with a 14 day rolling mean applied to the data.

Figure A.6 C and L band matching for area 8

Although there remains a difference between the two bands after matching the data of the C band for area 6, 7 and 8 look good enough for a historical analysis.

Analysis of Long time records

Figure A.7 shows the long soil moisture record for area 6, 7 and 8 respectively. The blue (long term) and orange (short term) lines are 14 day rolling mean averages. The green lines show the 365 days rolling mean. There is considerable difference between the years with 2014 - 2016 being relatively wet and the beginning of the record (2002-2007) relatively dry.
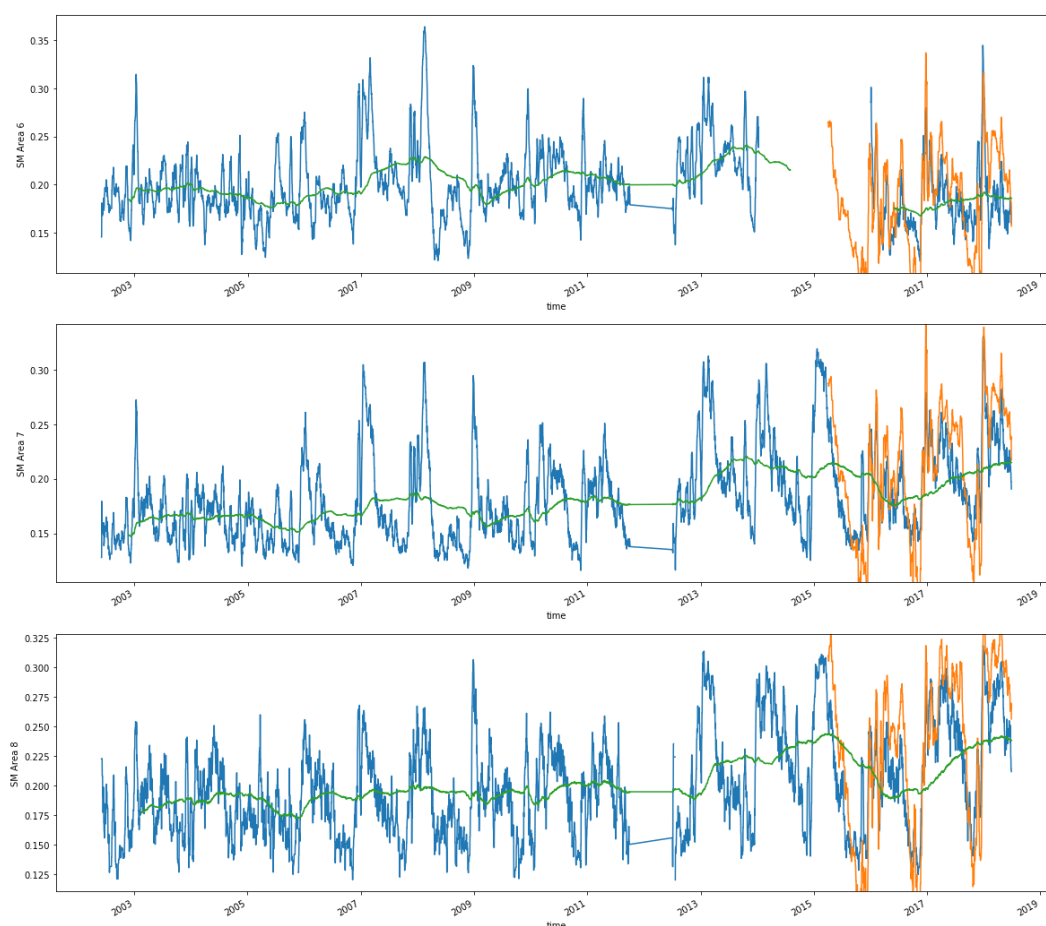

Figure A.7 Long term soil moisture record (14 day rolling mean) for area 6,7 and 8. The orange line shows the short term record (the L band), the green line the 365 day rolling mean.

For these areas we can now also determine the long term climatological variation (Figure A.8). This figure also show that climatology of the short time record (2015-2018) is different from the long time record (2002 - 2018).
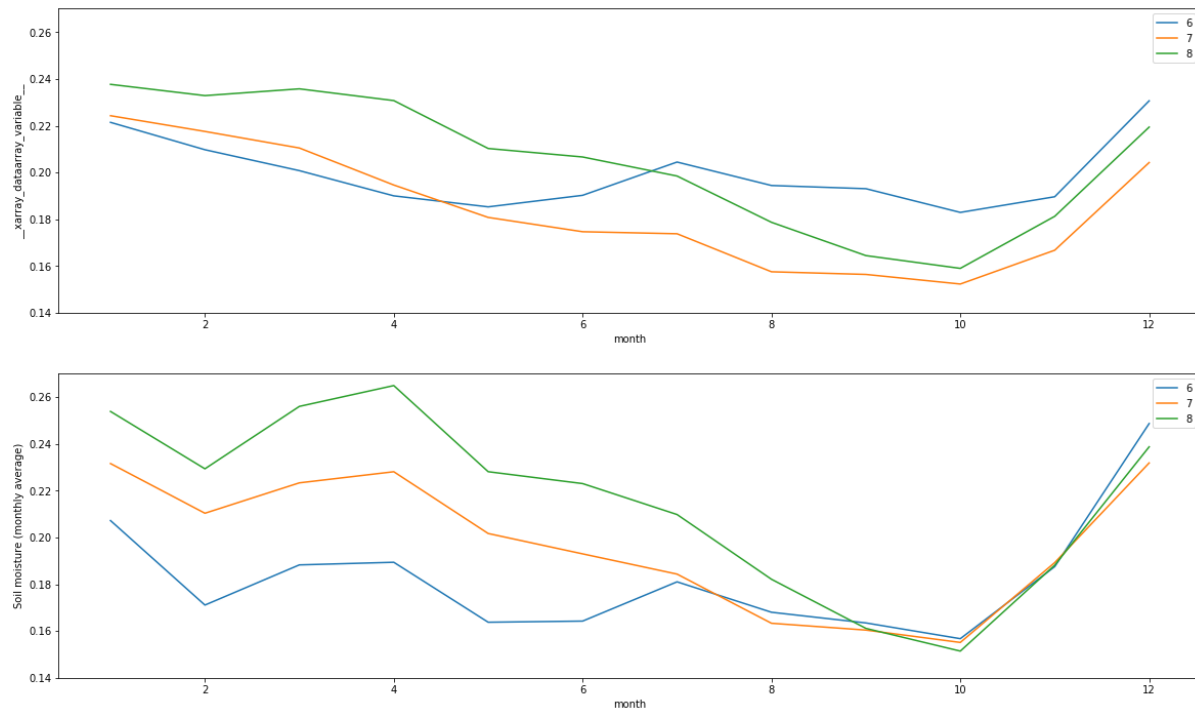
Figure A.8 Monthly climatology for the long time record (top panel) and the period of the L-Band (bottom panel).

In the plots in Figure A.9 30-day rolling mean of the soil moisture is shown for each area against the backdrop of the percentiles based on the climatology. This show how much the values deviate from the 'normal' monthly averages.
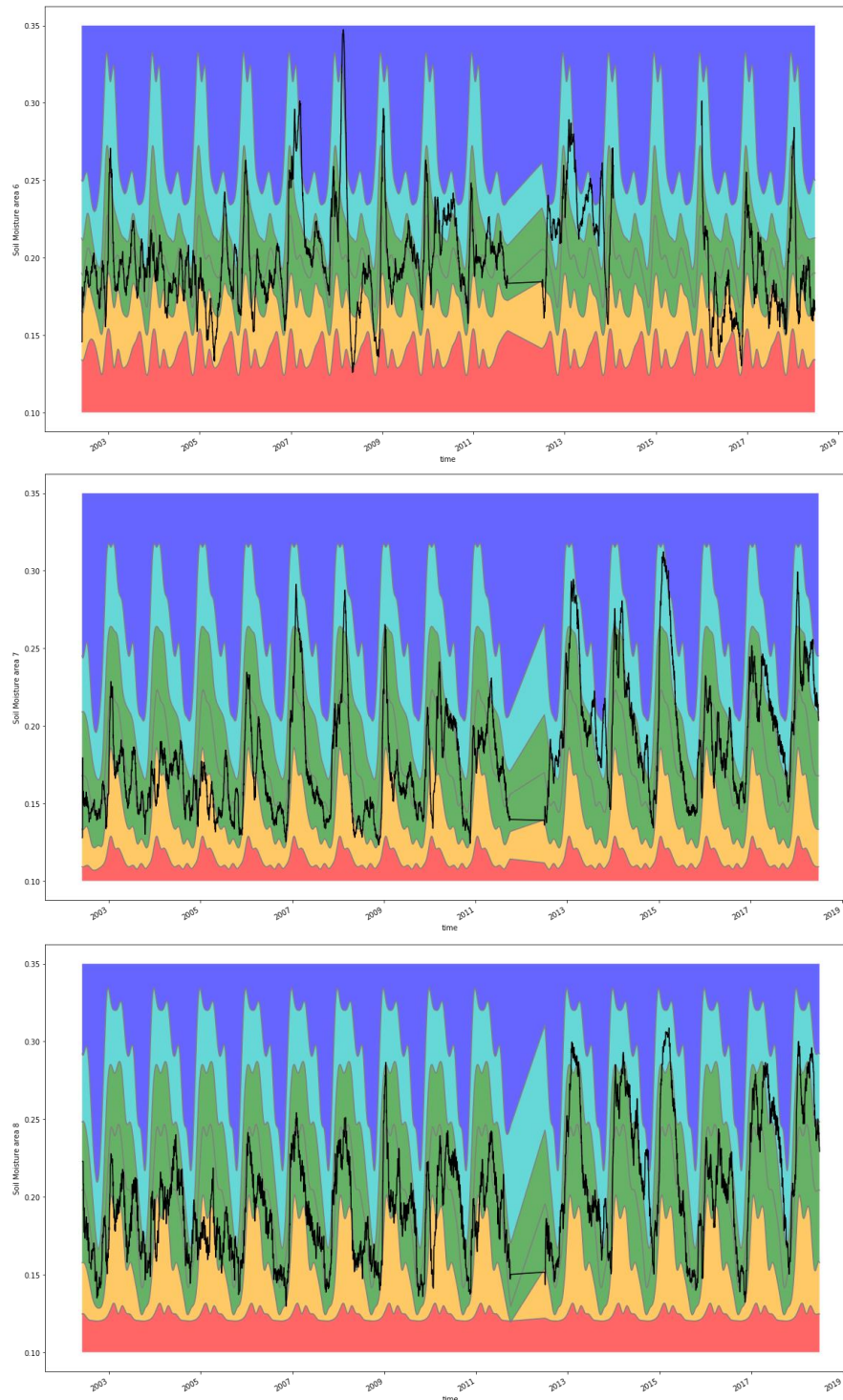
Figure A.9 Thirty day moving average (black line) for area 6, 7 and 8 respectively against a backdrop of the climatology percentiles: red 0- 10 %, orange 10-30%, green 30 - 70%, cyan 70-90%, blue 90 - 100%.

B Discharge changes for all sub-catchments

The Marromeu Complex can be sub-divided in five independent river catchments. The main report focusses on catchment 3 one of the two larger catchments. Part of catchment 2 is also discussed in more detail in the report – this is the area with irrigated sugar cane in the North-East (Area 6). In this Appendix the graphs with projected changes in discharge have been included for all five river catchments, to show the similarity in projected changes.
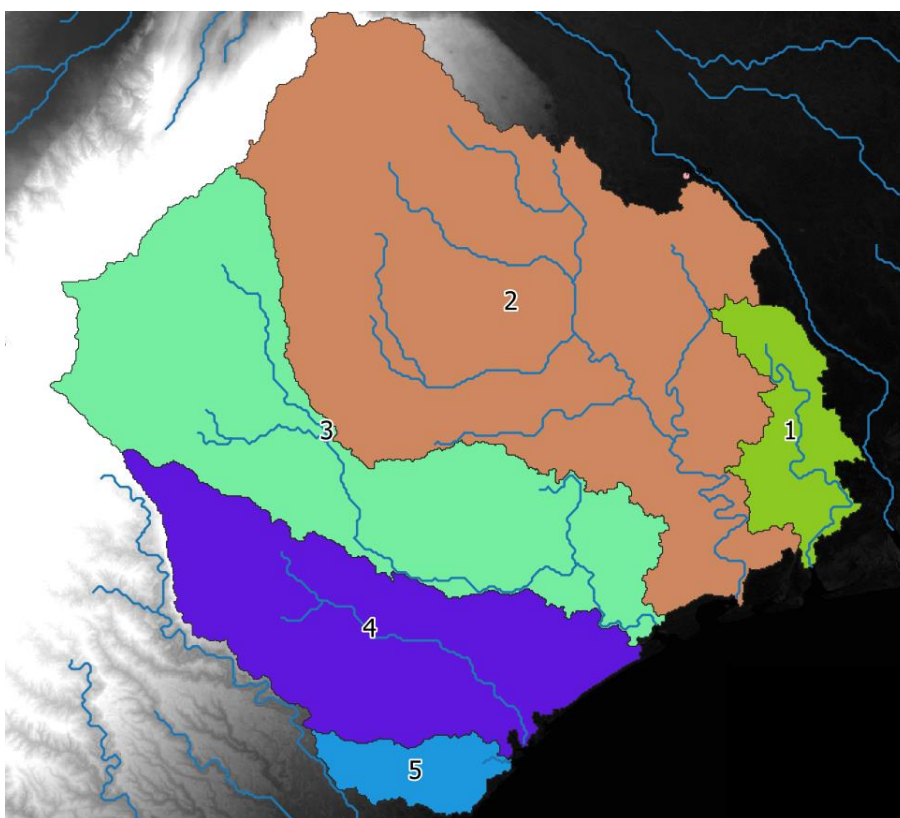

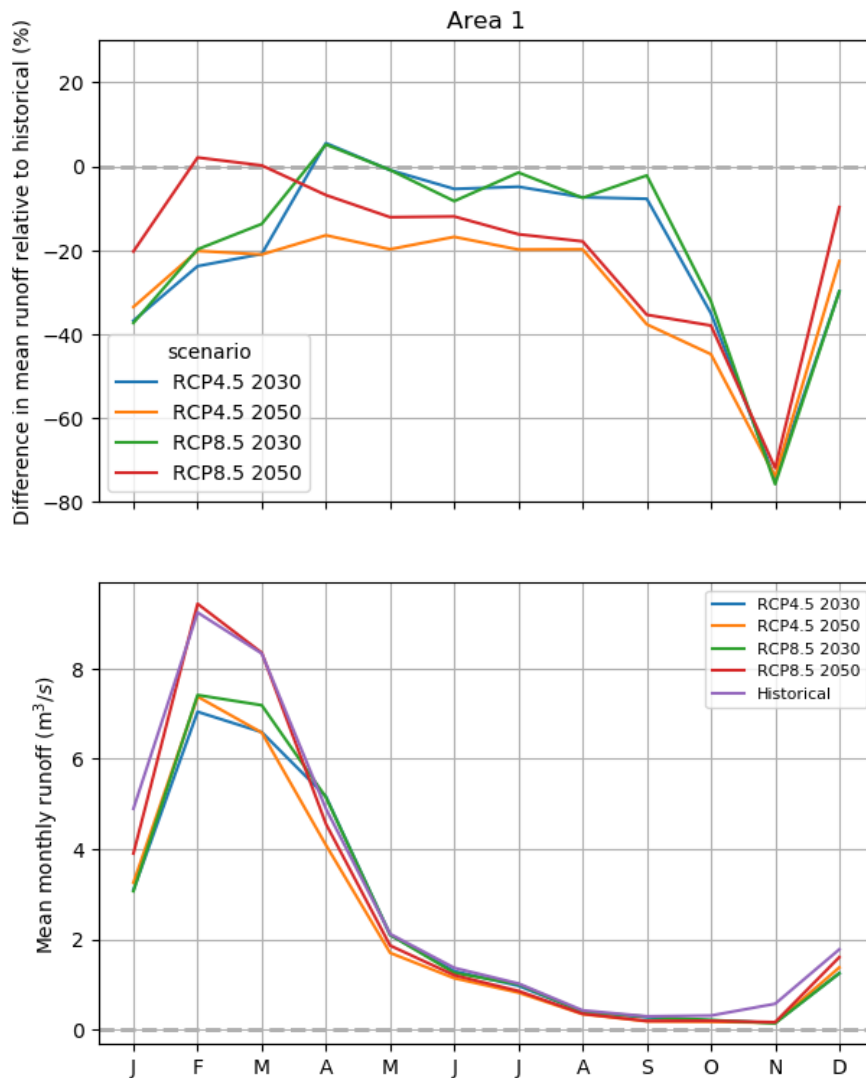*Figure B.1 Top: The five major river catchments of the Marromeu Complex*

Figure B.2 Top: Changes in mean monthly runoff (%) for the different scenarios relative to the historical model run in catchment area 1, below: mean monthly discharge (m³/s) for the different scenarios and historical period
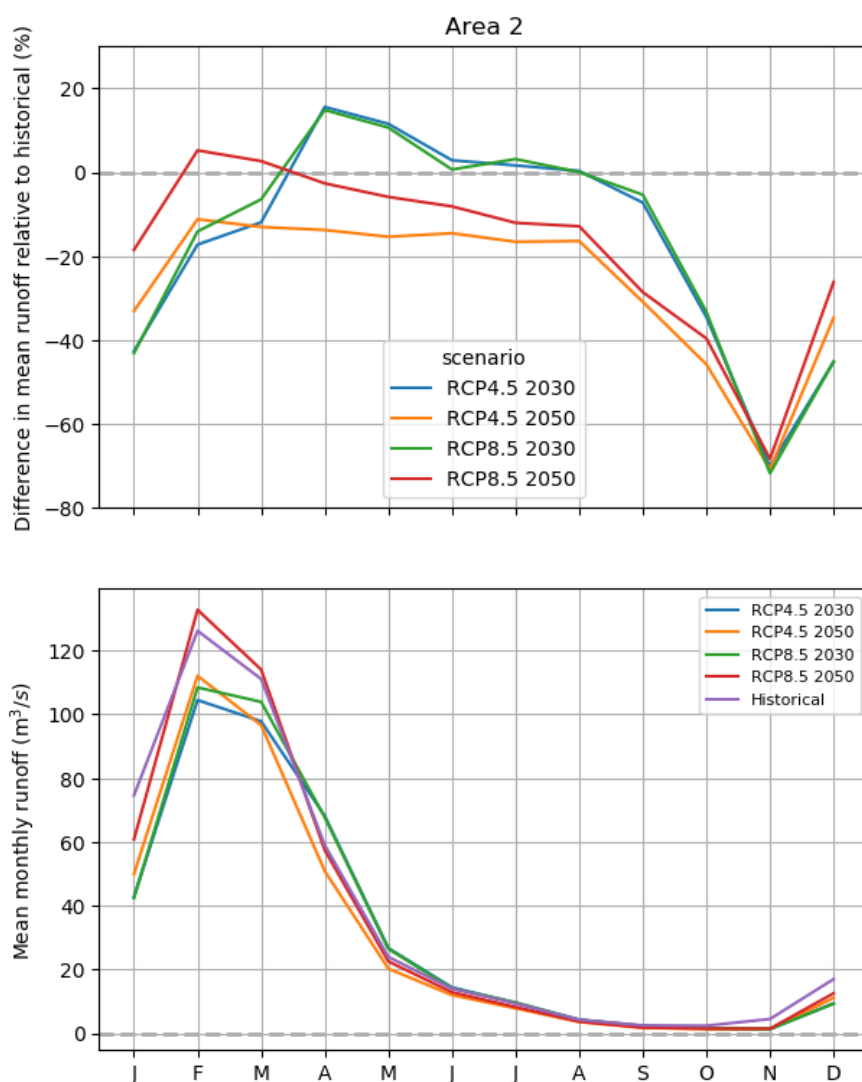
Figure B.3 Top: Changes in mean monthly runoff (%) for the different scenarios relative to the historical model run in catchment area 2, below: mean monthly discharge (m³/s) for the different scenarios and historical period
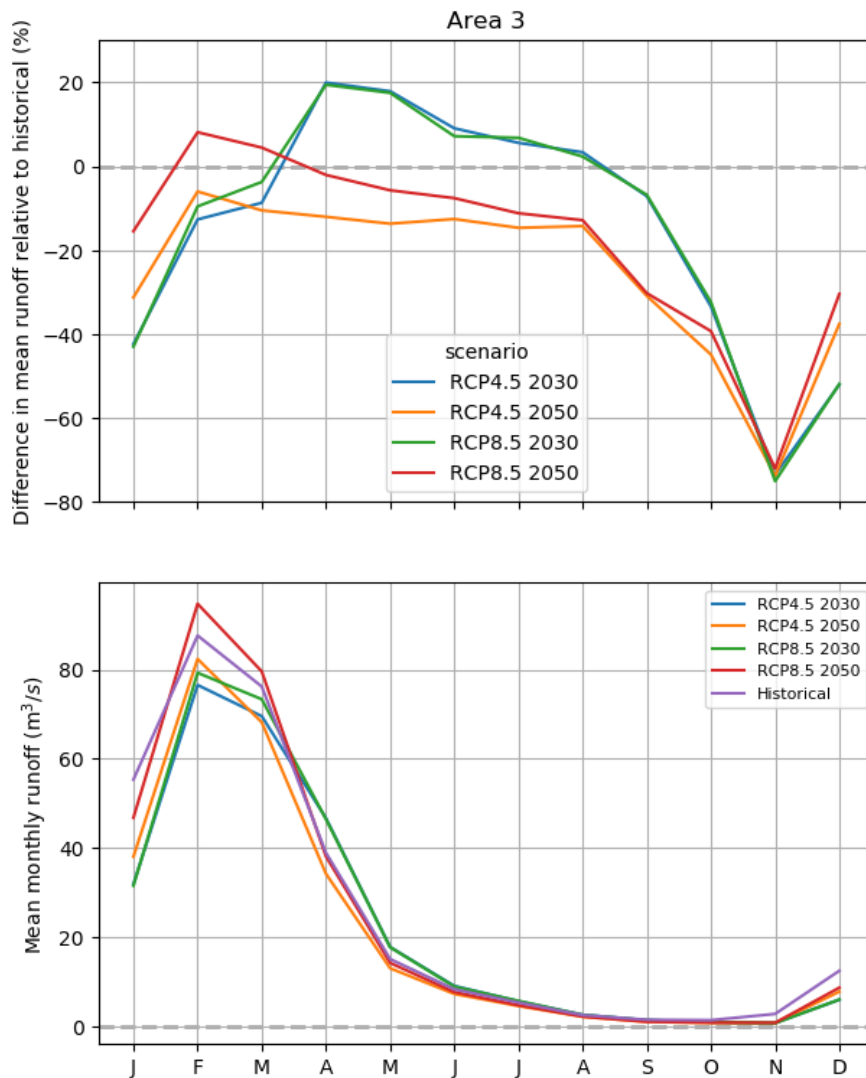
Figure B.4 Top: Changes in mean monthly runoff (%) for the different scenarios relative to the historical model run in catchment area 3, below: mean monthly discharge (m³/s) for the different scenarios and historical period
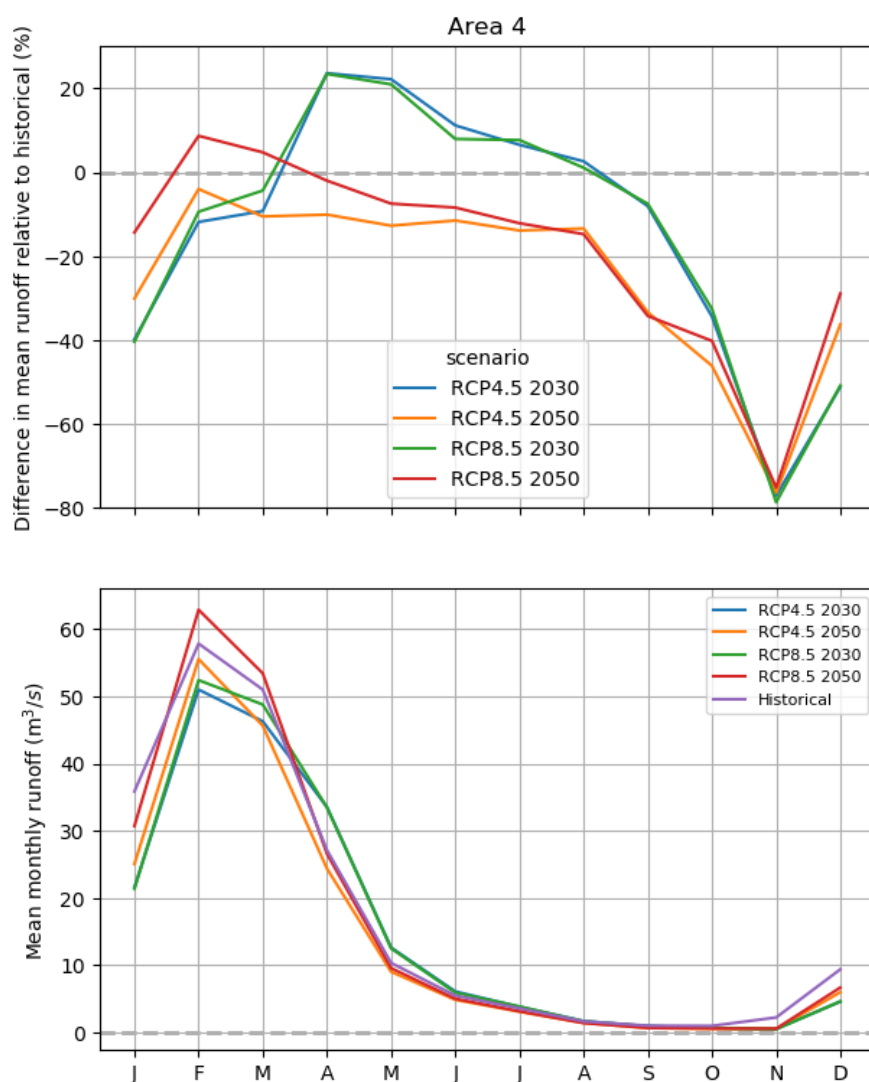
Figure B.5 Top: Changes in mean monthly runoff (%) for the different scenarios relative to the historical model run in catchment area 4, below: mean monthly discharge (m³/s) for the different scenarios and historical period
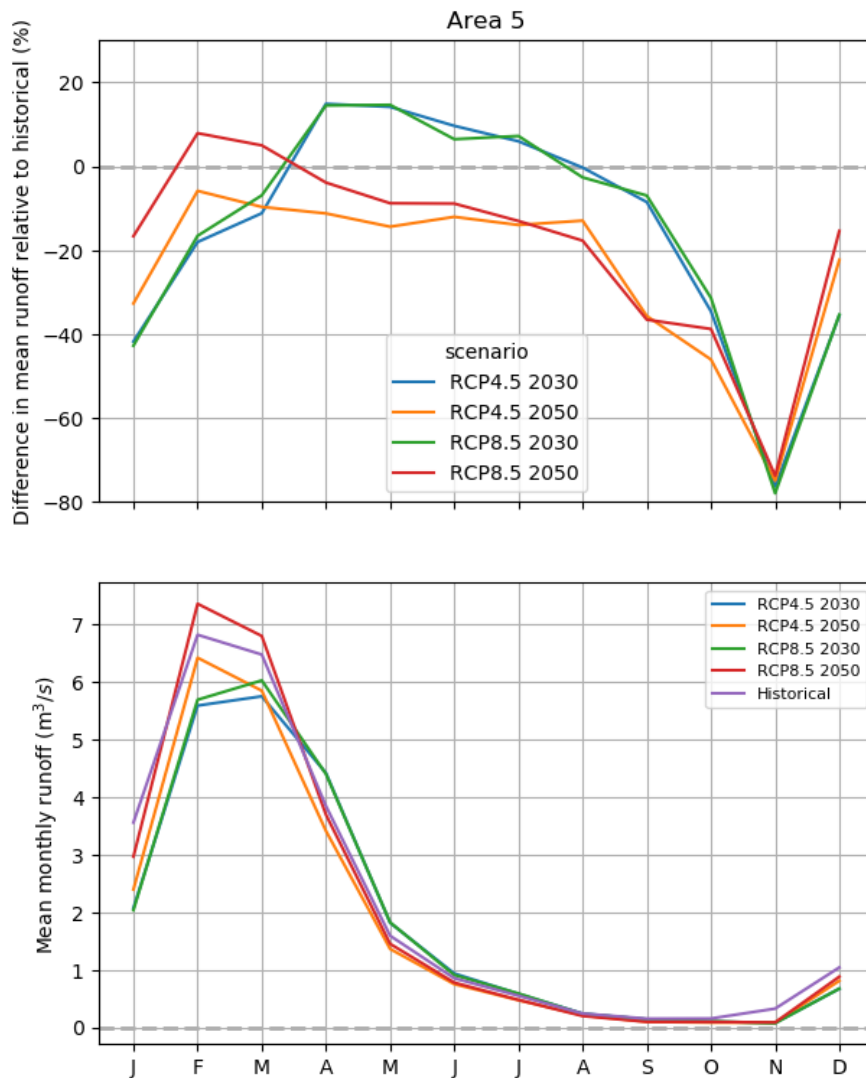
Figure B.6 Top: Changes in mean monthly runoff (%) for the different scenarios relative to the historical model run in catchment area 5, below: mean monthly discharge (m³/s) for the different scenarios and historical period

C Kart Analysis

This appendix focuses on the possibility of identifying the influence of a karstic system in the Cherringoma escarpment based on the in this study developed satellite-based soil moisture data.

The UNESCO-IHE report entitled "Feasibility Study to Reconnect the Salone River to the Main Zambezi – A Hydro-geomorphological Approach" (2014) mentions clear signs of karstic erosion along the Cherringoma escarpment for almost its entire length from South-West to North-East. The satellite-based soil moisture product from VanderSat is used to analyze the likely emergence of karstic waters at the foot of the escarpment.

In a first step, we plot the dynamics of mean soil wetness index (with parameter t = 30 days) in the escarpment, the lowlands and the border between the lowlands and the escarpment, see the boxes in Figure C.1.
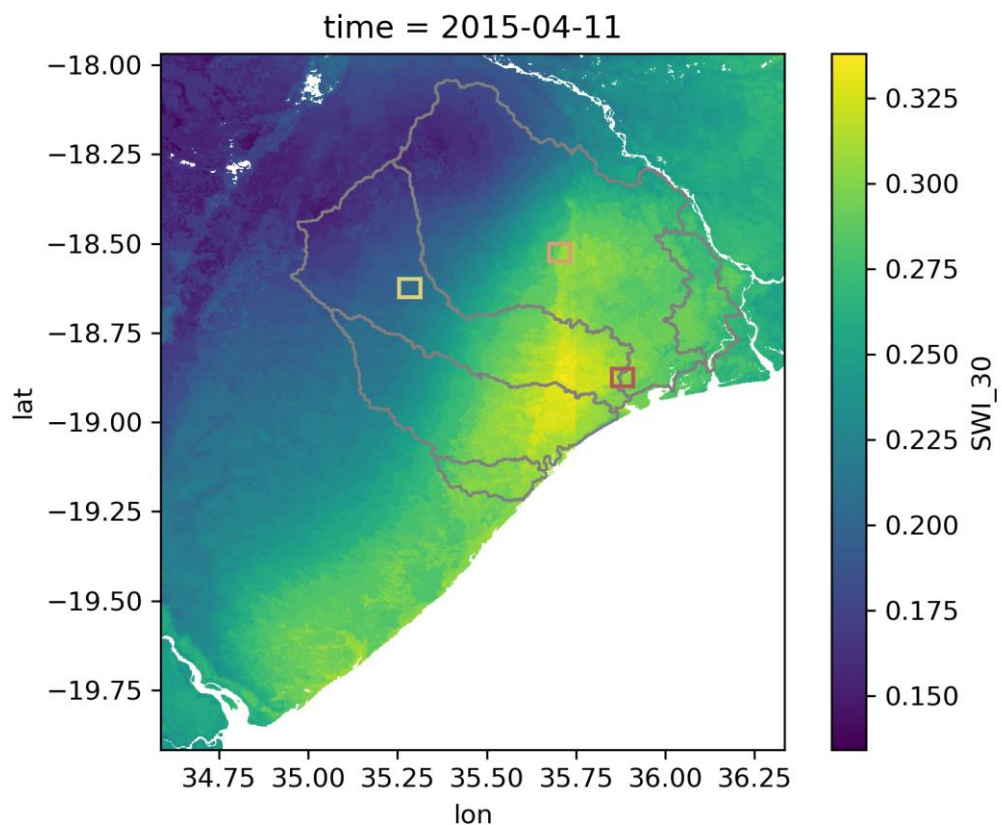

Figure C.1 Location of the mean soil moisture dynamics within the escarpment (yellow rectangle), the lowlands (red rectangle) and the border in between (orange rectangle). The background is the soil moisture estimates (soil wetness index) on 2015-04-11.
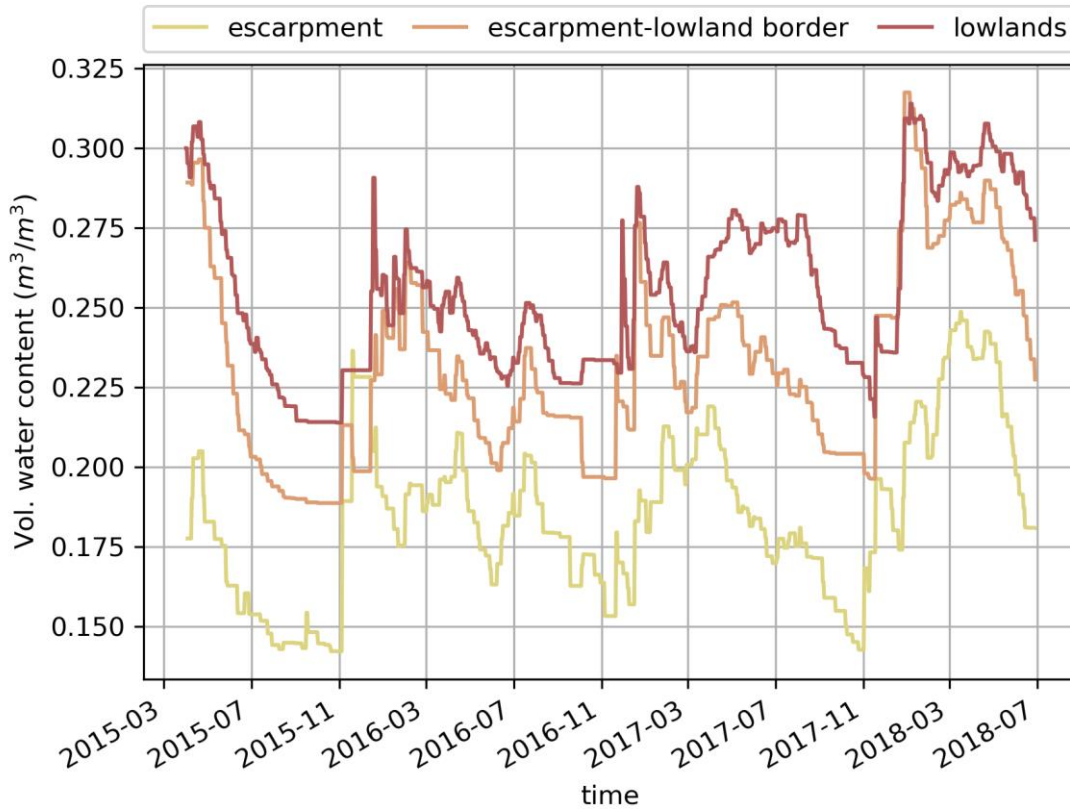
Figure C.2 Timeseries of mean soil moisture within the rectangles of the escarpments, the lowlands and the border in between both.

The dynamics of soil moisture in time are similar for the boxes assumed representative for the three areas (escarpments, lowlands and border between both) although shifted in terms of their absolute values, as shown in Figure C.2. We therefore do not observe different or time-shifted dynamics at the border of the escarpment and the lowlands, which could be linked to the presence of small springs from the karstic network that could delay the (subsurface) runoff process. However, if these springs are small (and we do not know their exact locations), they are probably not picked up by the soil moisture signal and would therefore not lead to a different dynamic. A different set of data is needed to further assess the presence of a karstic system in the area.

D Seasonal variation in surface water extents

The Sentinel-1 mission, carried out by the European Space Agency (ESA), consists of a constellation of two satellites (Sentinel 1A and 1B) with on board a C-band synthetic aperture radar (SAR). The satellites were launched in 2014 and provide radar backscatter, cloud free, images of the top layer of the soil. Radar backscatter is mainly influenced by the water content through the dielectric constant, geometry and roughness of the surface, and can therefore be used for surface water extent mapping.

For each Sentinel-1 image available since 2014, we tried to map surface water extent using a threshold on VV-backscatter to differentiate water pixels from land pixels. This was done using polygons which contain both land and water pixels as, shown in Figure D.1.
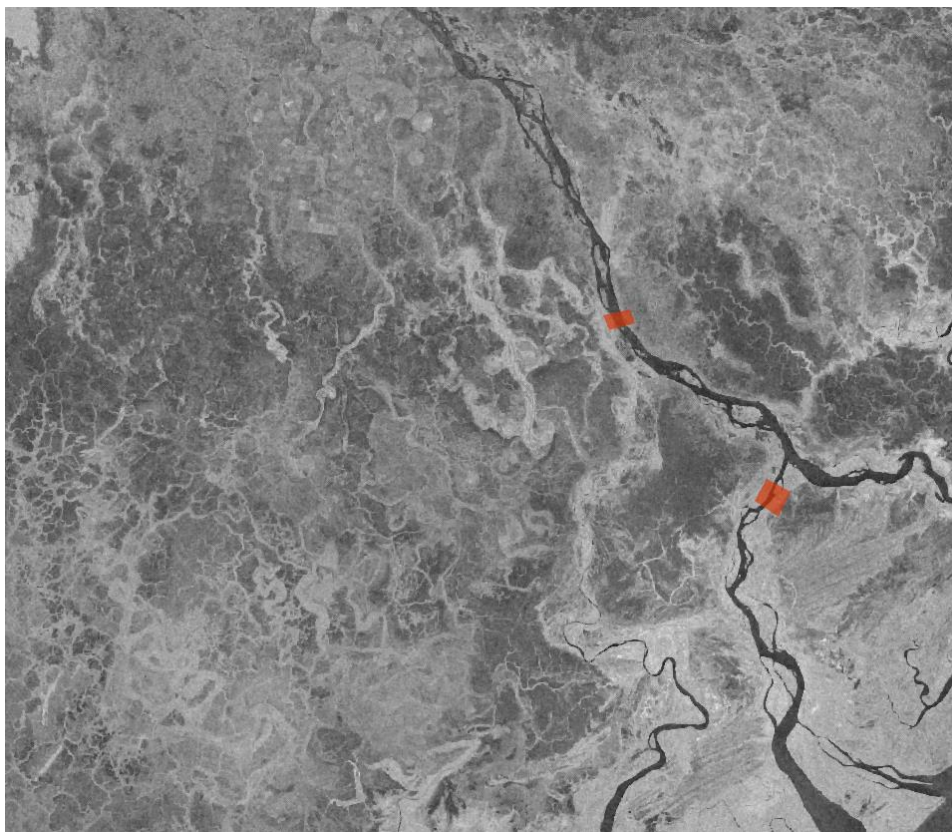

Figure D.1 Backscatter (VV) signal of Sentinel-1 image of 2016-10-19 with polygons (in red) containing water and land pixels.

Radar backscatter values of surface water are lower than the surrounding (and darker in Figure D.1) and a histogram of backscatter values within the polygons typically shows a bimodal shape, as shown in Figure D.2, with low backscatter values for water-pixels and higher backscatter values in land-pixels. This distribution van be used to determine the threshold to differentiate land and water pixel for the entire image area.
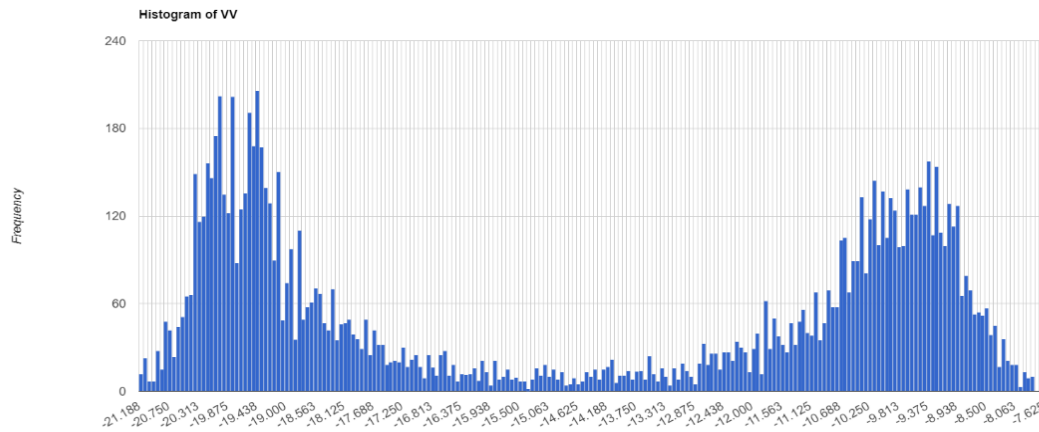
Figure D.2 Bimodal distribution of backscatter values of land (higher values) and water (lower values) within the red polygons shown in Figure B.1 to determine the threshold to distinguish water pixels from land pixels in the entire image (here, threshold = -14.97).

When applying the determined threshold to the rest of the image, we obtain the water extent shown in Figure D.3. We seem to encounter an overestimation of the surface water extent as this image is taken at the end of the dry season (2016-10-19) and we expect the area to be mostly dry.
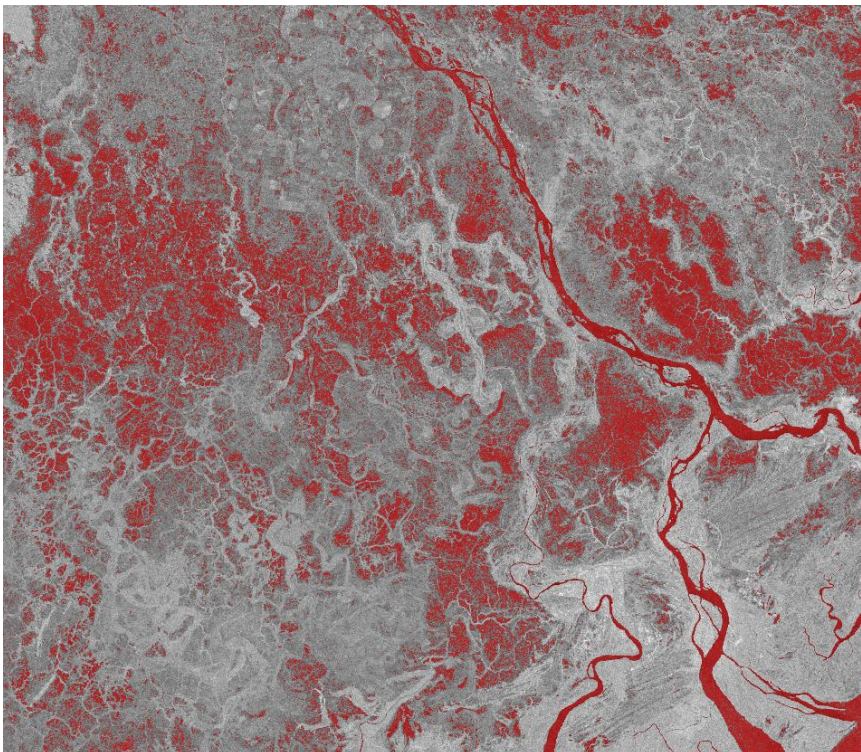

Figure D.3 Surface water extent (in red) found for 2016-10- using a threshold of -14.97 on the VV-backscatter. The problem here is an overestimation of surface water extent as this image is taken at the end of the dry season.

We therefore looked at an optical cloud-free image of the Sentinel-2 satellite (which is not able to see through clouds) taken at approximately the same time (2016-10-24) as shown in Figure D.4. When comparing this false coloring image with the surface water extent derived based on the Sentinel-1 radar images, we see a clear overestimation of surface water extent. This is likely due to the roughness of the vegetation which compares well with water pixels, but which makes it very difficult to determine surface water extent using Sentinel-1 images. We were therefore not able to determine surface water extent for each Sentinel-1 image in a reliable way to quantify the variability of surface water extent in the study area.

The difficulty to map surface water extent for each optical image of Sentinel-2 lies in the presence of clouds in optical images, which makes the analysis less straightforward and more complex. Especially during the wet period, clouds and clouds-shadow are present in the images.
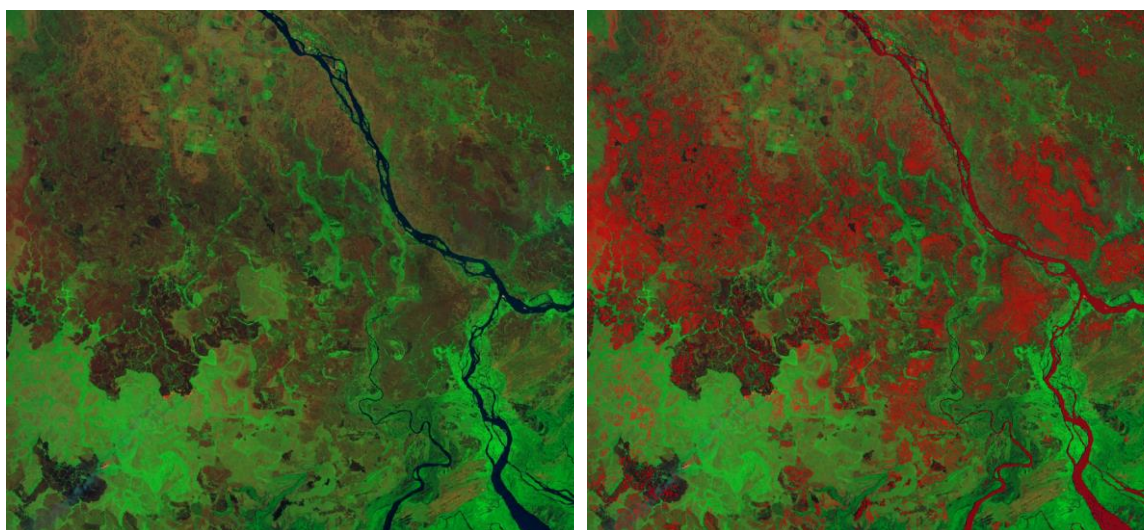

Figure D.4 Left: Sentinel-2 cloud-free image of 2016-10-24 (false coloring). Right: Sentinel-2 cloud-free image of 2016-10-24 overlaid by the surface water extent derived from the Sentinel-1 radar image (in red). We see an overestimation of surface water extent derived from Sentinel-1.

The same analysis was performed on an image during the wet season (2016-04-04) as shown in Figure D.5. Unfortunately, also for the wet season, we see an overestimation of surface water extent when using Sentinel-1 radar images compared to what we observe using optical images from Sentinel-2.
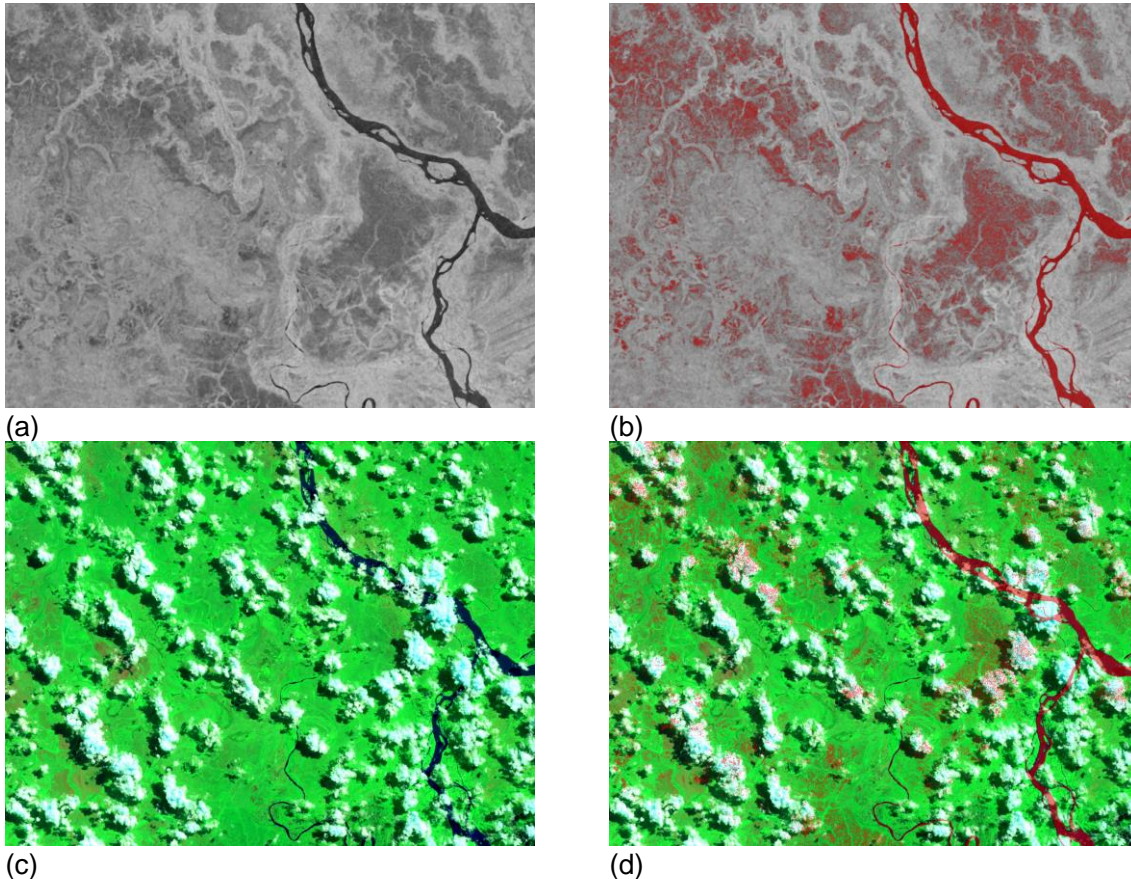

(a)

(b)

(c)

(d)

Figure D.5 (a) Sentinel-1 backscatter image (VV) of 2016-04-04. (b) Surface water extent in red based on threshold.
(c) Sentinel-2 optical image of 2016-03-30. (d) Sentinel-2 optical image of 2016-03-30 overlain by the
derived surface water extent based on Sentinel-1 analysis. Again, we see an overestimation of wet areas
compared to what we see in optical images, making this analysis unreliable for the current area.

Optical images by Sentinel-2 are affected by clouds and cloud-shadows and a relatively easy possibility to get rid of them is to create composite images of several images within a specific period and select one percentile value. In Figure D.6, we show composite images for the winter (January to April) and summer (June to September) period of 2016 for different percentile values. In doing so, cloud shadows appear in images with very low percentiles and clouds appear in images with very high percentiles (as also visible in Figure D.6e), and in between we can get an idea of cloud-free situations. The images obtained show that the chosen percentile has a high influence on what we see. It is for example not clear if the dark areas in Figure D.6b represent surface water areas; these dark areas also disappear for higher percentile values (Figure D.6f). This makes it difficult to classify surface water extent using optical images without ground field observations to validate the analysis.

(a) winter composite – percentile 30%

(b) summer composite – percentile 30%

(c) winter composite – percentile 40%

(d) summer composite – percentile 40%

(e) winter composite – percentile 60%

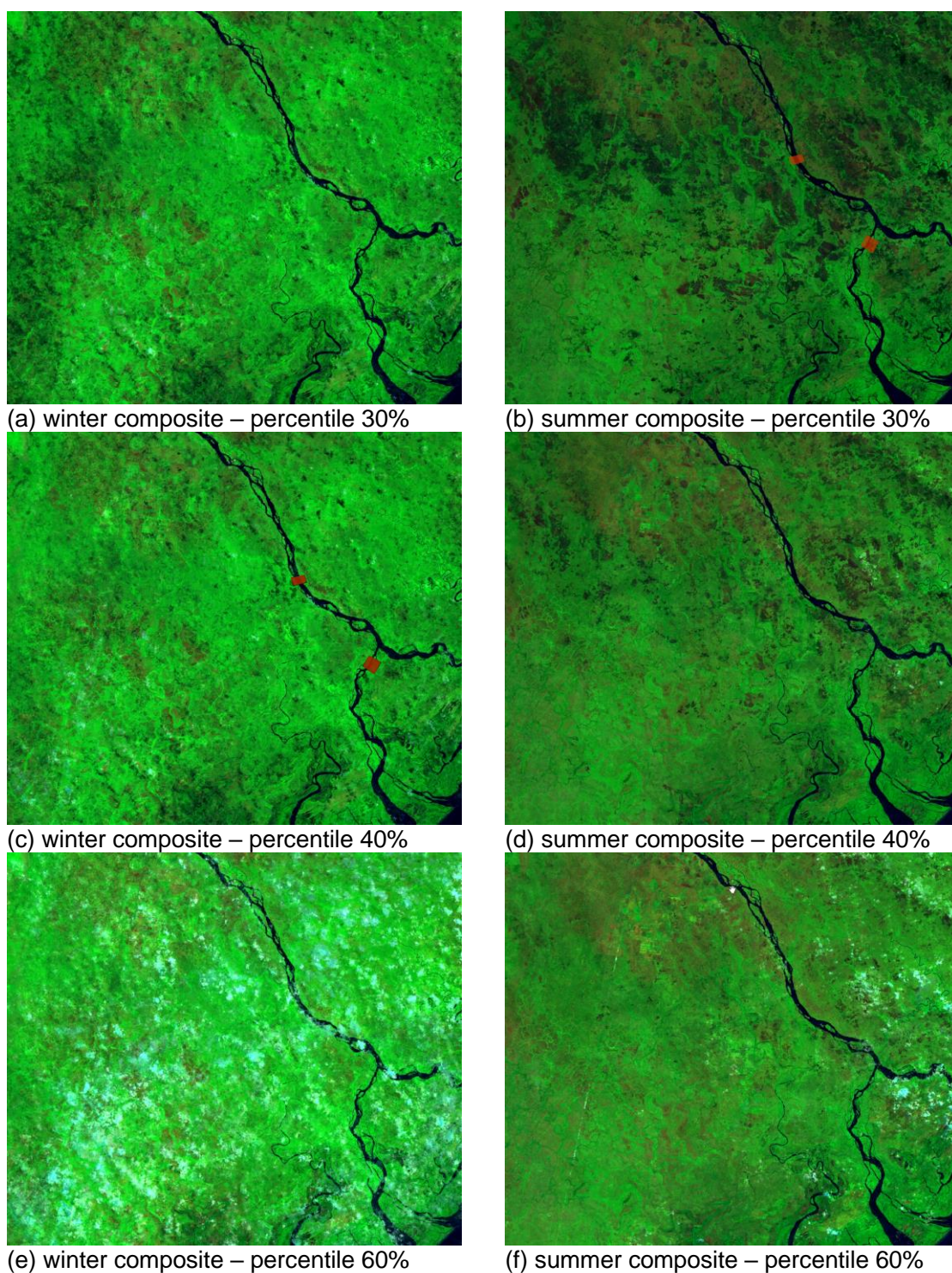(f) summer composite – percentile 60%

Figure D.6 Sentinel-2 based composites of the winter 2016 (2016-01-01 until 2016-04-30) and the summer of 2016 (2016-01-06 until 2016-09-30) for different percentile values.

A seasonal surface water extent analysis that could help to identify pools and their drying requires more extensive and in-depth analyses to provide reliable output.